Politecnico di Milano

Master Degree in Biomedical Engineering - Biomechanics and Biomaterials

Faculty of Industrial and Information Engineering
Department of Electronics Information and Bioengineering

Development of an in vitro platform to characterize Endothelial Cell-Platelet pro-thrombotic interaction mechanisms associated with Left Ventricular Assist Device therapy

Advisor:
Prof. Alberto Redaelli

Co-advisors:
Prof. Filippo Consolo
Prof. Marvin J. Slepian

Graduation Thesis of:
Alice Apostoli, 832780
Valentina Bianchi, 837461

Academic Year 2016-2017

Contents

List of Figures

List of Tables

List of abbreviations

HF	Heart Failure
MCS	Mechanical Circulatory Support
LVAD	Left Ventricular Assist Device
LV	Left Ventricle
EC	Endothelial Cell
HSD	Hemodynamic Shearing Device
TNF-α	Tumor Necrosis Factor α
CFD	Computational Fluid Dynamics
WSS	Wall Shear Stress
DTE	Device Thrombogenicity Emulation
PA	Platelet Activation
PAS	Platelet Activity State Assay
GFP	Gel Filtered Platelets
SEM	Scanning Electron Microscopy
ICAM-1	Intercellular Adhesion Molecule-1
VCAM-1	Vascular Adhesion Molecules-1
ELISA	Enzyme Linked ImmunoSorbent Assay
PRP	Platelet Rich Plasma
ATCC	American Type Culture Collection
HUVEC	Human Umbelical Venin Endothelial Cell
UDF	User Defined Function
INTERMACS	Interagency Registry for Mechanically Assisted Circulatory Support
GP	Glycoprotein
vWF	von Willebrand Factor
MRI	Magnetic Resonance Imaging
CT	Computed Tomography
PDF	Probability Density Function
FSI	Fluid-Structure Interaction
UHMWPE	Ultra-High Molecular Weight Polyethylene
PBS	Phosphate Buffer Saline

ASA	Acetylsalicyclic acid
IL	Interleukin
HLMVEC	Human Lung Microvascular Endothelial Cells
HAEC	Human Aortic Endothelial Cells
HCAECs	Human Coronary Artery Endothelial Cells
AA	Arachidonic Acid
SDS	Sodium Dodecyl Sulfate
FBS	Fetal Bovin Serum
P/S	Penicillin/Streptomycin
ECGS	Endothelial Cell Growth Supplement
ECGM	Endothelial Cell Complete Growth Medium
FCS	Fetal Calf Serum
SSECGM	Serum-Supplemented Endothelial Cell Growth Medium
DMSO	Dimetyl Sulfoxide
PBS	Phosphate Buffered Saline
MW	Multiwell
EPV	End Point Variable
HBS:BSA	Hepes Buffered Saline:Bovin Serum Albumin
$CaCl_2$	Calcium Chloride
PEG	Polyethylene Glycol
CH-TH	Chromazin - TH
EDTA	Ethylenediaminetetraacetic acid
HDMS	Hexamethyldisilazane
ANOVA	Analysis of Variance
MSS	Mean Sum of Squares
OD	Optical Density
SD	Standard Deviation
AT	Anti Thrombotic
PS	Polystyrene
Ag	Antigen
Ab	Antibody
ALP	Alkaline Phosphatase
pNPP	p-nitrophenylphosphate
FSC	Forward Scattered Channel
SSC	Side Scattered Channel
FACS	Fluorescence Activated Cell Sorter
SE	Secondary electrons
BSE	Backscattered electrons
SEI	Secondary electron imaging

Summary

Introduction

Heart failure (HF) is a chronic disease which severely compromises cardiac function leading to inadequate cardiac output. HF is one of the most critical public health burden of the 21^{th} century, affecting over 23 million people worldwide [1]. Preventive measures, medical therapy and heart transplantation are currently not able to counterbalance and/or reduce HF morbidity and mortality. This has brought to the development of mechanical circulatory support (MCS) devices, such as left ventricular assist devices (LVADs), which are intended to mechanically support or totally replace the pumping function of the failing left ventricle (LV). Nowadays, continuous-flow LVADs have become the mainstay of therapy for the treatment of HF, both as bridge to transplantation and destination therapy [2].
The current generation of LVADs have five main components, as shown in figure 1: the inflow cannula, the pump body (centrifugal or axial), the outflow cannula, the percutaneous drive-line and the electrical controller.

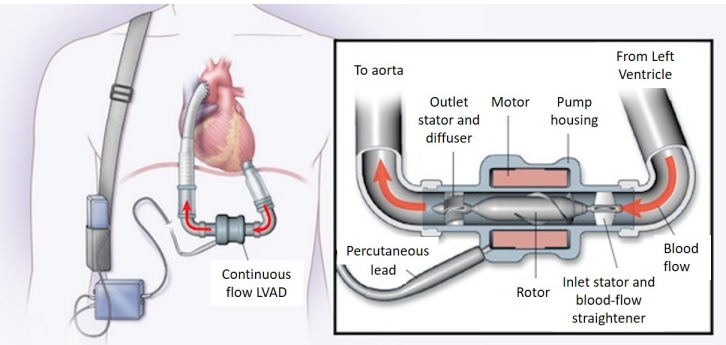

Figure 1: LVAD components [3]

Although survival rate associated with LVAD terhapy dramatically continues to improve, the therapy is still accompanied by the development of post-implant complications [4]. In particular, thrombosis represents one of the

most feared post-implant adverse events [5].
Thrombus formation in LVAD recipients is strictly driven by:

- the interaction between blood and device's artificial material;
- the disturbed flow dynamics associated with the pump.

In particular, pump-related altered hemodynamic conditions include hyper-shear stress due to the high impeller speed of the pump, and blood stasis and recirculation, mostly at the LV apex due to the reduced contractility of the LV [6] [7]. Both high shear stress magnitude and elongated shear exposure time may lead to platelet activation [8]. Activated platelets are prone to aggregation and thrombus formation [5]. In addition, the presence of stagnation regions exposes the ventricular endothelium to pro-thrombotic flow conditions, leading to endothelial activation. Endothelial activation represents a switch from a quiescent phenotype, characterized by an anti-adhesive, anti-coagulant and anti-inflammatory behaviour toward a pro-adhesive, pro-coagulant and pro-inflammatory one. This condition might become chronic, leading to endothelial injury enhancing thrombosis [9]. A further contribution to endothelium dysfunction is given by the placement of LVAD inflow cannula which further compromises normal LV hemodynamics enhancing blood stagnation and endothelial injury.
Even more critically, due to endothelium damage, complex interactions are induced between circulating activated platelets and inflamed endothelial cells (ECs). Platelet adhesion to endothelium is mediated by different adhesive proteins and mainly involves the endothelial receptors ICAM-1 and $\alpha_v\beta_3$ [28] [10]. This adhesive process is known to have a critical role in the pathogenesis of thrombosis in vivo.
However, endocardial dysfunction in LVAD recipients was poorly investigated so far and a clear understanding of the responsiveness of circulating activated platelets to the presence of an inflamed endothelium is lacking.

The present study is focused on the development of an experimental set-up able to characterize the interaction between activated platelets and inflamed ECs, in order to provide further insights into the mechanisms triggering thrombus formation in LVAD recipients. In particular, the adhesion mechanism, that is the first step of thrombus formation in-vivo, was investigated. To this purpose, platelets were incubated with cultured ECs and the interaction between the two cell types was evaluated in terms of platelet adhesion to the cell surface.
Four different conditions were considered:

- resting platelets incubated with non-activated ECs;

- shear activated platelets incubated with non-activated ECs;
- resting platelets incubated with inflamed ECs;
- shear activated platelets incubated with inflamed ECs.

Platelet activation was obtained through shear stress exposure, while ECs were chemically activated through the Tumor Necrosis Factor-α (TNF-α).
In addition, a computational fluid dynamics (CFD) patient-specific model of the LV chamber in presence of the LVAD inflow cannula was developed. The aim was to extract the wall shear stress (WSS) patterns at the LV apex-LVAD inflow cannula interface in order to settle the basis for a future improvement of the experimental set up, i.e. the in vitro replication of these WSS waveforms to induce mechanical stimulation of cultured ECs.

State of the Art

In the last few years, several studies in literature investigated the mechanisms driving thrombus formation in LVAD recipients. With the purpose of minimizing the thrombogenicity of LVADs, numerical and experimental tools were developed to evaluate the impact of the device on the biological environment.
Many CFD studies were focused on the evaluation of the disturbed fluid-dynamic conditions of the LV chamber in presence of the LVAD inflow cannula, whose geometry, position, insertion depth and angle may alter the intraventricular flow field. Some studies developed paradigmatic geometries to model the LV [11] [12], while others developed patient-specific LV models reconstructed from clinical imaging (Magnetic Resonance Imaging, MRI, or Computed Tomography, CT) [13] [14].
However, these CFD works have no direct correlation with platelet activation markers. Recently, in order to investigate the effect of abnormal flows on platelet thrombogenic markers, the Device Thrombogenicity Emulation (DTE) methodology was developed [15]. The DTE methodology couples in silico numerical simulations of LV-LVAD hemodynamics with in vitro measurement of platelet activation markers, and allows to predict the effects of design modifications and to optimize the thrombogenic performance of cardiovascular devices. Device-specific stress loading histories are extracted from numerical simulations and tested on a computer-controller hemodynamics emulating device (Hemodynamic Shearing Device, HSD), which is capable to uniformly expose platelets to constant or time-dependent shear stress waveforms. The HSD, whose schematic representation is shown in

figure 2a, combines the geometry of a cone and plate viscometer and a cylindrical coaxial Couette viscometer. At defined time points, the level of platelet activation deriving from the application of these shear flow can be quantified with a specific Platelet Activity State (PAS) assay.

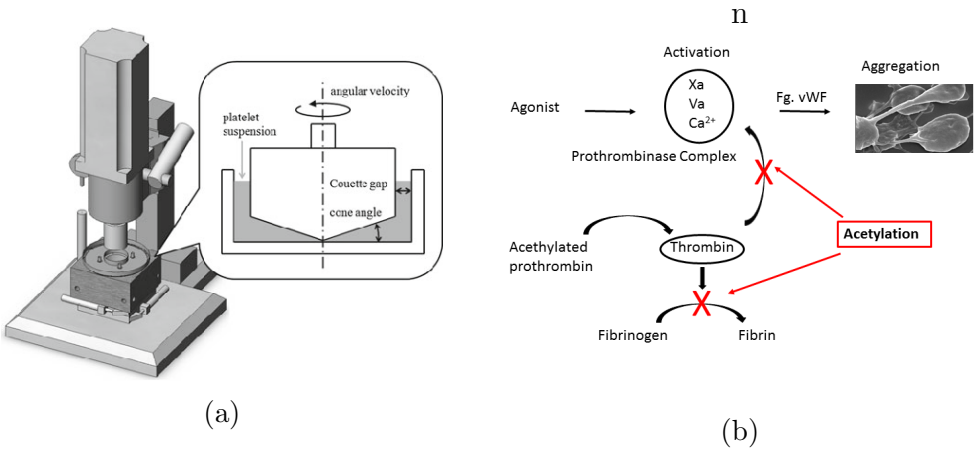

(a) (b)

Figure 2: Schematic representation of (a) HSD and (b) PAS assay

The PAS assay is a chemical assay able to measure the real-time thrombin production rate of activated platelets and to correlate it to the actual platelet activation level. Thrombin is a powerful marker of platelet activation, but in vivo the produced thrombin has a positive feedback response on platelet activation. By using a chemically modified prothrombin (acetylated prothrombin), able to remove the thrombin-mediated platelet activation positive feedback as shown in figure 2b, the PAS assay allows a reliable quantification of the platelet activation level [16].
So far, the PAS assay has been extensively used for in vitro studies of device-associated platelet activation. In particular, this technique was employed to measure the shear-mediated platelet activation induced by HSD stimulation [17].
Moreover, flow cytometry detection of platelet surface activation markers represents a valuable tool for the analysis of platelet activation. The most widely studied markers identifying procoagulant activity of platelets are P-selectin [18] [19] and Annexin V [20] [21], whose expression was demonstrated to be activation dependent.
Since shear stress has effects also on platelet shape, different studies in literature analysed through Scanning Electron Microscopy (SEM) imaging the changes in platelet morphology during the platelet adhesive process under flow.

Another important aspect related to thrombus formation in LVAD recipients

is the presence of endothelial inflammation.
Abnormal shear stress or chemical stimulation can modify the surface expression of various adhesion molecules, such as Intercellular Adhesion Molecule-1 (ICAM-1), Vascular Adhesion Molecule-1 (VCAM-1) and Endothelial Selectin (E-selectin), and release of these molecules in the extracellular fluid [22]. The incubation of cultured ECs with TNF-α demonstrated through both ELISA tests [23] and flow cytometry analysis [24] that this cytokine upregulates the expression of adhesion molecules and that the expression is dependent on TNF-α concentration and exposure time.
Regarding the mechanical stimulation, several studies in literature have shown that the structure and function of ECs are deeply affected by the nature of WSS waveforms. In particular, ECs are sensitive to (i) the direction of the flow and (ii) the magnitude of the resulting shear stress. Low and oscillating shear stresses were demonstrated to enhance the expression of adhesion molecules [25] and to induce morphological changes [26].

Materials and Methods

Platelet extraction and activation

In order to perform experiments involving platelets, Gel Filtered Platelets (GFP) were obtained through whole blood centrifugation followed by gel filtration of Platelet Rich Plasma (PRP). Aiming to shear platelets, the HSD was used to apply time-constant shear stress patterns of varying magnitude (i.e. 30, 50, 70 dyne/cm^2, 10 min).

Endothelial Cell culture and activation

Human Umbelical Vein Endothelial Cells (HUVECs) were chosen as cell line for the present study.
In order to characterize chemically-induced HUVECs inflammation potential, a preliminary experimental campaign was performed. HUVECs expression of soluble activation markers (ICAM-1, VCAM-1, E-Selectin) was measured using ELISA kits after exposure to TNF-α. Two variables were considered: TNF-α i) concentration and ii) exposure time. The characterization was repeated considering only 24h TNF-α exposure, performing both ELISA and flow cyotmetry for, respectively, soluble and surface ICAM-1, VCAM-1 and E-Selectin. According to the results of this campaign, two ECs inflammation protocols were defined for the subsequent experiments: i) TNF-α 10 ng/ml for 24h and ii) TNF-α 100 ng/ml for 24h.

Platelet-Endothelial Cell interaction

To evaluate the mutual interaction between sheared platelets and inflamed ECs, four main conditions were considered, as summarized in table 1, with the purpose to deconstruct this complex phenomena and analyse separately the mutual contribution offered by platelet activation and EC inflammation.

		Endothelial Cells	
		Non activated	TNFα-activated
Platelets	Resting	Experiment 1	Experiment 3
	HSD-sheared	Experiment 2	Experiment 4

Table 1: Summary of the four conducted experiments

Two characterization techniques were used to investigate variability in the activation level of the two cell types: i) PAS assay on platelet sample; ii) flow cytometry to determine HUVECs (i.e. ICAM-1, VCAM-1, E-Selectin) and platelet (i.e. P-Selectin and Annexin V) surface markers expression. In order to characterize the adhesion mechanism, two analysis techniques were used: i) SEM images acquisition and ii) flow cytometry to determine the expression level of the endothelial integrin $\alpha_V\beta_3$.

Computational Fluid Dynamics study

In order to characterize the LV-LVAD hemodynamics, CFD *patient-specific* models were developed, reconstructing the geometries from 3D-TT-ECHO (3D-TransThoracic-Echocardiography) images (figure 3).

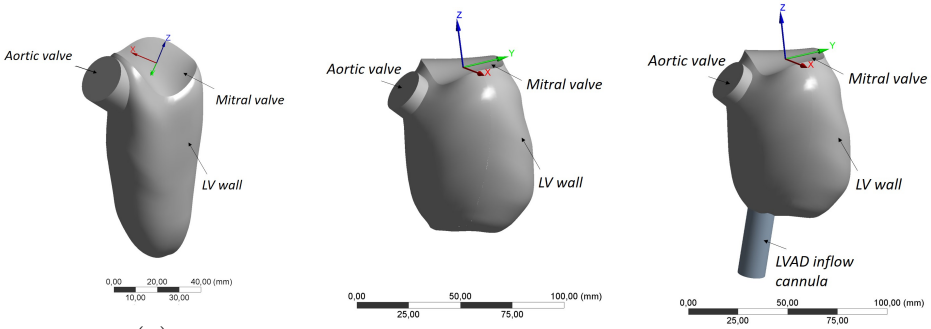

(a) (b) (c)

Figure 3: *Patient-specific* models: (a) healthy LV (b) HF LV pre-LVAD implant and (c) HF LV post-LVAD implant

Different conditions were simulated: i) healthy LV (figure 3a); ii) HF LV pre-

LVAD implant, i.e. dilated with reduced or negligible contractile capacity; iii) HF LV post-LVAD implant, i.e. dilated LV with negligible contractile capacity in presence of LVAD inflow cannula (figure 3c).
The dynamics of the cardiac cycle was simulated assigning a proper displacement to each node of the LV grid through the implementation of mesh motion User Defined Functions (UDFs). The resulting movement is i) contraction and twist during systole and ii) dilation and untwist during diastole. A different contractile capacity was simulated in the healthy LV with respect to the HF ones.

In order to define the shear stress patterns that ECs experience in the apical region of the LV, WSSs were extracted for each element of the apical ventricular wall, highlighted in green in figure 4.

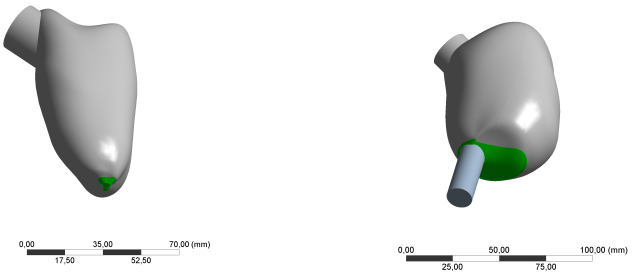

(a) (b)

Figure 4: Apical region in green where the zWSS trends were evaluated for the patient-specific healthy LV (a) and HF post-LVAD implant LV (b)

Results

Platelet-Endothelial Cell interaction

The interaction between platelets and cultured ECs was evaluated in terms of platelet adhesion to the cell surface, which was characterized through SEM imaging and flow cytometry analysis for the endothelial integrin $\alpha_v\beta_3$.
Figure 5 shows SEM images obtained for the 4 different experimental conditions reported in table 1.
Resting platelets bind minimally to non-activated HUVECs (figure 6a), while shear activated platelets adhere to non-activated ECs (figure 6b). On the other hand, TNF-α inflamed HUVECs resulted totally adhesive for platelets, both resting and shear activated (figures 6c and 6d).
The binding between sheared platelets and HUVECs was confirmed through

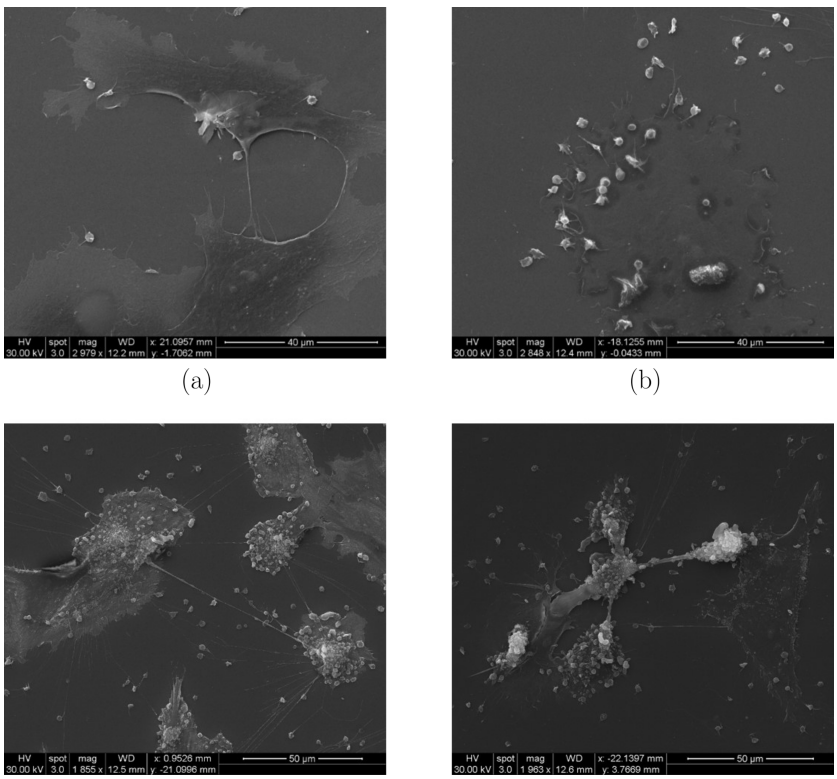

Figure 5: SEM images showing platelet adhesion to HUVEC, obtained incubating (a) non-activated platelets with non-activated HUVECs; (b) shear-activated platelets with non-activated HUVECs; (c) non-activated platelets with TNFα-activated HUVECs and (d) shear-activated platelets with TNFα-activated HUVECs

flow cytometry for the endothelial marker $\alpha_v\beta_3$, whose resulting histograms are shown in figure 6. $\alpha_v\beta_3$ expression resulted reduced after incubation with sheared platelets, demonstrating that the integrin is involved in the adhesion of platelets to the cell surface. The expression reduction is more evident when HUVECs are inflamed, confirming that the endothelial inflammation further enhances platelet adhesion.

Computational Fluid Dynamics study

In figure 7, the displacement achieved through the implemented UDFs is shown.

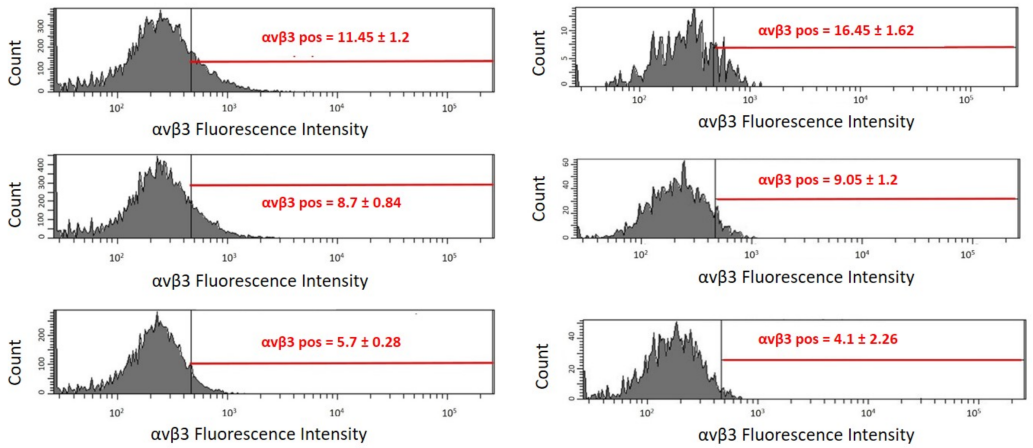

(a) (b)

Figure 6: 10 ng/ml TNF-α activated (a) and non-activated (b) HUVEC expression of $\alpha_V\beta_3$ according to flow cytometry without incubation with platelets (top), after 1h incubation with 50 dyne/cm^2 (center) and 70 dyne/cm^2 sheared platelets (bottom).

(a) (b) (c)

Figure 7: Superimposition of the end-diastolic and end-systolic configurations for the *patient-specific* LV models: (a) healthy LV, (b) HF-LV pre-LVAD implant with reduced contractile capacity and (c) HF-LV post-LVAD implant with negligible contractile capacity

Figure 8 shows the temporal trend of the axial component of the WSS extracted from the simulations. Both HF-LV models, i.e. pre and post LVAD implant, exhibit very low values of WSS (peak values are one order of magnitude lower compared to the healthy model), highlighting the presence of a stagnation region at the LV-LVAD inflow cannula interface.

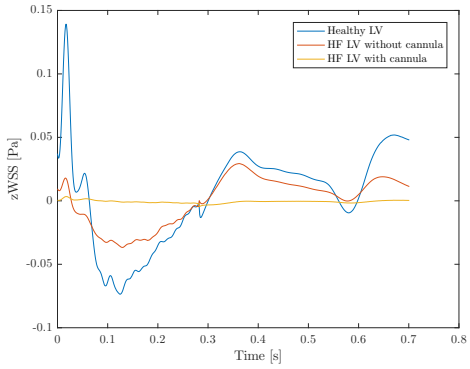

Figure 8: zWSS trends obtained for the three *patient-specific* models

Discussion and conclusions

LVAD is an established therapeutic strategy for patients with end-stage HF. Nevertheless, LVADs can activate the coagulation system resulting in device-related thrombus, mostly at the interface between the LV apex and the LVAD inflow cannula.
So far, thrombus formation in LVAD recipients was mainly ascribed to shear-mediated platelet activation. Another important aspect of thrombus formation is related to ECs inflammation which may lead to endothelial injury enhancing thrombosis. However, few studies in literature were focused on endocardial dysfunction in LVAD recipients. Moreover, the interactions between circulating activated platelets and inflamed ECs were poorly investigated.
In the present study, the interaction between sheared platelets and inflamed ECs was characterized through the development of an experimental set-up, able to investigate the mechanism of platelet adhesion to endothelium, which leads to thrombus formation in vivo.
It was demonstrated that the inflammation of cultured ECs induces adhesion of platelets to cell surface. Additionally, a decrease in the expression of the endothelial integrin $\alpha_v\beta_3$ after the incubation with platelets was observed, confirming the binding between the two cellular types. Shear activated platelets were shown to bind to unstimulated ECs as well, but the adhesion was lower with respect to the one induced by inflamed ECs.
In conclusion, the present study allowed to experimentally characterize the

role of platelet-endothelium interaction enhancing thrombus formation in LVAD recipients.

However, the experimental model is affected by various limitations that could be overcome.
Firstly, with the developed platform it is possible to investigate only platelet adhesion to ECs, which is just one of the mechanisms characterizing the complex phenomenon of thrombosis. However, this limitation represents an advantage too, allowing to analyse a single mechanism at once.
In addition, platelet activation was induced through HSD with time-constant shear stress patterns. An improvement could be to shear platelets replicating LVAD-specific waveforms extracted from in silico simulations.
Moreover, in the present study the contribution of blood contact with a foreign surface to thrombosis was neglected.
Finally, a very important future development of the present study is represented by the integration of the experimental set-up with a perfusion module able to replicate in silico extracted shear-flow patterns characteristic of the LV chamber with the LVAD, in order to mechanically stimulate cultured ECs, resembling in vivo EC inflammation pathways.

Bibliography

[1] Longjian Liu and Howard J Eisen, *Epidemiology of heart failure and scope of the problem*. Cardiology clinics, 32(1):1-8,2014.

[2] Joseph AR Englert III Jennifer A Davis and Selim R Krim, *Mechanical Circulatory Support for the Failing Heart: Continuous-Flow Left Ventricular Assist Devices*. The Ochsner Journal, 16(3):263-269, 2016.

[3] `http://rebelem.com/left-ventricular-assist-device/`

[4] Arman Kilic, Michael A Acker, and Pavan Atluri, *Dealing with surgical left ventricular assist device complications*. Journal of thoracic disease, 7(12):2158, 2015.

[5] Wei-Che Chiu, Gaurav Girdhar, Michalis Xenos, Yared Alemu, Jõao S Soares, Shmuel Einav, Marvin Slepian, and Danny Bluestein, *Thromboresistance comparison of the HeartMate II ventricular assist device with the device thrombogenicity emulation-optimized HeartAssist 5 VAD*. Journal of biomechanical engineering, 136(2):021014, 2014.

[6] Katharine H Fraser, Tao Zhang, M Ertan Taskin, Bartley P Griffith, and Zhongjun J Wu, *Computational fluid dynamics analysis of thrombosis potential in left ventricular assist device drainage cannulae.* ASAIO journal (American Society for Artificial Internal Organs: 1992), 56(3):157, 2010.

[7] Chitaru Kurihara, Minoru Ono, Takashi Nishimura, Aya Saito, Tsuyoshi Taketani, Motoyuki Hisagi, Kan Nawata, Osamu Kinoshita, Tetsurou Morota, Noboru Motomura, et al. *Use of DuraHeart® support for more than 1 year as the first successful bridge to heart transplantation in Japan.* Journal of Artificial Organs, 14(1):67-69, 2011.

[8] Jawaad Sheriff, Danny Bluestein, Gaurav Girdhar, and Jolyon Jesty, *High-shear stress sensitizes platelets to subsequent low-shear conditions.* Annals of biomedical engineering, 38(4):1442-1450, 2010.

[9] Jun Zhang, Albert F DeFelice, Joseph P Hanig, and Thomas Colatsky, *Biomarkers of endothelial cell activation serve as potential surrogate markers for drug-induced vascular injury.* Toxicologic pathology, 38(6):856-871, 2010.

[10] Dorothea I Siegel-Axel, and Meinrad Gawaz, *Platelets and endothelial cells.* Seminars in thrombosis and hemostasis, volume 33, pages 128-135. Copyright© 2007 by Thieme Medical Publishers, Inc., 333 Seventh Avenue, New York, NY 10001, USA, 2007.

[11] ChiWei Ong, Socrates Dokos, BeeTing Chan, Einly Lim, Amr Al Abed, NoorAzuanBinAbu Osman, Suhaini Kadiman, Nigel H Lovell, *Numerical investigation of the effect of cannula placement on thrombosis.* Theoretical Biology and Medical Modelling, 10(1):1, 2013.

[12] Guang-Mao Liu, Hai-Bo Chen, Fu-Liang Luo, Yan Zhang, Han-Song Sun, Jian-Ye Zhou, Sheng-Shou Hu, *Numerical simulation of LVAD inflow cannulas with different tip.* International Journal of Chemical Engineering, 2012, 2012.

[13] Anthony R Prisco, Alberto Aliseda, Jennifer A Beckman, Nahush A Mokadam, Claudius Mahr, and Guilherme JM Garcia, *Impact of LVAD Implantation Site on Ventricular Blood Stagnation.* ASAIO Journal, 2017.

[14] Sam Liao, Benjamin Simpson, Michael Neidlin, Tim AS Kaufmann, Zhiyong Li, Maria A Woodruff, and Shaun D Gregory, *Numerical prediction of thrombus risk in an anatomically dilated left ventricle: the effect*

of inflow cannula designs. BioMedical Engineering OnLine, 15(2):587, 2016.

[15] Danny Bluestein, KB Chandran, and KB Manning, *Towards non-thrombogenic performance of blood recirculating devices*. Annals of biomedical engineering, 38(3):1236-1256, 2010.

[16] Lorenzo Valerio, Filippo Consolo, Danny Bluestein, Phat Tran, Marvin Slepian, Alberto Redaelli, and Federico Pappalardo, *Shear-mediated platelet activation in patients implanted with continuous flow LVADs: A preliminary study utilizing the platelet activity state (PAS) assay*. In Engineering in Medicine and Biology Society (EMBC), 2015 37th Annual International Conference of the IEEE, pages 1255-1258. IEEE, 2015.

[17] Matteo Nobili, Jawaad Sheriff, Umberto Morbiducci, Alberto Redaelli, and Danny Bluestein, *Platelet activation due to hemodynamic shear stresses: damage accumulation model and comparison to in vitro measurements*. ASAIO journal (American Society for Artificial Internal Organs: 1992), 54(1):64, 2008.

[18] Qijin Lu, Bryan V Hofferbert, Grace Koo, and Richard A Malinauskas, *In Vitro Shear Stress-Induced Platelet Activation: Sensitivity of Human and Bovine Blood*. Artificial organs, 37(10):894-903, 2013.

[19] M Griesshammer, H Beneke, B Nussbaumer, M Grünewald, M Bangerter, and L Bergmann, *Increased platelet surface expression of P-selectin and thrombospondin as markers of platelet activation in essential thrombocythaemia*. Thrombosis research, 96(3):191-196, 1999.

[20] Eleni Tzima, Patrick J Trotter, Margaret A Orchard, and John H Walker, *Annexin V relocates to the platelet cytoskeleton upon activation and binds to a specific isoform of actin*. European Journal of Biochemistry, 267(15):4720-4730, 2000.

[21] Jeanne Dachary-Prigent, Jean-Marie Freyssinet, Jean-Max Pasquet, Jean-Claude Carron, and Alan T Nurden, *Annexin V as a probe of aminophospholipid exposure and platelet membrane vesiculation: a flow cytometry study showing a role for free sulfhydryl groups*. Blood, 81(10):2554-2565, 1993.

[22] Ryan B Huang, and Omolola Eniola-Adefeso, *Shear stress modulation of IL-1β-induced E-selectin expression in human endothelial cells*. PloS one, 7(2):e31874, 2012.

[23] MWJ Boehme, U Raeth, WA Scherbaum, PR Galle, and W Stremmel, *Interaction of endothelial cells and neutrophils in vitro: kinetics of thrombomodulin, intercellular adhesion molecule-1 (ICAM-1), E-selectin, and vascular cell adhesion molecule-1 (VCAM-1): implications for the relevance as serological disease activity markers in vasculitides.* Clinical & Experimental Immunology, 119(1):250-254, 2000.

[24] Fabienne Mackay, Hansruedi Loetscher, Dietrich Stueber, Gisela Gehr, and Werner Lesslauer, *Tumor necrosis factor alpha (TNF-alpha)-induced cell adhesion to human endothelial cells is under dominant control of one TNF receptor type, TNF-R55.* The Journal of experimental medicine, 177(5):1277-1286, 1993.

[25] David C Chappell, Signe E Varner, Robert M Nerem, Russell M Medford, R Wayne Alexander, *Oscillatory shear stress stimulates adhesion molecule expression in cultured human endothelium.* Circulation research, 82(5):532-539, 1998.

[26] Wei Yin, Saravan Kumar Shanmugavelayudam, and David A Rubenstein, *The effect of physiologically relevant dynamic shear stress on platelet and endothelial cell activation.* Thrombosis research, 127(3):235-241, 2011.

[27] Robert L Czervionke, John C Hoak, and Glenna L Fry, *Effect of aspirin on thrombin-induced adherence of platelets to cultured cells from the blood vessel wall.* Journal of Clinical Investigation, 62(4):847, 1978.

[28] Thomas Bombeli, Barbara R Schwartz, and John M Harlan, *Adhesion of activated platelets to endothelial cells: evidence for a GPIIbIIIa-dependent bridging mechanism and novel roles for endothelial intercellular adhesion molecule 1 (ICAM-1), $\alpha v\beta 3$ integrin, and GPIbα.* The Journal of experimental medicine, 187(3):329-339, 1998.

[29] Wei Yin, Farzana Rouf, Saravan K Shanmugavelayudam, and David A Rubenstein, *Endothelial cells modulate platelet response to dynamic shear stress.* Cardiovascular Engineering and Technology, 5(2):145-153, 2014.

[30] CW Ong, BT Chan, E Lim, NA Abu Osman, AA Abed, S Dokos, and NH Lovell, *Fluid structure interaction simulation of left ventricular flow dynamics under left ventricular assist device support.* In 2012 Annual International Conference of the IEEE Engineering in Medicine and Biology Society, pages 6293-6296. IEEE, 2012.

Sommario

Introduzione

L'insufficienza cardiaca (IC) è una malattia cronica che compromette gravemente la funzionalità cardiaca causando una portata sanguigna inadeguata. L'IC colpisce circa 23 milioni di persone nel mondo [1] ed è per questo considerata una delle patologie del XXI secolo con maggiore incidenza sulla salute della popolazione mondiale. Le misure preventive, la terapia medica e il trapianto cardiaco non sono in grado di contrastare e/o ridurre la mortalità e la morbilità associate all'IC. Questo ha portato allo sviluppo di dispositivi meccanici di supporto circolatorio (Mechanical Circulatory Support devices, MCS devices), come i dispositivi di assistenza ventricolare sinistra (Left Ventricular Assist Devices, LVAD) il cui obiettivo è fornire un supporto o sostituire completamente la funzione pompante del ventricolo sinistro (VS). I LVAD a flusso continuo rappresentano un supporto per la terapia per l'IC, sia come ponte al trapianto cardiaco, che come terapia definitiva [2].
L'attuale generazione di LVAD prevede cinque componenti principali (figura 9): la cannula di afflusso, la pompa(centrifuga o assiale), la cannula di efflusso, la linea di trasmissione percutanea e il controllore elettronico.

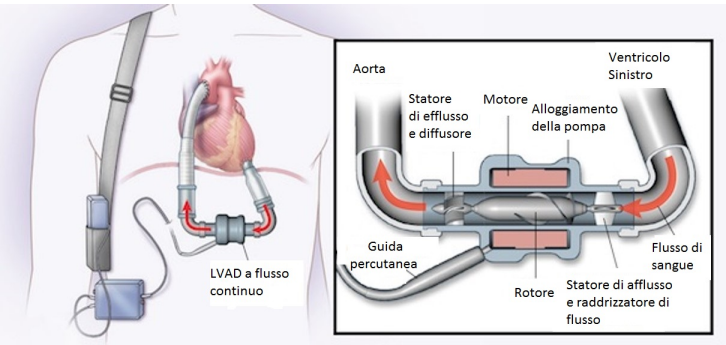

Figura 9: Componenti di un LVAD [3]

Nonostante il tasso di sopravvivenza associato a questi dispositivi sia in

continua crescita, la terapia è soggetta allo sviluppo di complicazioni post-impianto [4]. In particolare, la trombosi rapprenta una delle più temute complicazioni [5].
La formazione di trombi nei soggetti con LVAD è strettamente legata a:

- l'interazione tra il sangue e il materiale artificiale del dispositivo;
- la fluidodinamica disturbata associata alla pompa.

In particolare, le condizioni emodinamiche alterate includono alti sforzi di taglio (hyper-shear) dovuti alla elevata velocità di rotazione dell'impeller della pompa, e il ristagno e ricircolo di sangue principalmente nella porzione apicale del VS a causa della ridotta contrattilità di quest'ultimo [6] [7]. Sia l'elevata ampiezza degli sforzi di taglio che i lunghi tempi di esposizione allo shear possono portare all'attivazione piastrinica [8]. Le piastrine attivate tendono all'aggregazione e alla formazione di trombo [5].
Inoltre, la presenza di regioni di ristagno espone l'endotelio ventricolare a condizioni di flusso pro-trombotiche che possono indurne l'attivazione. L'attivazione dell'endotelio rappresenta un passaggio da un fenotipo quiescente, caratterizzato da comportamento anti-adesivo, anti-coagulante e anti-infiammatorio, ad uno pro-adesivo, pro-coagulante e pro-infiammatorio. Questa condizione può diventare cronica, causando danno endoteliale e aggravando la trombosi [9]. La presenza della cannula di afflusso del VAD contribuisce alla disfunzione endoteliale, compromettendo ulteriormente la normale emodinamica del VS, accentuando il ristagno di sangue e il danno endoteliale.
Inoltre, il danno endoteliale induce complesse interazioni tra le piastrine attivate circolanti e le cellule endoteliali (CE). L'adesione piastrinica all'endotelio è mediata da diverse proteine adesive e coinvolge principalmente i recettori endoteliali ICAM-1 (Inter Cellular Adhesion Molecule-1) e $\alpha_v\beta_3$ [28] [10]. Questo processo adesivo è noto avere un ruolo critico nella patogenesi della trombosi in vivo.
Tuttavia, pochi lavori si sono focalizzati sulla disfunzionalità dell'endocardio nei pazienti con LVAD e non è ancora chiaro quale sia la risposta delle piastrine attivate circolanti alla presenza di endotelio infiammato,

Il presente studio è focalizzato sullo sviluppo di un set-up sperimentale per caratterizzare l'interazione tra piastrine attivate e CE infiammate per comprendere i meccanismi responsabili della formazione di trombo nei pazienti con LVAD impiantato. In particolare, è stato investigato il meccanismo di adesione, primo step della formazione di trombo in vivo. Con questo obiettivo, le piastrine sono state incubate con CE in coltura e l'interazione tra i due tipi cellulari è stata valutata in termini di adesione piastrinica alle CE. Quattro diverse condizioni sono state considerate:

- piastrine non attivate incubate con CE non attivate;
- piastrine attivate tramite shear incubate con CE non attivate;
- piastrine non attivate incubate con CE infiammate;
- piastrine attivate tramite shear incubate con CE infiammate;

L'attivazione piastrinica è stata ottenuta tramite esposizione a sforiz di taglio, mentre le CE sono state attivate chimicamente attraverso il fattore di necrosi tumorale α (TNF-α).
Inoltre, è stato sviluppato uno modello CFD (Computational Fluid Dynamics) paziente-specifico della camera ventricolare in presenza della cannula di afflusso di un LVAD. Lo scopo è stato quello di estrarre l'andamento degli sforzi di taglio a parete (Wall Shear Stress, WSS) nella regione di interfaccia tra l'apice del VS e la cannula del LVAD in modo da consentire uno sviluppo futuro del set-up sperimentale, ovvero la replica in vitro delle forme d'onda dei WSS per stimolare meccanicamente CE in coltura.

Stato dell'arte

Negli ultimi anni, molti studi in letteratura hanno esaminato i meccanismi che portano alla formazione di trombo nei pazienti con LVAD impiantato. Numerosi strumenti numerici e sperimentali sono stati sviluppati per valutare l'impatto del dispositivo sull'ambiente biologico, con l'obiettivo finale di minimizzare la trombogenicità dei LVAD.
Molti studi CFD si sono focalizzati sull'analisi delle condizioni fluidodinamiche disturbate del VS in presenza della cannula di afflusso del LVAD, la cui geometria, posizione, profondità e angolo di inserzione possono alterare il campo di flusso intraventricolare.
Alcuni lavori hanno utilizzato geometrie paradigmatiche per modellizzare il VS [11] [12], mentre altri hanno sviluppato dei modelli paziente-specifico ricostruiti a partire da immagini ottenute tramite tecniche di imaging (Magnetic Resonance Imaging, MRI, or Computed Tomography, CT) [13] [14].
Tuttavia, questi lavori CFD non hanno nessuna correlazione diretta con i marcatori di attivazione piastrinica. Per investigare l'effetto che l'emodinamica alterata ha sui marker piastrinici trombogenici, è stata sviluppata la metodologia DTE (Device Thrombogenicity Emulation) [15]. Quest'ultima combina simulazioni numeriche in silico dell'emodinamica del VS con LVAD con misurazioni in vitro relative ai marcatori di attivazione piastrinica, e consente quindi di predire gli effetti di modifiche del design dei dispositivi

cardiovascolari e di ottimizzarne la performance trombogenica. Storie di carico paziente-specifiche vengono estratte dalle simulazioni numeriche e poi testate su un dispositivo di emulazione emodinamica (Hemodynamic Shearing Device, HSD), capace di esporre uniformemente le piastrine a forme d'onda di sforzo di taglio costanti oppure tempo varianti. L'HSD, la cui rappresentazione schematica è mostrata in figura 10a, combina la geometria di un viscosimetro a cono e piatto con quella di un viscosimetro cilindrico coassiale di tipo Couette. A istanti di tempo predefiniti, il livello di attivazione piastrinica derivante dall'applicazione di un certo shear viene quantificato tramite uno specifico saggio detto Platelet Activity State (PAS) assay.

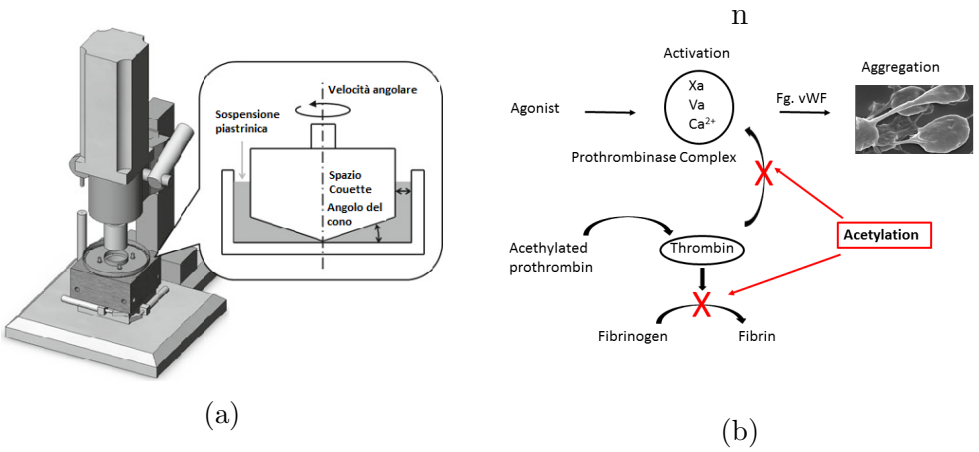

(a) (b)

Figura 10: Rappresentazione schematica di (a) HSD e (b) PAS assay

Il PAS assay è un saggio chimico in grado di misurare in tempo reale la produzione di trombina da parte delle piastrine attivate e di correrla al livello di attivazione piastrinica. La trombina è un potente marker di attivazione piastrinica, ma, in vivo, la trombina prodotta ha un feedback positivo sull'attivazione piastrinica. Utilizzando dunque una protrombina chimicamente modificata (protrombina acetilata), capace di rimuovere il feedback positivo sull'attivazione piastrinica mediato dalla trombina come mostrato in figura 10b, il PAS assay consente di quantificare in modo affidabile il livello di attivazione piastrinica [16].
Finora, il PAS assay è stato ampiamente utilizzato in vitro per studiare l'attivazione piastrinica associata a dispositivi. In particolare, questa tecnica è stata usata per misurare l'attivazione piastrinica indotta da sforzo di taglio attraverso la stimolazione con HSD [17].
Inoltre, la misura dell'espressione dei marcatori piastrinici di superficie tramite citometria a flusso rappresenta un valido strumento per l'analisi dell'attivazione piastrinica. Tra i marker che indicano un'attività procoagulante delle

piastrine, i più studiati sono la P-selectina [18] [19] e l'Annessina V [20] [21], la cui espressione è attivazione-dipendente.
Dato che gli sforzi di taglio hanno effetto anche sulla forma delle piastrine, alcuni studi in letteratura hanno esaminato attraverso il microscopio a scansione elettronica (SEM) i cambiamenti nella morfologia piastrinica durante il processo adesivo delle piastrine sotto flusso.

Un altro aspetto importante relativo alla formazione di trombo nei pazienti che hanno subito impianto di LVAD è la presenza di infiammazione endoteliale.
Sforzi di taglio non fisiologici o stimolazione chimica possono modificare l'espressione da parte delle CE di diverse molecole di adesione, come la molecola di adesione intercellulare (ICAM-1), la molecola di adesione cellulare vascolare (VCAM-1) e la selectina endoliale (E-selectina), e rilascio di queste molecole nel fluido extracellulare [22]. L'incubazione di CE in coltura con TNF-α ha dimostrato attraverso ELISA [23] e citometria a flusso [24] che questa citochina regola l'espressione delle molecole di adesione e che l'espressione dipende dalla concentrazione di TNF-α e dal tempo di esposizione.
Relativamente alla stimolazione meccanica, numerosi studi in letteratura hanno mostrato che la struttura e la funzionalità delle CE sono profondamente influenzate dalla natura della forma d'onda di WSS. In particolare le CE sono sensibili a i) direzione del flusso e ii) ampiezza dello sforzo di taglio risultante. Sforzi di taglio bassi ed oscillanti provocano un aumento dell'espressione delle molecule di adesione [25] e inducono cambiamenti morfologici [26].

Materiali e Metodi

Estrazione ed attivazione piastrinica

Per svolgere esperimenti con le piastrine, il GFP (gel-filtered platelets) è stato ottenuto tramite centrifuga di sangue intero seguita da gel-filtrazione del PRP (platelet rich plasma). Le piastrine sono state sottoposte tramite HSD a sforzi di taglio costanti nel tempo di diversa ampiezza (i.e. 30, 50, 70 dyne/cm^2, 10 min).

Coltura ed attivazione di Cellule Endoteliali

Human Umbelical Vein Endothelial Cells (HUVECs) sono state scelte come linea cellulare per il presente studio.
E' stata condotta una campagna sperimentale preliminare con lo scopo di caratterizzare il potenziale infiammatorio delle HUVECs indotto da stimo-

lazione chimica. L'espressione da parte delle HUVECs di marcatori solubili di attivazione (ICAM-1, VCAM-1, E-selettina) è stata misurata tramite kit ELISA in seguito a incubazione con TNF-α. Sono state considerate due variabili: i) concentrazione di TNF-α e ii) tempo di esposizione al TNF-α. Tale caratterizzazione è stata ripetuta considerando soltanto 24 h di esposizione al TNF-α. Sia l'ELISA che la citometria a flusso sono stati eseguiti per valutare l'espressione dei marcatori solubili e di superficie ICAM-1, VCAM-1 ed E-Selettina. Sulla base dei risultati di tale campagna sperimentale, due protocolli di infiammazione sono stati definiti: i) TNF-α 10 ng/ml per 24h and ii) TNF-α 100 ng/ml per 24h.

Interazione Piastrine-Cellule Endoteliali

Per valutare la mutua interazione tra piastrine sottoposte a sforzo di taglio e CE infiammate, sono state considerate quattro condizioni, come riassunto in tabella 2, con lo scopo di scomporre tale complesso fenomeno e di analizzare separatamente il contributo di attivazione piastrinica e infiammazione endoteliale.

		Cellule Endoteliali	
		Non attivate	Attivate con TNFα
Piastrine	Non stimolate	Esperimento 1	Esperimento 3
	Stimolate con HSD	Esperimento 2	Esperimento 4

Tabella 2: Riassunto dei quattro esperimenti condotti

Due tecniche di caratterizzazione sono state utilizate per investigare variabilità nel livello di attivazione dei due tipi cellulari: i) PAS assay su campioni piastrinici ii) citometria a flusso, per determinare l'espressione dei marcatori di superficie delle HUVECs (i.e. ICAM-1, VCAM-1, E-Selettina e $\alpha_V\beta_3$) e delle piastrine (i.e. P-Selettina e Annessina V). Il meccanismo di adesione, invece, è stato caratterizzato tramite: i) acquisizione di immagini SEM e ii) citometria a flusso per quantificare l'espressione dell'integrina endoteliale $\alpha_V\beta_3$.

Studio di fluidodinamica computazionale

Con l'obiettivo di caratterizzare l'emodinamica del VS in presenza di LVAD, sono stati sviluppati modelli CFD *paziente-specifici* i.e. VS ricostruiti da immagini 3D-TT-ECHO (3D-TransThoracic-Echocardiography) (figura 11).

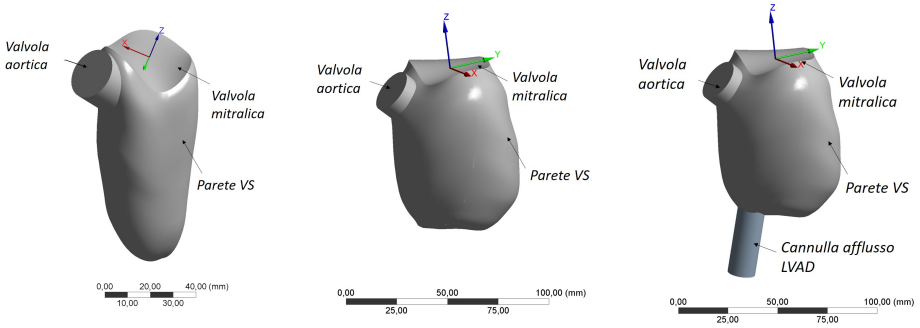

Figura 11: Modelli *paziente-specifico*: (a) VS sano e (b) IC-VS pre impianto LVAD (c) IC-VS post impianto LVAD

Sono state simulate diverse condizioni: i) VS sano (figura 11a); ii) IC-VS pre impianto LVAD, i.e. VS dilatato con contrattilità residua ridotta o trascurabile; iii) IC-VS post impianto LVAD, i.e. VS dilatato con contrattilità trascurabile in presenza della cannula di afflusso del LVAD (figura 11c).

La dinamica del ciclo cardiaco è stata simulata assegnando un opportuno spostamento ad ogni nodo della griglia del VS, implementando User Defined Functions (UDFs) di movimento della mesh. Il movimento risultante è i) contrazione e twist durante la sistole e ii) dilatazione e untwist durante la diastole. Inoltre, è stata simulata una diversa contrattilità del ventricolo sano rispetto a quelli dilatati.

Per ottenere l'andamento dei WSS a cui le CE sono soggette nella regione apicale del VS, sono stati estratti i valori di WSS per ogni elemento della superficie evidenziata in verde in figura 12.

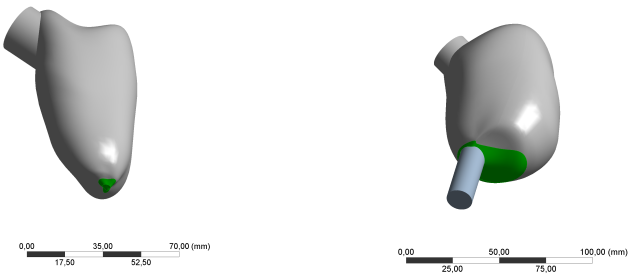

Figura 12: Regione apicale (in verde) dove i valori di zWSS vengono valutati per i modelli *paziente-specifici* (a) sano e (b) IC post impianto LVAD

Risultati

Interazione Piastrine-Cellule Endoteliali

L'interazione tra piastrine e CE in coltura è stata valutata in termine di adesione piastrinica alla superficie cellulare, la quale è stata caratterizzata attraverso l'acquisizione di immagini al SEM e l'analisi citofluorimetrica per l'espressione dell'integrina endoteliale $\alpha_v\beta_3$.
La figura 13 mostra le immagini SEM ottenute per le 4 diverse condizioni sperimentali, riportate in tabella 2.

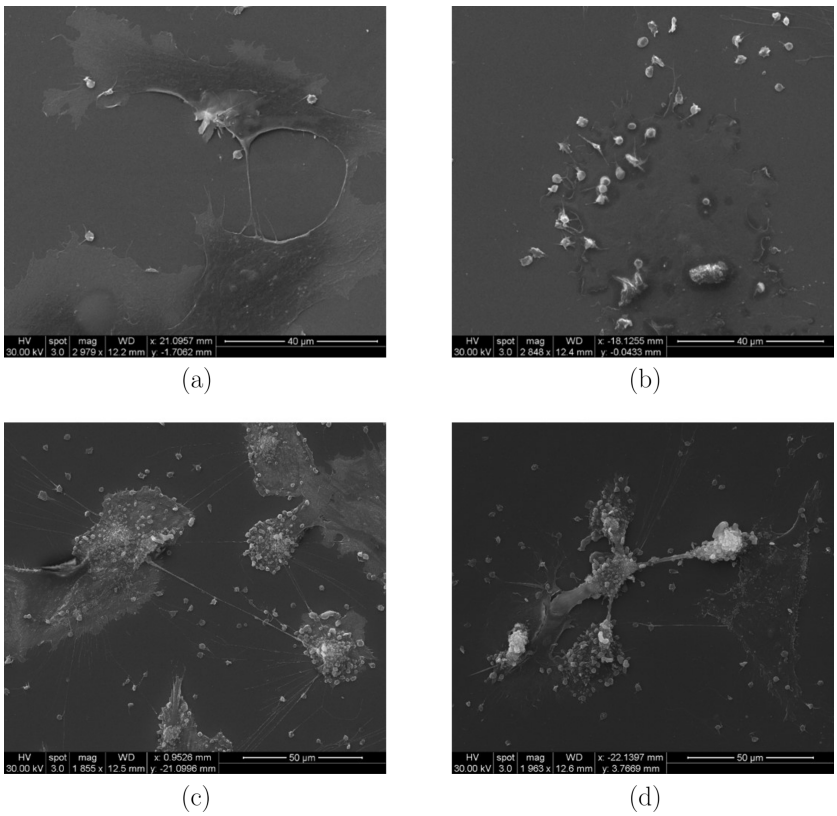

Figura 13: Immagini SEM che mostrano l'adesione piastrinica alle HUVEC, ottenute incubando: (a) piastrine non attivate con CE non attivate; (b) piastrine attivate tramite shear con CE non attivate; (c) piastrine non attivate con CE stimolate con TNFα e (d) piastrine attivate tramite shear con CE stimolate con TNFα

E' possibile notare che le piastrine non attivate si legano minimamente alle HUVEC non stimolate (figura 13a), mentre le piastrine attivate tramite shear aderiscono alle CE non attivate (figura 13b). Inoltre, le HUVEC chimicamente infiammate sono risultate completamente adesive per le piastrine,

sia attivate che non (figure 13c e 13d).
Il legame tra piastrine soggette a shear e HUVEC è stato confermato dalla citometria a flusso per il marcatore endoteliale $\alpha_v\beta_3$. Gli istogrammi ottenuti sono mostrati in figura 14

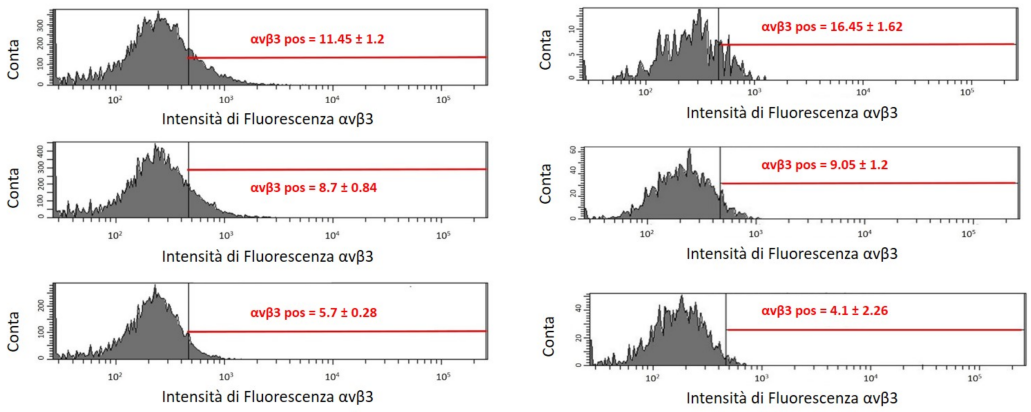

Figura 14: Espressione di $\alpha_V\beta_3$ ottenuta tramite citometria a flusso per CE (a) attivate con 10 ng/ml di TNF-α e (b) non attivate, dopo 1 ora di incubazione con piastrine attivate tramite shear pari a 50 dyne/cm^2 (centro) e 70 dyne/cm^2 (in basso) e in assenza di incubazione con le piastrine (in alto)

L'espressione di $\alpha_V\beta_3$ è risultata ridotta in seguito all'incubazione con piastrine attivate tramite shear, dimostrando che l'integrina è coinvolta nell'adesione piastrinica all'endotelio. La diminuzione dell'espressione è più evidente quando le HUVEC sono infiammate, confermando che l'infiammazione endoteliale accentua l'adesione piastrinica.

Studio di fluidodinamica computazionale

Il movimento ottenuto grazie alle UDF implementate è mostrato in figura 15.

In figura 16 è mostrato l'andamento temporale della componente assiale di WSS estratta dalle simulazioni. Entrambi i modelli pre/post impianto di LVAD mostrano valori di WSS estremamente bassi (valori di picco un ordine di grandezza inferiori rispetto a quelli ottenuti per il modello sano), evidenziando la presenza di una regione di ristagno all'interfaccia VS-cannula di afflusso del LVAD.

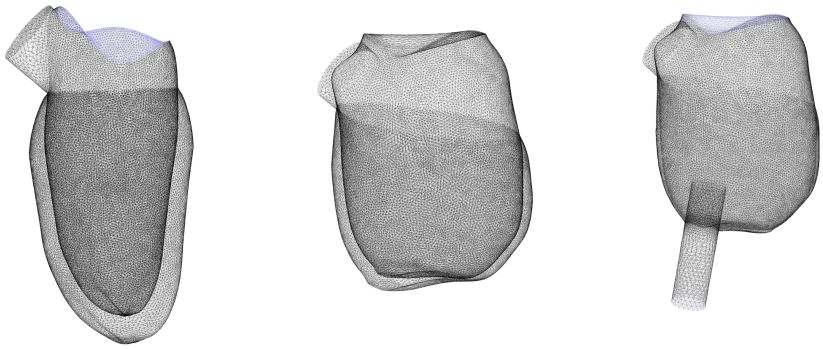

(a) (b) (c)

Figura 15: Sovrapposizione delle configurazione fine-sistole e fine-diastole per i modelli *paziente-specifici*: (a) VS sano, (b) IC-VS con contrattilità ridotta pre impianto LVAD e (c) IC VS con contrattilità trascurabile post impianto LVAD

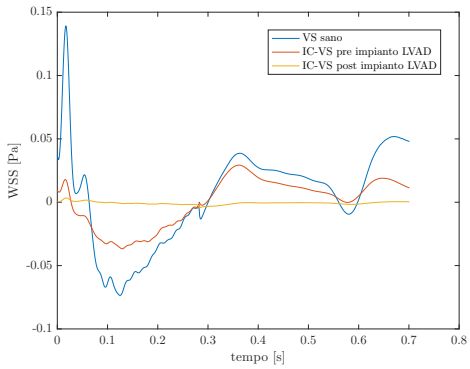

Figura 16: Andamenti di zWSS ottenuti per i tre modelli *paziente-specifici*

Discussione e conclusioni

L'impianto del LVAD è ormai una strategia terapeutica per i pazienti affetti da IC. Nonostante ciò, i LVAD possono provocare attivazione del sistema della coagulazione portando a formazione di trombo, in particolare all'interfaccia tra l'apice del VS e la cannula di afflusso del LVAD.
Finora, la formazione di trombi in pazienti con LVAD impiantato è stata studiata principalmente in relazione all'attivazione piastrinica mediata dallo shear. Un altro aspetto importante relativo alla formazione di trombi è l'infiammazione endoteliale, la quale può degenerare in danno endoteliale, aggravando la trombosi. Tuttavia, pochi studi in letteratura si sono focalizzati

sulla disfunzionalità dell'endocardio in soggetti portatori di LVAD. Inoltre, le interazioni tra piastrine attivate circolanti e le CE infiammate non sono state analizzate in modo approfondito.
Nel presente progetto di tesi, l'interazione tra piastrine soggette a shear e CE infiammate è stata caratterizzata grazie allo sviluppo di un set-up sperimentale in grado di investigare il meccanismo di adesione piastrinica all'endotelio, processo che in vivo porta alla trombosi.
E' stato dimostrato che la stimolazione di CE in coltura induce l'adesione delle piastrine alla superficie cellulare. Inoltre, la diminuzione dell'espressione dell'integrina endoteliale $\alpha_v\beta_3$ in seguito all'incubazione con le piastrine, ha confermato la presenza di adesione delle piastrine. E' risultato che le piastrine attivate tramite shear si legano anche alle CE non stimolate. Tuttavia, l'adesione è nettamente inferiore a quella indotta dall'endotelio infiammato.
In conclusione, il presente studio ha consentito di caratterizzare sperimentalmente il ruolo dell'interazione piastrine-endotelio nella formazione di trombo nei pazienti con impianto di LVAD.

Il modello sperimentale presenta, tuttavia, diverse limitazioni.
Innanzitutto, con la piattaforma sviluppata è possibile valutare esclusivamente l'adesione piastrinica alle CE, la quale rappresenta solo uno dei meccanismi che caratterizzano il fenomeno complesso della trombosi. Questo limite, però, può essere visto allo stesso tempo anche come un vantaggio, in quanto consente di focalizzarsi su un singolo meccanismo alla volta.
In aggiunta, l'attivazione piastrinica è stata indotta tramite HSD con un livello di shear costante nel tempo per 10 minuti. Sottoporre le piastrine a shear che replicano pattern LVAD-specifici estratti da simulazioni numeriche porterebbe a un miglioramento della piattaforma sperimentale.
Inoltre, è stato trascurato il contributo dell'interazione tra sangue e materiale artificiale alla trombosi.
Infine, un importante sviluppo futuro del seguente progetto di tesi è rappresentato dalla possibilità di integrare il set-up sperimentale con un modulo di perfusione in grado di replicare sforzi di taglio estratti da simulazioni numeriche caratteristici del VS con LVAD, per stimolare meccanicamente le CE in coltura.

Bibliografia

[1] Longjian Liu and Howard J Eisen, *Epidemiology of heart failure and scope of the problem.* Cardiology clinics, 32(1):1-8,2014.

[2] Joseph AR Englert III Jennifer A Davis and Selim R Krim, *Mechanical Circulatory Support for the Failing Heart: Continuous-Flow Left Ventricular Assist Devices*. The Ochsner Journal, 16(3):263-269, 2016.

[3] `http://rebelem.com/left-ventricular-assist-device/`

[4] Arman Kilic, Michael A Acker, and Pavan Atluri, *Dealing with surgical left ventricular assist device complications*. Journal of thoracic disease, 7(12):2158, 2015.

[5] Wei-Che Chiu, Gaurav Girdhar, Michalis Xenos, Yared Alemu, Jõao S Soares, Shmuel Einav, Marvin Slepian, and Danny Bluestein, *Thromboresistance comparison of the HeartMate II ventricular assist device with the device thrombogenicity emulation-optimized HeartAssist 5 VAD*. Journal of biomechanical engineering, 136(2):021014, 2014.

[6] Katharine H Fraser, Tao Zhang, M Ertan Taskin, Bartley P Griffith, and Zhongjun J Wu, *Computational fluid dynamics analysis of thrombosis potential in left ventricular assist device drainage cannulae*. ASAIO journal (American Society for Artificial Internal Organs: 1992), 56(3):157, 2010.

[7] Chitaru Kurihara, Minoru Ono, Takashi Nishimura, Aya Saito, Tsuyoshi Taketani, Motoyuki Hisagi, Kan Nawata, Osamu Kinoshita, Tetsurou Morota, Noboru Motomura, et al. *Use of DuraHeart® support for more than 1 year as the first successful bridge to heart transplantation in Japan*. Journal of Artificial Organs, 14(1):67-69, 2011.

[8] Jawaad Sheriff, Danny Bluestein, Gaurav Girdhar, and Jolyon Jesty, *High-shear stress sensitizes platelets to subsequent low-shear conditions*. Annals of biomedical engineering, 38(4):1442-1450, 2010.

[9] Jun Zhang, Albert F DeFelice, Joseph P Hanig, and Thomas Colatsky, *Biomarkers of endothelial cell activation serve as potential surrogate markers for drug-induced vascular injury*. Toxicologic pathology, 38(6):856-871, 2010.

[10] Dorothea I Siegel-Axel, and Meinrad Gawaz, *Platelets and endothelial cells*. Seminars in thrombosis and hemostasis, volume 33, pages 128-135. Copyright© 2007 by Thieme Medical Publishers, Inc., 333 Seventh Avenue, New York, NY 10001, USA, 2007.

[11] ChiWei Ong, Socrates Dokos, BeeTing Chan, Einly Lim, Amr Al Abed, NoorAzuanBinAbu Osman, Suhaini Kadiman, Nigel H Lovell, *Numerical investigation of the effect of cannula placement on thrombosis.* Theoretical Biology and Medical Modelling, 10(1):1, 2013.

[12] Guang-Mao Liu, Hai-Bo Chen, Fu-Liang Luo, Yan Zhang, Han-Song Sun, Jian-Ye Zhou, Sheng-Shou Hu, *Numerical simulation of LVAD inflow cannulas with different tip.* International Journal of Chemical Engineering, 2012, 2012.

[13] Anthony R Prisco, Alberto Aliseda, Jennifer A Beckman, Nahush A Mokadam, Claudius Mahr, and Guilherme JM Garcia, *Impact of LVAD Implantation Site on Ventricular Blood Stagnation.* ASAIO Journal, 2017.

[14] Sam Liao, Benjamin Simpson, Michael Neidlin, Tim AS Kaufmann, Zhiyong Li, Maria A Woodruff, and Shaun D Gregory, *Numerical prediction of thrombus risk in an anatomically dilated left ventricle: the effect of inflow cannula designs.* BioMedical Engineering OnLine, 15(2):587, 2016.

[15] Danny Bluestein, KB Chandran, and KB Manning, *Towards non-thrombogenic performance of blood recirculating devices.* Annals of biomedical engineering, 38(3):1236-1256, 2010.

[16] Lorenzo Valerio, Filippo Consolo, Danny Bluestein, Phat Tran, Marvin Slepian, Alberto Redaelli, and Federico Pappalardo, *Shear-mediated platelet activation in patients implanted with continuous flow LVADs: A preliminary study utilizing the platelet activity state (PAS) assay.* In Engineering in Medicine and Biology Society (EMBC), 2015 37th Annual International Conference of the IEEE, pages 1255-1258. IEEE, 2015.

[17] Matteo Nobili, Jawaad Sheriff, Umberto Morbiducci, Alberto Redaelli, and Danny Bluestein, *Platelet activation due to hemodynamic shear stresses: damage accumulation model and comparison to in vitro measurements.* ASAIO journal (American Society for Artificial Internal Organs: 1992), 54(1):64, 2008.

[18] Qijin Lu, Bryan V Hofferbert, Grace Koo, and Richard A Malinauskas, *In Vitro Shear Stress-Induced Platelet Activation: Sensitivity of Human and Bovine Blood.* Artificial organs, 37(10):894-903, 2013.

[19] M Griesshammer, H Beneke, B Nussbaumer, M Grünewald, M Bangerter, and L Bergmann, *Increased platelet surface expression of P-selectina*

and thrombospondin as markers of platelet activation in essential thrombocythaemia. Thrombosis research, 96(3):191-196, 1999.

[20] Eleni Tzima, Patrick J Trotter, Margaret A Orchard, and John H Walker, *Annexin V relocates to the platelet cytoskeleton upon activation and binds to a specific isoform of actin.* European Journal of Biochemistry, 267(15):4720-4730, 2000.

[21] Jeanne Dachary-Prigent, Jean-Marie Freyssinet, Jean-Max Pasquet, Jean-Claude Carron, and Alan T Nurden, *Annexin V as a probe of aminophospholipid exposure and platelet membrane vesiculation: a flow cytometry study showing a role for free sulfhydryl groups.* Blood, 81(10):2554-2565, 1993.

[22] Ryan B Huang, and Omolola Eniola-Adefeso, *Shear stress modulation of IL-1β-induced E-selectin expression in human endothelial cells.* PloS one, 7(2):e31874, 2012.

[23] MWJ Boehme, U Raeth, WA Scherbaum, PR Galle, and W Stremmel, *Interaction of endothelial cells and neutrophils in vitro: kinetics of thrombomodulin, intercellular adhesion molecule-1 (ICAM-1), E-selectin, and vascular cell adhesion molecule-1 (VCAM-1): implications for the relevance as serological disease activity markers in vasculitides.* Clinical & Experimental Immunology, 119(1):250-254, 2000.

[24] Fabienne Mackay, Hansruedi Loetscher, Dietrich Stueber, Gisela Gehr, and Werner Lesslauer, *Tumor necrosis factor alpha (TNF-alpha)-induced cell adhesion to human endothelial cells is under dominant control of one TNF receptor type, TNF-R55.* The Journal of experimental medicine, 177(5):1277-1286, 1993.

[25] David C Chappell, Signe E Varner, Robert M Nerem, Russell M Medford, R Wayne Alexander, *Oscillatory shear stress stimulates adhesion molecule expression in cultured human endothelium.* Circulation research, 82(5):532-539, 1998.

[26] Wei Yin, Saravan Kumar Shanmugavelayudam, and David A Rubenstein, *The effect of physiologically relevant dynamic shear stress on platelet and endothelial cell activation.* Thrombosis research, 127(3):235-241, 2011.

[27] Robert L Czervionke, John C Hoak, and Glenna L Fry, *Effect of aspirin on thrombin-induced adherence of platelets to cultured cells from the blood vessel wall.* Journal of Clinical Investigation, 62(4):847, 1978.

[28] Thomas Bombeli, Barbara R Schwartz, and John M Harlan, *Adhesion of activated platelets to endothelial cells: evidence for a GPIIbIIIa-dependent bridging mechanism and novel roles for endothelial intercellular adhesion molecule 1 (ICAM-1), $\alpha v\beta 3$ integrin, and GPIbα*. The Journal of experimental medicine, 187(3):329-339, 1998.

[29] Wei Yin, Farzana Rouf, Saravan K Shanmugavelayudam, and David A Rubenstein, *Endothelial cells modulate platelet response to dynamic shear stress*. Cardiovascular Engineering and Technology, 5(2):145-153, 2014.

[30] CW Ong, BT Chan, E Lim, NA Abu Osman, AA Abed, S Dokos, and NH Lovell, *Fluid structure interaction simulation of left ventricular flow dynamics under left ventricular assist device support*. In 2012 Annual International Conference of the IEEE Engineering in Medicine and Biology Society, pages 6293-6296. IEEE, 2012.

Chapter 1

Introduction

1.1 Background

Heart Failure (HF) is a chronic disease, generally characterized by a progressive deterioration occurring over a period of years or even decades. This condition can affect one side of the heart only, but in the majority of the cases it involves both sides. Affected by this progressive pathology, the heart muscle is unable to pump enough blood to meet the body's needs. It can be either that the heart can not fill with enough blood and that it does not have the adequate force to pump blood to the rest of the body, or both of them. The leading causes of HF are diseases such as coronary heart disease, high blood pressure and diabetes [1].
HF is having a growing diffusion in the world and can be considered one of the most serious public health burden of the 21^{st} century. It affects nearly 5.8 million people in the United States and over 23 million worldwide [2]. This pathology is accompanied by increasing clinical costs and a need for devices able to restore the correct function of the heart. So far, heart transplant represents the most prominent solution for the treatment of advanced HF. However, the paucity of heart donors compared to the large need of heart replacement, long wait times and long-term complications of immunosuppressive therapy have brought to the development of blood recirculating devices. These devices include Mechanical Circulatory Support (MCS) implants, such as left ventricular assist devices (LVADs).
Nowadays, the implantation of LVADs represents an important technological solution for the treatment of HF, requiring a challenging integration of technical, clinical and biological expertise. In particular, continuous-flow LVADs have become standard therapy for the management of HF both for patients who will eventually receive a transplant (bridge to transplantation) and as an option for those who may not qualify for transplant but qualify for long-

term MCS (destination therapy) [3]. The LVAD is intended to partially or totally replace the function of the diseased left ventricle (LV). The first generation devices tried to replicate the pulsatile flow of the heart. Since they showed several limitations (i.e. large dimension, noise, short durability), in the last years these devices moved from pulsatile to continuous-flow technology, which allows to overcome the previous problems.
The current generation of LVADs (e.g. HeartMate II or III, HeartWare VAD) have five main components:

- the inflow cannula;
- the pump body (axial or centrifugal);
- the outflow cannula;
- the percutaneous drive-line;
- the electrical controller.

As shown in figure 1.1, the inflow cannula is inserted into the apex of the LV and the outflow is anastomosed to the ascending aorta. In this way, the pump is able to draw blood from the LV and move it into the aorta. Once the blood reaches the aorta, it can flow toward the rest of the body. The drive-line is connected to the pump, exits the body through a small incision in the skin and connects to the controller.

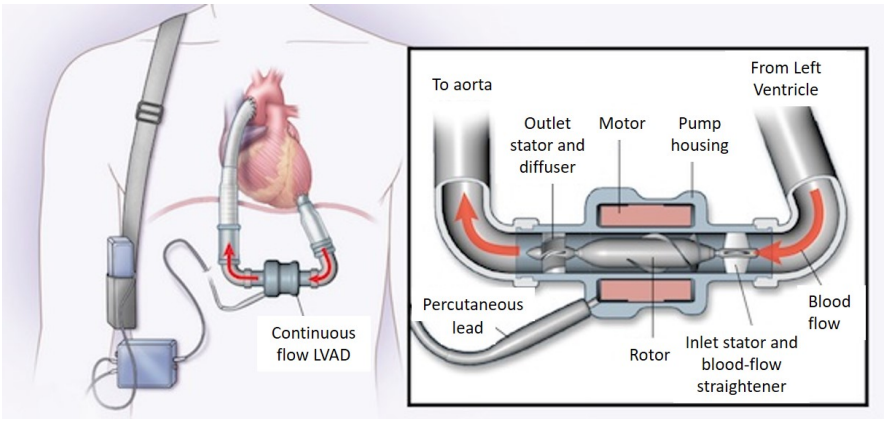

Figure 1.1: LVAD components [4]

A recent analysis of the Interagency Registry for Mechanically Assisted Circulatory Support (INTERMACS) demonstrated that destination therapy LVAD patients had comparable 2-year survival rates as heart transplant recipients [5]. However, although outcomes continue to improve thanks to

enormous investment of both human and financial resources, these devices are affected by post-implant complications, such as thromboembolic events or pump thrombosis leading to complete device obstruction/malfunction [6]. Due to these complications, LVAD recipients undergo anti-coagulation treatments, which lead to secondary complications, such as thrombocytopenia or bleeding events.
Starling et al. [7] outlined a rising rate of thrombosis with the HeartMate II and a significant increase of device-related failure of the implant. In particular, confirmed pump thrombosis occurs early and peaks 1 month after implantation, with a reduction in risk by 6 months, as shown in figure 1.2a. Moreover, patients with pump thrombosis have increased morbidity and substantially increased mortality unless the pump is replaced or cardiac transplantation is performed, as outlined in figure 1.2b.

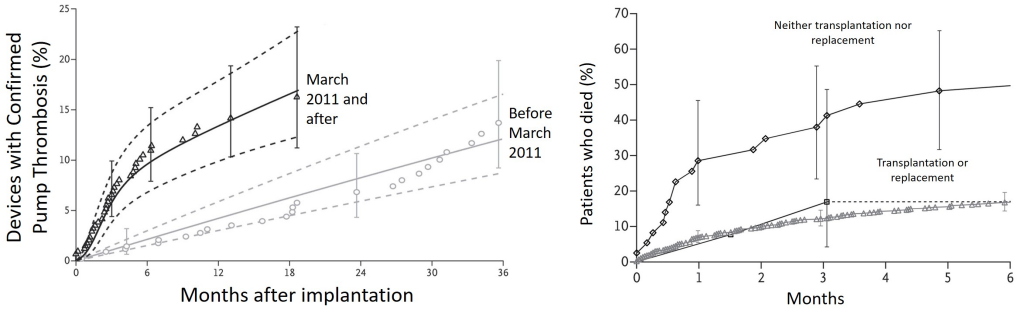

(a) (b)

Figure 1.2: (a) Occurrence and incidence of confirmed pump thrombosis stratified according to implantation date, adapted from [7]; (b) mortality according to management strategy after confirmed pump thrombosis adapted from [7]

The MOMENTUM 3 [8], ENDURANCE [9] and ADVANCE [10] clinical trials compared the thrombotic rate of the new bearingless magnetically levitated centrifugal continuous-flow pump (HeartMate III, St Jude Medical, Minneapolis, MN, USA), the small intrapericardial centrifugal-flow device (HeartWare HVAD, HeartWare Inc., Miami, FL, USA) and the axial-flow LVAD technology (HeartMate II, Thoratec Corp., Pleasanton, CA, USA). Only the HeartMate III was reported to not induce pump thrombosis (0% vs. 10.1% for the HeartMate II). In addition, the HeartMate III was associated with a higher rate of survival and a more evident improvement in clinical outcomes, with respect to the HeartMate II. On the other hand, it was not free from thrombembolic complications and stroke with a rate of events not different from that of the HeartMate II (7.9% vs. 10.9%). Regarding the

HeartWare HVAD3, it was reported that pump thrombosis occurs at a rate of 0.08 events per patient-year in patients receiving this device, and no significant difference in the rate of device thrombosis was found between the HVAD and the HeartMate 22. Furthermore, the HVAD was associated with significantly higher rates of ischemic and hemorrhagic stroke than the HeartMate II (29.7% vs. 12.1%).

The two main reasons that can lead to thrombus formation in LVAD recipients are:

- the contact of blood with a foreign surface (the pump is in direct contact with the blood circulation);
- the altered rheologic conditions, including i) the hyper-shear within the artificial pump and ii) blood stasis, characterized by the presence of stagnant, slow or recirculating flows, mostly at the LV apex-LVAD inflow cannula interface [11] [12].

In the present study, only the second point (i.e. altered rheology) was be investigated.
Concerning the hyper-shear condition, in continuous flow LVADs, the blood is constantly propelled out from the apex of the LV by a turbine, and returned to the ascending aorta. In order to generate physiological cardiac outputs, VADs operate at very high impeller speeds (2500-3000 rpm for the HeartWare VAD, $>$ 4500 rpm for HeartMate III), which generate non-physiological high shear stress levels in specific locations, like the impeller-shroud gaps and regions of elevated residence time such as in the rear (inlet) and front (outlet) hubs. These high shear stress accumulation regions may irreversibly damage blood cells flowing through the device. In particular, with recirculation, repeated platelet injury can lead to platelet activation. Activated platelets are prone to aggregation and thrombus formation [6].
Regarding the presence of slow or stagnant flows, it is known that recirculation areas may trap platelets, increasing their exposure time to the artificial surface while also increasing the local concentrations of agonist released from previously adhering platelets.
In addition, endothelial injury due to altered shear stress might enhance thrombus formation. It is widely established that significant endothelial dysfunction occurs in patients with end stage HF requiring LVAD placement, as well as in LVAD recipients [13]. The ventricular endothelium is in fact subjected to pro-thrombotic flow conditions (i.e. presence of stagnation regions and recirculating flows), due to:

- dilated heart and reduced contractility;

- cannula placement, which alters the LV hemodynamics.

J. Ranjit et al. [13] performed a study of endothelial and coagulation systems in LVAD recipients and demonstrated a significant activation of both the endothelial and coagulation systems, with a persistent activation of the endothelium up to post-operative day 180. The study proved that the vast endothelial surface can provide an important pathophysiologic trigger for the coagulation abnormalities, suggesting activation of the extrinsic (tissue factor) coagulation pathway .

In order to improve outcomes of LVAD therapy, a detailed understanding of the impact of the device on the biological environment in which the device is meant to operate is crucial. A combination of technical and biological efforts is fundamental to promote the development of less thrombogenic devices, capable of restoring the normal blood flow in the body limiting detrimental impact on biological structures. Within the design constraints of blood recirculating devices and their functionality, thrombogenicity minimization is probably the most important design goal.

1.2 Thrombus formation

In thrombosis, a pathological clot, due to abnormal coagulation reactions, uncontrollably grows and occludes the lumen of a blood vessel, obstructing the flow of blood. In 1856, Rudolf Virchow postulated that the three main factors that influence thrombus formation, as shown in figure 1.3, are [14]:

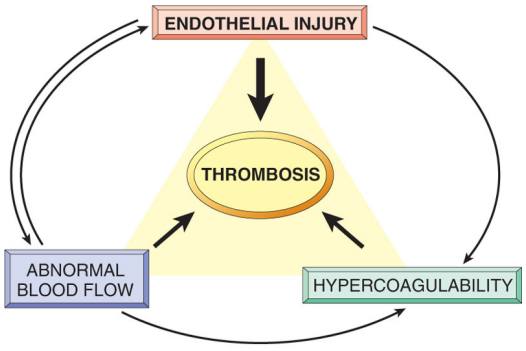

Figure 1.3: The three main causes of thrombosis are given in Virchow's triad [14]

- Endothelial injury: it is the main cause of thrombus formation in the heart and the arterial circulation [15]. The main causes of endothe-

lial injury are changes in shear stress associated with hypertension, disturbed flow conditions or traumatic vascular injury.

- Hypercoagulability of the blood: it is generally less important than endothelial injury in predisposing to thrombosis. It refers to an abnormally heightened coagulation response to vascular injury resulting from either primary (genetic) or secondary (acquired) disorders.

- Abnormalities in blood flow: it refers to non-physiological fluid dynamic conditions (i.e. non-physiological shear stresses) in the vessels, such as areas of turbulent flow or local pockets where stasis of fluid occurs. Abnormal blood flow may promote both platelet and endothelial cell (EC) activation.

In the present study three aspects of thrombus formation in VAD recipients are taken into account:

- shear-mediated platelet activation within the pump;

- EC inflammation leading to increased expression of inflammatory cytokines and adhesion molecules, generating a shift of ECs towards a prothrombotic phenotype;

- mutual interaction between platelets and ECs as a further contributory effect to thrombosis.

1.2.1 Platelet activation

Resting platelets are discoid anuclear cells and have a smooth, rippled surface, with an average diameter of 2-4 μm. Normal platelet count is in the range 150 x10^3 - 350 x10^3 pl/μll and they have a life span of approximately 8-10 days. Platelets are derived from the fragmentation of megakaryocytes' cytoplasm. They lack genomic DNA, but contain megakaryocyte-derived messenger RNA and the translational machinery needed for protein synthesis. The outermost layer of the platelet is a surface coat made up of glycoproteins (GP). This layer plays a very important role in platelet function, including adhesion and aggregation, and thus, contributes to hemostasis and pathobiologic thrombosis. There are several receptors on this layer, including the selectins (P-selectin), the integrins (GP I, GP II), the immunoglobulins and other receptors such as those for collagen or thrombin. All these elements assist platelets during the adhesion or aggregation process. In fact, GPIIb-IIIa contributes towards adhesion to fibrin and the binding of fibrinogen that facilitate platelet-platelet interaction, while GPIb is important in

the attachment of platelets to von Willebrand Factor (vWF) and the vascular sub-endothelium. Furthermore, GPIa-IIa has a role in the adhesion to collagen. Platelets intracellular organelles in the cytoplasm include α granules, mitochondria, a tubular system, lysosomes. α granules store a variety of proteins such as β thromboglobulin, fibrinogen, vWF, fibronectin and other clotting factors [16].
Platelets are the primary cellular clotting elements in blood. They are essential for hemostasis and repair of the injured vascular endothelium, but pathological activation of platelets can induce occlusive thrombosis. The contribution of platelets to both physiologic hemostasis and pathological thrombosis rests with their ability to adhere, activate and aggregate. Activation follows adherence and is designated to recruit additional platelets to the site of injury.
As previously described, platelet activation is one of the major driver of post-implantation thrombotic complications affecting LVADs. In fact, in the case of contact with artificial surfaces, as within LVADs, platelets adhesion and activation are emphasized. When a LVAD is implanted, the first hemostatic reaction in case of vascular endothelial damage is vasoconstriction. Thereafter, due to the disruption of the vascular endothelial layer, tissue factors are exposed, initiating the coagulation cascade. In presence of artificial surfaces, platelets form a thin monolayer over the material which serves as a base for thrombin generation and platelet aggregation. Adhered platelets undergo shape change and form podocytes. Platelets aggregates attract more activated platelets, speeding up the coagulation cascade. This leads to thrombus formation by increasing Factor Xa activation and converting prothrombin into thrombin. The final step in the thrombus formation is represented by the thrombin-mediated conversion of fibrinogen in fibrin.

Within MCS devices, the most relevant mechanical agonist to platelet-mediated thrombosis is represented by fluid mechanical shear stress. Physical agonists, like flow induced forces, trigger platelet activation, just as chemical agonists. Normal vascular flow is characterized by low wall and fluid shear stresses, ranging from 1 to 10 dyne/cm^2 in venous flow, to 50 dyne/cm^2 in arterial flow, peaking at approximately 60 dyne/cm^2 in the arterioles. Both higher shear stress magnitude and elongated shear exposure time may lead to detectable level of platelet activation [17].
Numerical simulations of the MicroMed HeartAssist 5 showed that passage through the VAD exposes platelets to peak shear stresses of 1000-2000 dyne/cm^2 [6]. Thamsen et al. [18] compared the HVAD and HeartMate II pumps in terms of volumetric distribution of shear stresses and residence times, with regard to specified threshold for vWF damage (90 dyne/cm^2),

platelet activation (500 dyne/cm^2) and hemolysis (1500 dyne/cm^2). The results are shown in figure 1.4. Regarding shear stresses above 500 dyne/cm^2 and 1500 dyne/cm^2, the volumetric differences between the two pumps are marginal, while the overall residence times are longer in the HVAD for all thresholds, suggesting higher tendencies to platelet activation and hemolysis.

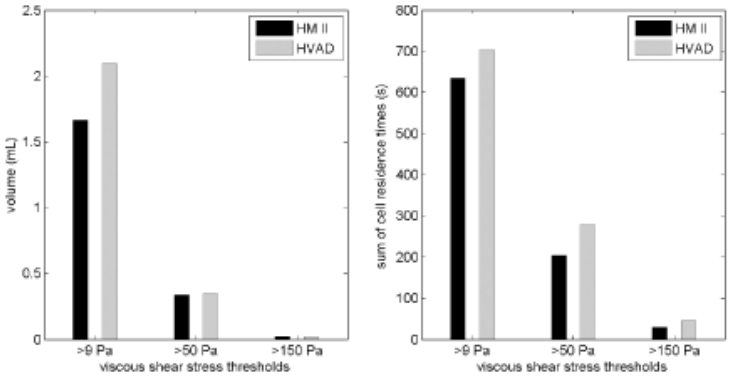

Figure 1.4: Volume fractions (left) subjected to specified shear stress thresholds and corresponding sums of cell residence times (right) [18]

Fraser and co-workers [19] analysed through a CFD study the hemodynamics in five different VADs in terms of shear stress, residence time and hemolysis. Depending upon the VAD, operating condition and location, the scalar shear stresses ranged from 0 to 3060 Pa. The shear stress in the three axial-flow pumps spanned a wider range than in the two centrifugal VADs, resulting in higher mean and maximum shear stresses and larger percentage volumes experiencing high shear stresses. All five VADs had regions of shear stresses > 150 Pa at all the operating conditions investigated.

1.2.2 Endothelial cell activation

As previously described, it is widely established that significant activation of the endothelial system occurs in LVAD recipients [13]. EC activation is distinct from endothelial injury; however, the two phenomena may be associated with the development of thrombosis [20].
EC activation represents a reversible alteration resulting in morphological rearrangements, but without loss of endothelial integrity. However, EC activation process can progress and lead to endothelial injury, which is known to be one of the main cause of thrombus formation in the heart and in the arterial circulation [15].
Specifically, EC activation is an immunological and inflammatory response that promotes expression of adhesion molecules, such as the intercellular ad-

hesion molecule-1 (ICAM-1), the vascular adhesion molecule-1 (VCAM-1) and the endothelial selectin (E-selectin), the secretion of pro-inflammatory cytokines, the elaboration of chemokines and the induction of procoagulant molecules. For these reasons, EC activation represents a switch from a quiescent phenotype, characterized by an anti-adhesive, anti-coagulant and anti-inflammatory behaviour toward a pro-adhesive, pro-coagulant and pro-inflammatory one. EC activation is divided into two stages [20]:

- Type I EC activation: it occurs immediately following stimulation and causes releasing of endothelial adhesion and antithrombotic molecules.
- Type II EC activation: it is a delayed response, which is dependent on the synthesis of proteins, such as adhesion molecules, cytokines, chemokines and procoagulant factors.

Both these stages are reversible when endothelial activators are withdrawn. Otherwise, the activation becomes chronic and leads to EC injury with cells detachment, resulting in circulating ECs and release of microparticles, as for LVAD recipients.

1.2.3 Platelets adhesion to endothelial cells

Interactions between platelets and endothelium are involved in many disease processes. In particular, as previously described, both cell types participate in the pathogenesis of thrombosis.
Under physiological conditions, in the human vascular system platelets continuously flow, without adhering or aggregating on ECs. The intact endothelium, in fact, represents a barrier separating platelets from adhesive substrates in the subendothelial matrix. However, after damage to the endothelium cell surface and the resulting dysfunction, complex interactions are induced among circulating platelets and ECs. The two cell types interfere with each other and regulate their activities via direct and indirect interactions. The interaction between platelets and the vessel wall involves cellular receptor on the surface of ECs, such as integrins ($\alpha_v\beta_3$), ICAM-1 and GPIbα, and it is mediated by adhesive proteins, such as vWF, fibronectin and fibrinogen.
Platelet adhesion is a multistep process, in which platelets initially tether to the vessel wall, then roll along it and in the end they firmly adhere. Activated ECs express P-selectin on their surface. Platelet tethering is mediated as a consequence of the interaction between platelet surface receptors P-selectin glycoprotein ligand 1 (PSGL-1) with endothelial P-selectin. Rolling involves also interactions between glycoprotein Ibα of platelets and vWF expressed

by ECs. The subsequent firm adhesion is mediated by integrins.
From a mechanistic standpoint, platelets and ECs communicate on multiple levels. Cross-talk may occur over a distance (paracrine signaling), via transient interactions or through receptor-mediated cell-cell adhesion. Platelets may release or transfer substances that influence EC function and vice versa. ECs express cell surface receptors or soluble mediators that either inhibit platelet function or promote platelet activation [21]. Platelets can affect endothelial function by the release of vasoactive substances from storage granules, that may mediate vasodilation [22].

1.3 Aim of the thesis

The present study arises from an international research project between three institutions, namely i) Università Vita Salute San Raffaele of Milan (project coordinator), ii) the Biomechanics research group of the Department of Electronics, Information and Bioengineering (DEIB) of Politecnico di Milano and iii) Sarver Heart Center of University of Arizona. The experimental activities were conducted at the laboratory facilities of Politecnico di Milano, both of the Department of Chemistry, Materials and Chemical Engineering "G.Natta" and of the Biomechanics Laboratory, and of the University od Arizona.
The study is focused on the development of an experimental set-up with the purpose to emulate the interaction between activated platelets and inflamed ECs, in order to characterize the mechanisms responsible for thrombus formation, which takes place in vivo at the LV-LVAD inflow cannula interface in LVAD recipients. In particular, the adhesion mechanism of platelet on ECs, which is the first step of thrombus formation in vivo, was characterized.
In order to characterize the mutual interaction between the two cell types, platelets were incubated with cultured ECs in different conditions. In particular, the following steps were followed:

- characterization of the interaction between resting platelets and non-activated ECs;
- characterization of the interaction between shear activated platelets and non-activated ECs;
- characterization of the interaction between resting platelets and activated ECs;
- characterization of the interaction between shear activated platelets and activated ECs.

In order to faithfully replicate the pathological environment, platelets were shear-activated through the Hemodynamic Shearing Device (HSD), emulating the passage through the artificial LVAD pump, and cultured ECs where forced to switch toward a pro-thrombotic phenotype, through the exposure to a known chemical activator (Tumor Necrosis Factor-α, TNF-α). Taking advantage of biotechnological techniques and assays (i.e. Enzyme Linked Immunosorbent Assay - ELISA, flow cytometry, Platelet Activity State - PAS assay), we measured the activation level of both platelets and ECs. Scanning Electron Microscope (SEM) imaging technique, coupled with flow cytometry for the endothelial integrin $\alpha_v\beta_3$, was used to characterize the adhesion mechanism of platelets to ECs in the four experimental conditions.
So far, thrombus formation in LVAD recipients was mainly ascribed to hyper-shear platelets activation. With the present study, it is possible to better define the role of ECs in the thrombus formation phenomenon.
In addition, we settled the basis for an improvement of the experimental set up, i.e. the substitution of the chemical activation of ECs with an in-silico-derived patient-specific mechanical stimulation of ECs. For this aim, a computational fluid dynamics (CFD) approach was employed to develop a patient-specific model of the LV chamber, simulating the presence of the LVAD inflow cannula, and to extract the wall shear stress (WSS) trends in the apical portion of the ventricular wall. These time-varying (i.e. along the cardiac cycle) WSS waveforms represent the WSS values which cardiac ECs are subjected to at the LV-LVAD inflow cannula interface.

1.4 Outline

The present thesis is structured as follows:

- Chapter 2 describes the most outstanding results associated with methods developed for the assessment of the thrombogenicity of MCS devices. Moreoever, the state of the art regarding the evaluation of platelet activation, EC activation and the characterization of their mutual interaction is presented .

- The first part of Chapter 3 describes the experimental set up and protocols for the evaluation of the interaction between platelets and ECs. In particular, details about platelets extraction and EC culture are given and the procedures for both platelet and EC activation are described. Moreover, the analysis techniques used for the measurement of the activation level of the two cell types and for the visualization of platelet adhesion to EC surface are illustrated.

The second part of Chapter 3 is focused on the CFD study aimed to model the LV chamber in both healthy and pathological conditions (pre- and post - LVAD implant). Details about the developed tools are given. Finally, the extraction of the WSS trends in the LV apical region is described.

- Chapter 4 describes the results obtained in both the experimental and the in-silico parts of the present study.
- In Chapter 5 a critical discussion of the obtained results and the conclusive remarks are presented, together with limitations of the study and envisioned future developments.

Chapter 2

State of the Art

Minimization of the thrombogenicity of LVADs is currently the most important goal for improving the outcomes of these devices. For this aim, a detailed understanding of the impact of the device on the biological environment is crucial. In the last few years, different approaches and methodologies have been developed to elucidate the mechanism driving the shear-mediated platelet activation and to identify possible design solutions to minimize the device-associated thrombogenicity. These include numerical and experimental tools, often used in combination, to model shear stress waveforms and to predict and characterize platelet response. In the present chapter the most outstanding numerical studies aimed at evaluating the fluid-dynamic conditions of the LV in presence of LVAD and experimental studies aimed at examining the impact of LVAD on platelet and EC activation, are described.

2.1 Numerical characterization of the LV - LVAD hemodynamics

Several studies in literature investigated the disturbed flow dynamics and the thrombogenic potential of the LV in presence of LVAD, through CFD approach which provides detailed ventricular flow characteristics, such as velocity profiles, shear stress distributions and re-circulation. The most crucial element that can alter the physiological hemodynamics of the LV is the inflow cannula, whose geometry, insertion depth, insertion angle and position may alter the intraventricular flow fields.
Ong et al. [23] studied the effect of cannula placement on thrombosis, simulating three different insertion lengths of a trumpet tipped inflow cannula, as shown in figure 2.1. The risk of thrombosis was evaluated by intraventricular vorticity distributions, intensities, stagnation and wall shear stress. It was

found that the cannula inserted one-fourth into the LV achieved the best performances in terms of reducing the risk of thrombus formation, resulting in negligible fluid stagnation and higher vortex intensities.

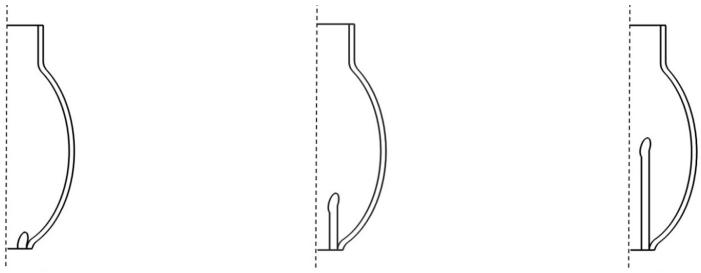

(a) (b) (c)

Figure 2.1: The three different configurations of cannula placement in simulations [23]: (a) near the apex, (b) one fourth of LV and (c) half LV

Liu et al. [24] investigated four different geometries of cannulae: blunt, beveled, trumpet and caged. They concluded that the trumpet-tipped inflow cannula owned the best performance, ensuring smooth flow velocity distribution without backflow, low velocity flow or myocardial obstruction.
These two studies are limited by the lack of anatomically correct LV geometry. Both developed paradigmatic LV models (an ellipsoid [23] and a conical volume [24]). Fraser et al. [11] employed a Magnetic Resonance Imaging (MRI) segmented LV model (set of MR images derived from an healthy patient) to compare the thrombogenic potential of three different cannulae (Medtronic DLP 12, 16 and 24 F). It was found that 12 and 16 F cannulae were superior due to lower fluid stagnation volumes, as shown in figure 2.2.

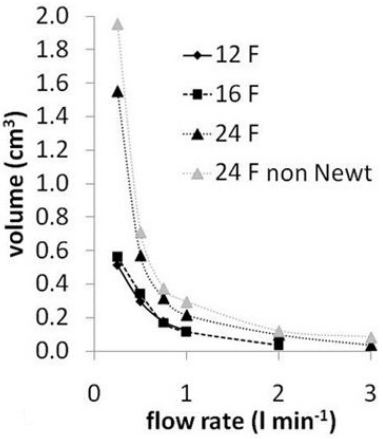

Figure 2.2: Volume of the cannula with velocity magnitude < 1 mm/s [11].

Liao et al. [25] developed a patient-specific LV model to determine the effects of various inflow cannula geometries on the intraventricular flow in terms of thrombus risk (i.e. low velocity magnitude coupled with low strain rate), blood residence time and LV washout. A computed tomography (CT) angiography was performed on a rotary blood pump candidate to reconstruct the ventricular geometry. The heart failure was simulated through a null ventricular contractility. They showed that the inferiorly flared cannula has the potential to reduce incidences of thrombus formation with comparatively lower stagnation regions, while all cannulae resulted in similar LV washout and blood residence time. The highest and most consistent areas of thrombus risk occurred at the interface between the cannula and endocardium. The major limitation of this model was the static ventricular wall, since in most instances some residual contractility of the LV is still present. In addition, this model did not include ventricular valve movements.
Prisco et al. [26] developed a computational model to investigate if the LVAD implantation site affects stagnation of blood within the LV, and therefore, the thrombogenic potential. A 3D model of the LV was reconstructed from clinical imaging of a heart failure patient prior to LVAD implantation and a LVAD inflow cannula was virtually implanted in both apical and diaphragmatic configurations, as shown in figure 2.3. The simulations suggested a higher risk for thromboembolic events with a diaphragmatic implantation due to greater blood stagnation.

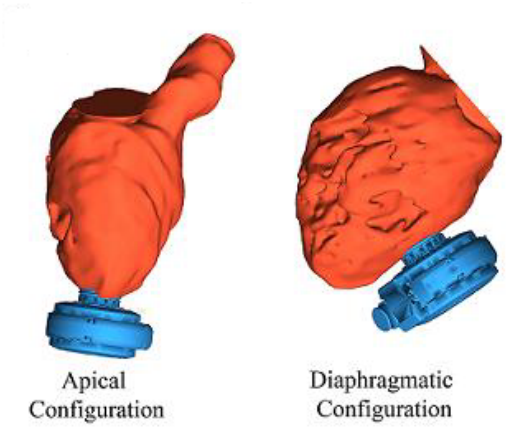

Figure 2.3: Combination of the LVAD geometry with the heart geometry to represent two surgical configurations: apical and diaphragmatic [26].

2.2 Device Thrombogenicity Emulation

The development of tools for predicting thrombus formation in silico was certainly helped by the advances in computing power, mathematical modeling and diagnostic imaging techniques. Nevertheless, those CFD research efforts have no direct correlation to platelet activation markers. To bridge this gap, the device hemodynamics was integrated with the corresponding thrombogenic markers thanks to the introduction of a thrombogenicity predictive technology (Device Thrombogenicity Emulation, DTE) [27].
Figure 2.4 illustrates the DTE optimization iterative process.

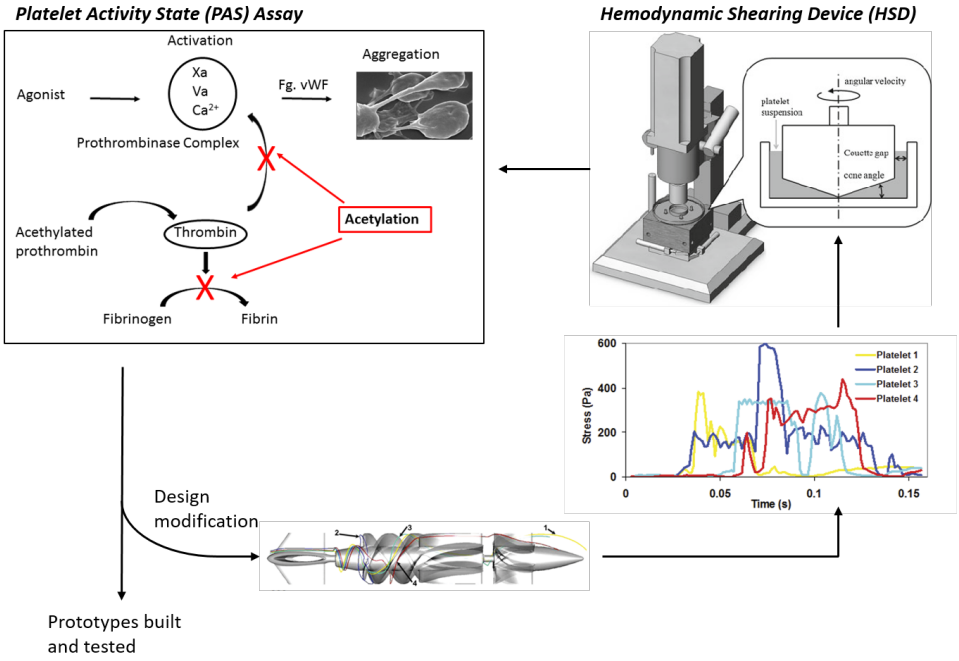

Figure 2.4: Schematic of the DTE. (bottom center) Representative platelets trajectories in the flow field of a LVAD from [28]; (bottom right) Emulation of stress histories of typical platelets trajectories from [28]; (top right) Computer controlled HSD where platelets are exposed to uniform shear stress; (top left) Principle of the PAS assay used to measure the activity state of platelets sampled from the HSD.

The DTE was developed by researchers from Stony Brook University in collaborations with the bioengineering groups of the University of Arizona and Politecnico di Milano, with the aim of optimizing the thrombogenic performance of blood recirculating devices (e.g. artificial heart valves, LVADs). This methodology combines *in silico* numerical simulations with *in vitro* mea-

surement of platelet activation markers, allowing the prediction of the effects of modifications to the design of a given device on its thrombogenicity. The composite approach of the DTE is based on two complementary activities:

- Numerical results, obtained from two-phase CFD simulations of blood flow in the device, are used to gather data concerning the stress history experienced by each particle within the blood flow, after repeated recirculation within the device. Cumulative stresses that may drive platelets beyond the activation threshold are calculated along multiple trajectories and collapsed into probability density functions (PDFs), representing the device "thrombogenic fooprint" [28]. CFD results are then coupled with mathematical models for cumulative damage prediction.

- Representative trajectories, called hot spot trajectories (bottom center in figure 2.4), are selected from numerical simulations according to their stress accumulation in time (bottom right in figure 2.4) and are tested on a computer-controlled programmable hemodyanamics emulating device (HSD, top right in figure 2.4). Platelet activation level deriving from the application of these flow-induced mechanical loads is quantified with a specific Platelet Activity State (PAS) assay (top left in figure 2.4).

Depending on the resultant platelet activation level measured with the PAS assay, a design modification of the device can be performed, or alternatively, a prototype can be built and tested. In this way, iterative virtual design modifications of the original device geometry can be performed and tested in vitro, optimizing the thrombogenic performance of the updated device.
Girdhar and co-workers [28] adopted the DTE methodology to compare the thrombogenic risk of two LVADs. Flow within the devices was modeled with a two-phase fluid-structure interaction (FSI) simulation resolving all components of the stress tensor that are relevant to flow-induced thrombogenicity. Subsequently, the loading history of platelets in the flow field was tracked down, identifying trajectories that may drive them beyond the activation threshold. Platelet activity measurements performed in the actual pump prototypes under clinical conditions in circulation flow loops showed a significantly lower platelet activity rate after optimization with the DTE methodology.

2.2.1 The Hemodynamic Shearing Device

As just described, DTE method allows to expose platelets to realistic shear stress waveforms extracted from CFD simulations. The in silico anal-

ysis in the modeling domain is followed by the experimental emulation of the device specific stress loading histories in vitro, using the HSD. The subsequent platelet activation after shear exposure is measured using the PAS assay.
The HSD is a computer-controlled device capable of emulating device and cardiovascular pathologies hemodynamics while uniformly exposing platelets to constant or dynamic time-dependent shear stress waveforms. The HSD, whose schematic representation is shown in the top right of figure 2.4, combines the geometry of a cone and plate viscometer and a cylindrical coaxial Couette viscometer.
The HSD was specifically designed to guarantee a uniform flow field within the device. According to this feature, shear stresses generating in the cone and plate and couette region are uniform too [29]. The equations 2.2.1 and 2.2.2 describe the shear stresses in both cone-plate and couette regions:

$$\tau_{cone-plate} = \tau_{Couette} \tag{2.2.1}$$

$$\mu\frac{\omega}{\alpha} = 2\mu\frac{R_0^2 R_i^2}{R_0^2 - R_i^2}\left(\frac{1}{r^2}\right)|_{r=R_i} \tag{2.2.2}$$

The parameter μ indicates the viscosity of the fluid, ω represents the angular velocity of the cone, which varies depending on the shear rate of interest, and α is the cone angle, that is equal to 1°. Finally, R_0 is the inner radius of the ring and R_i the outer radius of the cone.
The blood-contacting surfaces are manufactured from blood compatible ultra-high molecular weight polyethylene (UHMWPE), treated with silicone. The electrical components of the HSD comprise a high-torque servo-motor controller system with a programmable interface. The highly controllable motor is mounted onto a mortiser support attacched to the cone. Precise positioning of the cone height above the base-plate is achieved with a dual-bearing-support and the Couette gap between the cone and ring is controlled with X-Y positioning micrometers. The platelet sample occupies the Couette and conical spaces [30]; at the defined time points, the platelets are withdrawn from this region and processed for the PAS assay.

2.2.2 The Platelet Activity State assay

Thrombin generation is a powerful marker of platelet activation in response to several biochemical and mechanical agonists. When platelets are activated, phospholipids on their membranes become negatively charged. Prothrombin (FII), in conjunction with activated factor X (FXa) and activated factor V (FVa), in the presence of Ca^{2+}, forms the prothrombinase

complex on the negatively charged surface and generates thrombin (FIIa). Thrombin catalyses the formation of fibrin from fibrinogen to allow clot formation.
The PAS assay is a modified prothrombinase method able to measure the near-real time rate of thrombin formation by activated platelets and to correlate it with their activation level. This laboratory technique, developed at Stony Brook University [31], is particularly well suited for identifying activation due to physical forces, such as fluid shear forces. Although thrombin generation is a powerful marker of platelet activation, in vivo the produced thrombin has a positive feedback response on platelet activation. Conversely, with PAS assay there is a linear relationship between platelet activation and the thrombin formation rate. To block thrombin feedback and ensure this one-to-one relationship, acetylated prothrombin (Ac-FIIa) is used as the thrombin substrate. Ac-FIIa does not feedback on the factor Xa complex to further activate platelets or convert fibrinogen to fibrin. The removal of the positive feedback activation by thrombin is essential for reliable quantification of platelet activation level [32]. The modification to the thrombin generation cascade is highlighted in the top left of figure 2.4.
The test is performed with gel-filtered platelets (GFP), obtained through the following procedure, shown in figure 2.5:

- Blood centrifugation to obtain platelet-rich plasma (PRP);
- Separation of platelets from PRP by gel filtration.

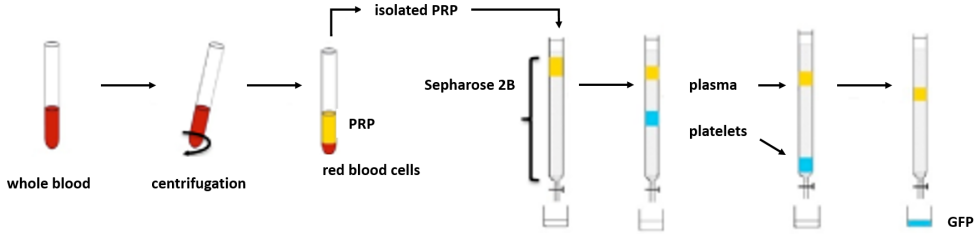

Figure 2.5: GFP extraction procedure [32]

Gel filtration is a technique used to separate molecules on the basis of molecular size, whose schematic representation is shown in figure 2.6. It is performed on a column packed with Sepharose 2B beads (60-200 μm diameter, 2% agarose; Sigma-Aldrich). Such beads will allow all solutes (up to very large molecular weights) to enter the gel matrix. Cellular elements such as platelets, due to their size, are restricted to the spaces between the beads. Therefore, when PRP is loaded into the column, the platelets pass through the column at a higher speed than the plasma constituents and are eluted

in advance and well separated from all plasma solutes that are not tightly adsorbed to the platelet surface [33].

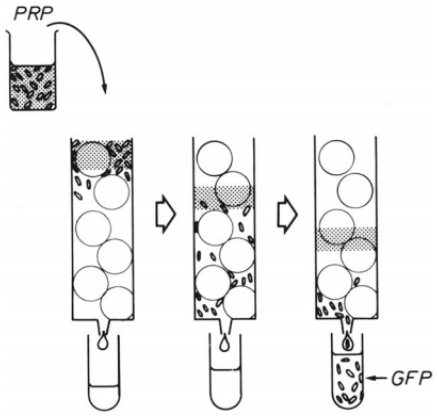

Figure 2.6: Schematic illustration of the principle of gel filtration of PRP. Plasma solutes, platelets, and beads of Sepharose 2B are represented by the small dots, the eliptical shapes and the circles respectively [33]

The PAS assay has been utilized extensively for in vitro studies of device-associated platelet activation. In particular, several studies in literature support the ability of the PAS assay for assessing VAD-associated shear-mediated platelet activation in vitro [28]. This technique can be employed, as prevously mentioned, to measure the shear induced platelet activation caused by HSD stimulation or to characterize the dynamics of platelet activation within flow loop systems where platelets are recirculated and thrombogenicity is measured in timed samples extracted from the loop [34].
Additionally, the PAS assay can be employed in the clinical settings. The first attempt to connect such methodology to clinically relevant diagnostics is represented by the study of Valerio and co-workers [32]. The PAS assay appeared to be a sensitive tool for detecting abnornal levels of platelet activation in association with VAD-related thrombosis, compared to standard clinical diagnostic tools.

2.3 Platelet activation: in vitro studies

Over the years, a variety of in vitro methods have been developed to study platelet activation due to pathological shear stresses and exposure times. Among the established methods for the in vitro investigation of the device-associated platelet activation, most of them evaluate the thrombogenic potential in the presence of a mechanical load by measuring the PAS.

Bluestein and colleagues performed several studies using in vitro VAD loops or cone-plate viscometer with the purpose of correlating shear stress profiles and correspondent level of platelet activation, computed performing PAS assay [17] [27]. The results showed that stenotic flow conditions increased the level of platelet activation with respect to the non-stenotic control.
Nobili et al. [29] used the HSD to subject platelets to different shear stress waveforms and measured platelet activation level through the PAS assay. The so-obtained results are shown in figure 2.6.

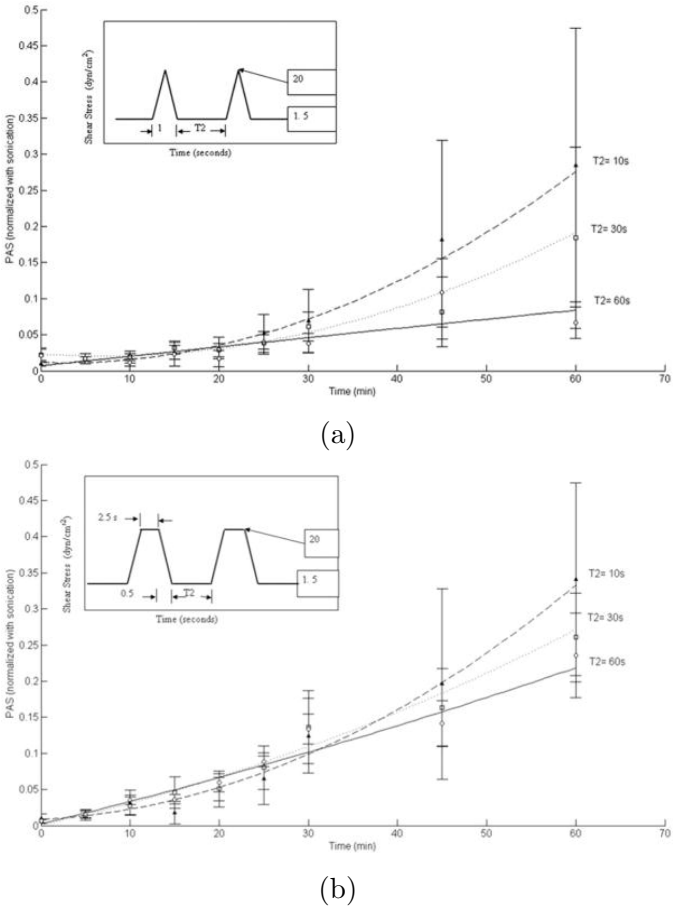

Figure 2.6: Normalized PAS values for triangular (a) and square (b) shear stress waveforms [29].

Triangular and square waveform were applied to simulate repeated passages through a generic device. Each waveform had a baseline shear of 1.5 dyne/cm^2 imposed for a time period T2, and peak shear of 20 dyne/cm^2, for a period T1. The normalized PAS values obtained for triangular and square shear stress waveforms are shown respectively in figures 2.6a and 2.6b. It

was demonstrated that the PAS increases decreasing the "relaxation" time (T2) between pulses.
Sheriff et al [35] developed a closed-loop recirculating syringe-capillary viscometer device - the "platelet hammer" - capable of repeatedly exposing platelets to wall shear stresses up to 2000 dyne/cm^2 for brief durations. The range of shear stresses and exposure times may allow the investigation of pathologies and measures associated with MCS devices. Sheriff et al. demonstrated that platelets activate, sensitize and change shape in response to both single and repeated passages though a variety of shear stresses and exposure times, and their resulting stress accumulation. In particular, according to PAS assay results, a single passage through shear stress conditions approaching 1000 dyne/cm^2 (WSS up to 2000 dyne/cm^2) for 25 ms activated platelets and repeated passages (74 loops at $\tau = 350 dyne/cm^2$ for 50 ms) significantly increased the PAS when compared to unsheared platelets. Moreover, the role of hypershear in platelet sensitization was examined. As shown in figure 2.7, platelets exposed to very high shear stress for brief exposures continue to activate despite subsequent exposure to low shear stress.

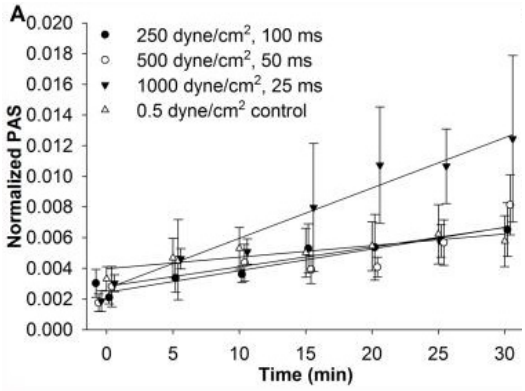

Figure 2.7: Normalized PAS trend in time obtained exposing platelets once to very high shear stresses for durations on the order of milliseconds, followed by subsequent 30 min exposure to 0.5 dyne/cm^2 in the HSD. Sample are assayed for PAS at regular intervals [35]

In order to analyze the role of repeated pathological shear stress exposure on shape change, SEM images, reported in figure 2.8, were obtained for platelets exposed to average peak shear stresses of 50, 150, 400 and 500 dyne/cm^2. It was demonstrated that baseline platelets have a discoid shape with little or no pseudopods, which increase in length and number as the stress accumulation is increased.
Since patients on continuous-flow VADs undergo pharmacotherapy including both anticoagulant and antiplatelet prophylaxis, several studies examined

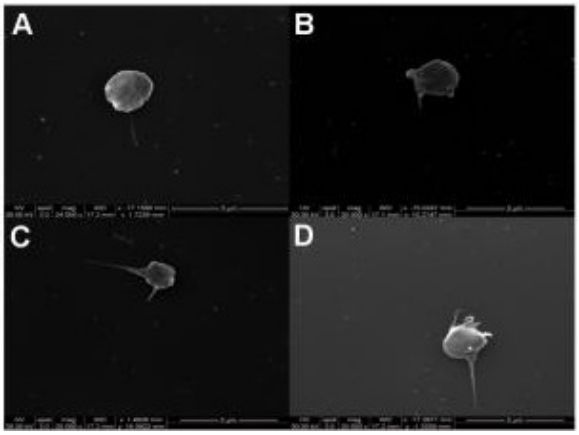

Figure 2.8: Shape change observed for platelets exposed to different shear stresses: baseline platelets (A), 50 dyne/cm^2 for 300 ms (B), 250 dyne/cm^2 for 60 ms, 500 dyne/cm^2 for 63 ms (D) [35]

the effect of antiplatelet agents on shear-induced platelet activation in vitro. Sheriff and colleagues [36] studied the effects of aspirin (acetylsalicyclic acid, ASA) as it is routinely prescribed to limit the effects of flow-induced platelet activation in most MCS devices. Results of the PAS assay are shown in figure 2.9.

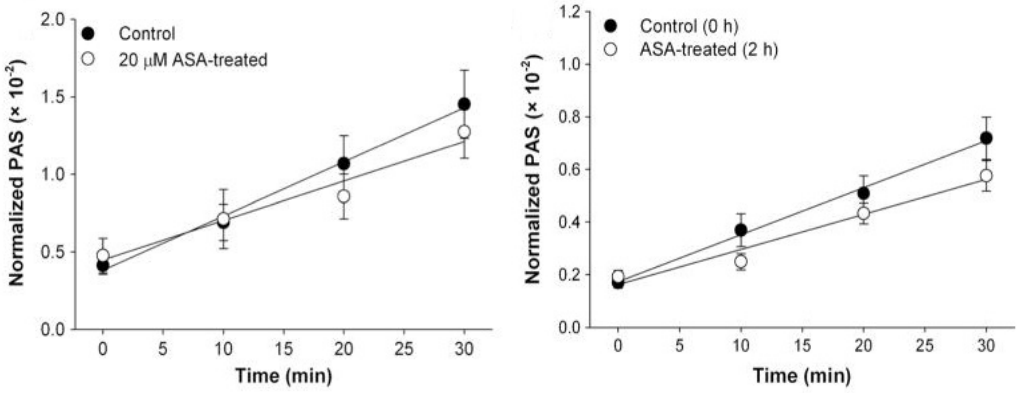

(a) (b)

Figure 2.9: Platelet activation post-in vitro ASA treatment (a) and 2h post-in vivo ASA treatment (b) [36].

In particular, the evolution of PAS of platelets during repeated passages in a flow loop containing a DeBakey VAD after in vitro administration or in vivo metabolism of aspirin was examined. It was demonstrated that direct treatment with aspirin is as effective as in vivo metabolized aspirin in reduc-

ing platelet activation. Moreover, it was shown that in vitro treatment with antiplatelet agents coupled with design optimization techniques, such as the DTE, may reduce the platelet activation even further.

Activated platelets release the content of their intracellular granules and so their activation can be estimated by measuring the level of proteins released into the extracellular fluid, which is usually performed through ELISA kits. At the same time, flow cytometry detection of intra- and extra-cellular antigens specific for platelets granules and negatively charged phospholipids on the external surface of platelets membrane can be an additional tool for the analysis of platelet activation. The most widely studied types of activation-dependent monoclonal antibodies directed against membrane proteins are P-selectin specific. P-selectin (CD62p) is a GP of the α-granule membrane of resting platelets and it is incorporated into the plasma membrane upon activation and granule secretion [37]. Therefore, a P-selectin specific monoclonal antibody only binds to degranulated platelets, not to resting ones [38]. Griesshammer et al. [39] used a flow cytometric assay to demonstrate that P-selectin expression is activation dependent.
Lu and co-workers [40] analyzed the sensitivity of human platelets to shear stress stimulation, using a cone-plate rheometer to test blood samples at shear stresses up to 400 dyne/cm^2 for 2 minutes. Different platelet activation markers, such as platelet count and platelet surface P-selectin expression, were used to assess the response to shear. They showed that exposure to shear stresses above 200 dynes/cm^2 caused changes in platelet markers. Platelet counts decreased with increasing shear stress, dropping to less than 40% of the baseline level at shear stresses of 200 and 400 dyne/cm^2. In addition, a significant increase in P-selectin expression resulted after shear stress exposure.
Another common marker identifying procoagulant activity of platelets is Annexin V. Stimulation of platelets induces an increase in intracellular calcium which causes the relocation of Annexin V to the cytoplasmatic side of plasma membrane where it associates with actin [41] [42]. In particular Tzima et al. [43] showed that upon stimulation of platelets with thrombin there is a ninefold increase in the amount of Annexin V in the cytoskeleton fraction of activated platelets with respect to resting ones. Moreover, Dachary-Prigent and colleagues [44] incubated samples of stimulated and control platelets with Annexin V-FITC and then analysed them using a FACScan flow cytometer. They demonstrated that when platelets were activated with agonists, the presence of a specific subpopulation expressing maximal binding of Annexin V was clearly observed.
Some studies in literature are focused on shear stress effects on platelet func-

tion and shape and showed that platelets follow different biochemical pathways at elevated shear stress compared to low shear stress environment [45]. Kuwahara et al. [46] observed real-time changes in platelet morphology on a thrombogenic surface during the platelet adhesive process in blood perfusion by using a parallel-plate flow chamber, epifluorescence and SEM imaging. They tested washed platelets resuspended in HEPES buffer and demonstrated that platelets exposed to physiological rapid blood flow changes dynamically modify their shape at distinct phases of the adhesive process to complete successful thrombogenesis. In particular, the SEM images reported in figure 2.10 showed three distinct morphological groups: ball-shaped with filopods, hemisphere-shaped with filopods, and extensively spread. These data illustrate the typical scenario of shape changes during the adhesive process: ball-shaped platelets roll, gradually flatten to a hemispherical shape and finally adhere to the surface. Then, the platelets that have firmly adhered are spread extensively over the surface under flow conditions.

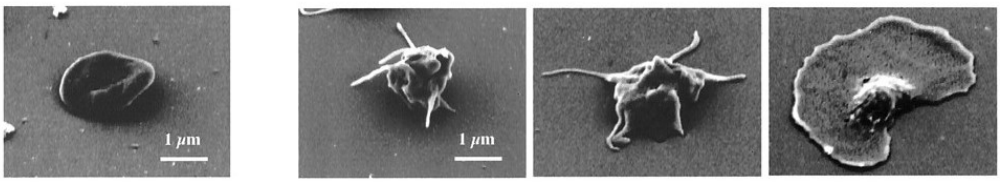

Figure 2.10: Time-course shape changes in an individual platelet during a real-time adhesive process under flow conditions [46].

2.4 Endothelial cell activation: in vitro studies

It is known that ECs can be activated through both chemical and mechanical stimulation. The response of ECs to fluid shear stress (mechanical stimulation) and various chemical agonists (chemical stimulation) such as Tumor Necrosis Factor-α (TNF-α) and Interleukin-1β (IL-1β) results in the surface expression of various adhesion molecules and is critical to the balance between healthy and pathogenic inflammation response [47].
Biomarkers of endothelial activation include different families [20]:

- Selectins: this family includes the E-selectin which is a specific marker of EC activation and is expressed solely on the activated cells.
- Immunoglobulins: this family includes two important adhesion molecules, ICAM-1 and VCAM-1, which partecipate in the cascade and in the co-

ordination of adhesion events between leukocytes and the activated ECs.

- Integrins: they are heterodimeric glycoproteins consisting of α and β subunits, which mediate EC-leukocyte and EC-extracellular matrix interactions. Among the integrins, only the $\alpha_v\beta_3$ heterodimer is an endothelial adhesion molecule and is expressed by the activated ECs.

ICAM-1, VCAM-1 and E-selectin are three important adhesion molecules that are upregulated during endothelial activation. For this reason, these markers are of interest to quantify the degree of endothelial activation. Measurement of circulating adhesion molecules is one option. Even if these circulating molecules may have functions of their own by binding to receptors on blood leukocytes, they are considered as mirroring the expression changes on the endhotelial surfaces when used as markers of activation.
Leeuwenberg et al. [48] showed that the amount of soluble ICAM-1 and E-selectin could be correlated to their level of surface expression. Videm et al. [49] demonstrated that soluble VCAM-1 concentration well represents surface expression changes in Human Umbelical Vein Endothelial Cell (HUVEC) cultures undergoing endotoxin stimulation.
All these soluble markers can be detected using commercial ELISA kits [50], while the surface expression of the molecules can be evaluated through flow citometry analysis.

2.4.1 Endothelial cell chemical activation

Normally, ECs maintain an anticoagulant surface by expressing heparin-like structures, thrombomodulin and components of the fibrinolytic system. However, in vitro, cytokines such as TNF-α, IL-1 and endotoxin are known to shift ECs from an antihemostatic to a procoagulant state. ECs synthesize and express on their surface numerous adhesins and other molecules which participate in leukocyte and platelet recruitment, coagulation and inflammation. In particular, TNF-α is a mediator of systemic inflammation and immune-responses. A major site of action of TNF is the vascular endothelium, where it induces inflammatory responses by enhancing adhesion molecule expression and cytokine secretion. TNF-α activates ECs and changes the expression of many genes responsible for an endothelium phenotype prone to facilitate transmigration of leukocytes and to reduce anti-thrombotic properties. The binding of this factor to the TNFR1 receptor on ECs is followed by rapid translocation of the transcription factor NF-KB from the cytoplasm to the nucleus. This translocation is important for stimuating the transcription of the adhesion molecules E-selectin, ICAM-1 and VCAM-1 [51].

Mackay et al. [52] stimulated cultured HUVECs from 0 to 10 h with human TNF. Through cytofluorimetric analysis, whose results are shown in figure 2.11, ICAM-1 was found to be expressed on unstimulated cultured HUVECs at high levels, whereas E-selectin and VCAM-1 were essentially absent. The chemical stimulation triggered the upregulation of ICAM-1 and the induction of E-selectin and VCAM-1 expression. The modulation of ICAM-1 and VCAM-1 expression was detectable after 2h of TNF stimulation and reached a sustained maximum level after 6-8 h, contrasting with the expression of E-selectin where induction was maximum after 2h and declined after 10 h.

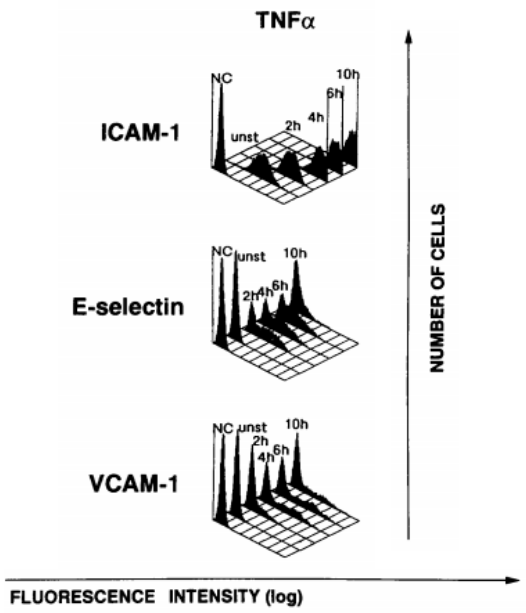

Figure 2.11: Cytofluorimetric profiles of ICAM-1, E-selectin and VCAM-1 expression on HUVECs stimulated in culture for 2, 4, 6 and 10 h with 10 ng/ml TNF-α [52]

Tsai et al. [53] incubated confluent Human Lung Microvascular Endothelial Cells (HLMVECs) cultured in a microdevice with 10 ng/ml of inflammatory cytokine TNF-α in medium and demonstrated that EC activation with the TNF-α upregulates expression of adhesion molecules such as VCAM-1 and ICAM-1.
Nawroth et al [54] incubated purified recombinant TNF with cultured ECs (both bovine aortic cells and HUVECs). Monolayers of these two cell lines were incubated with a fixed concentration of TNF (10 nM) for 12 hours or, alternatively, with increasing doses of TNF (logarithmic scale) for a fixed time interval (12h). These incubations resulted in a time and dose dependent acquisition of procoagulant activity, i.e. induction of EC tissue factor and

suppression of endothelial anticoagulant function.
Finally, Boehme and colleagues [55] activated cultured HUVECs with 10 ng/ml of TNF-α and determined the levels of soluble ICAM-1, VCAM-1 and E-selectin through commercialy available ELISAs. Significantly increased levels of the three markers were measured in the presence of TNF-α.

2.4.2 Endothelial cell mechanical activation

ECs are capable of discriminating between various flow types. The differential responses to the flow environment are reflected both in different levels of adhesion molecule expression and in morphological responses.
ECs in vivo are constantly exposed to blood flow and the resulting frictional force, i.e. the WSS, varies in magnitude and direction with time, depending on the cardiac cycle and vasculature geometry [56]. Several studies in literature have shown that the structure and function of ECs are deeply affected by the nature of WSS waveforms. Pathological shear stresses have been of special interest to many researchers, due to their potential role in endothelial damage and dysfunction. Moreover, it is known that shear stress modulates the extrinsic activation of coagulation mediated by perturbed ECs.
In particular, the two characteristics of blood flow that influence endothelial function and phenotype are:

- magnitude of the resulting shear stress;
- direction of flow.

Regarding the WSS magnitude, some in vitro studies have demonstrated that shear stress between 10 and 15 dyne/cm^2 promotes endothelial quiescience and an atheroprotective gene expression profile, while low shear stress ($<$4 dyne/cm^2), which is prevalent at atherosclerosis-prone sites, stimulates an atherogenic phenotype [57].
Concerning flow direction, studies in literature have shown that oscillatory flow, i.e. oscillatory shear stress defined as a bidirectional shear stress with a close-to-zero time average, has the capacity to alterate the endothelial morphology and to induce adhesion molecule expression. Chappel et al. [58] exposed HUVEC monolayers to oscillatory shear stresses (between 0.5/-0.5 Pa s, f=1Hz), imposed in an in vitro environment through a flow system (parallel plate flow chamber). They demonstrated that oscillatory flow directly modifies intracellular signaling mechanism, leading to enhanced expression of VCAM-1 ICAM-1 and E-selectin, while steady shear stresses don't have significant effects on upregulation of the adhesion molecules. These results,

shown in figure 2.12, highlight that oscillatory shear stress provides a proinflammatory stimulus to ECs.

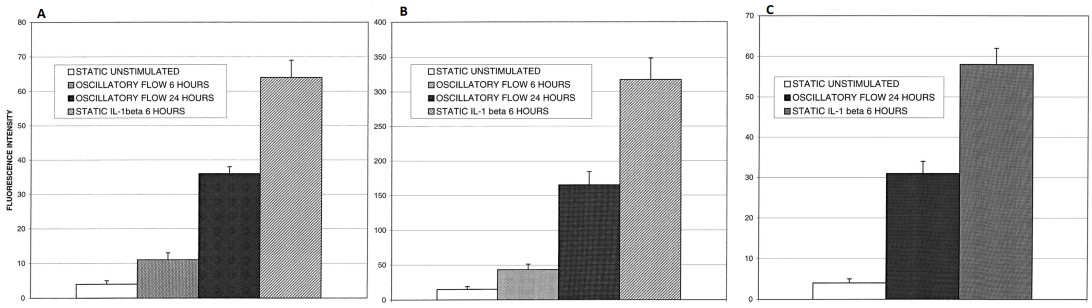

Figure 2.12: Representative histograms of the level of VCAM-1 (A), ICAM-1 (B), E-selectin (C) expressions. The histograms show fluorescence intensities for statically cultured cells and HUVEC monolayers exposed to oscillatory flow [58].

Regarding the morphological response, Estrada et al. [59] demonstrated that ECs subjected to a disturbed flow condition (low and oscillating shear stresses with average value equal to 0.13 Pa) have rounded or cuboidal shape, as shown in figure 2.13, with shortly and randomly oriented actin filaments and with a compromised impermeability. In this study they replicated shear stress waveforms associated with both normal and disturbed flow to stimulate an endothelial monolayer of Human Aortic Endothelial Cells (HAECs) cultured in a microfluidic chamber.
Finally, Yin et co-workers [60] exposed confluent HUVECs to pulsatile shear stress using a cone and plate shearing device, replicating both normal and pathological conditions (stenosis and recirculation zone). After 30-minutes of shear application, compared to normal shear stress, both recirculation and stenosis shear stresses induced a marginal increase in ICAM-1 expression. The recirculation shear stress led to the maximum amount of cell surface tissue factor expression, compared to normal and stenosis ones.

2.5 Platelets-endothelium interaction

As described in chapter 1, the interaction between circulating platelets and vascular wall ECs plays critical roles in pathogenesis of thrombosis and atherosclerosis, which can also be affected by shear stress. Shear stress activated ECs can initiate coagulation and shear stress activated platelets can bind to ECs, enhancing inflammatory responses.

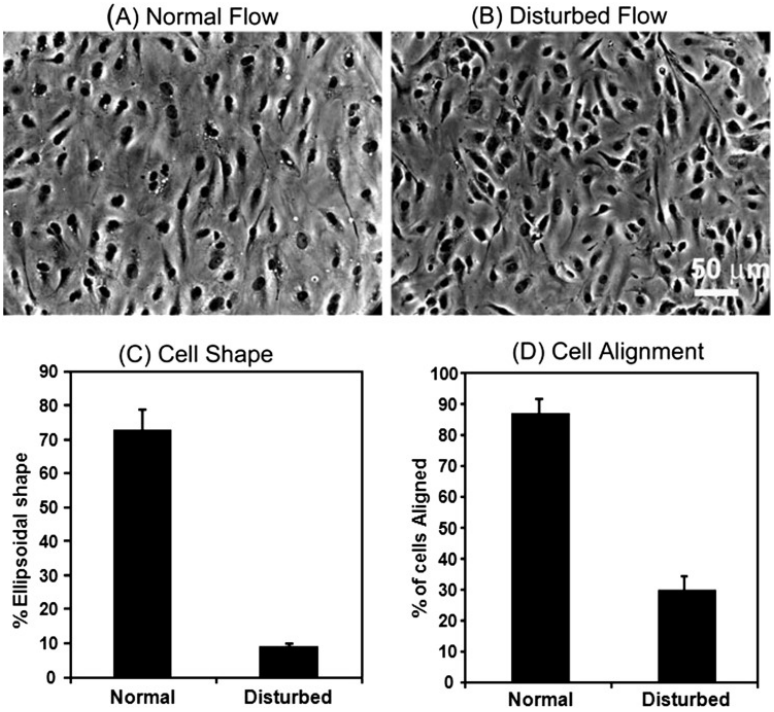

Figure 2.13: Phase contrast images of cells cultured under conditions of (A) normal and (B) disturbed flow. Graphs quantifying % of cultured cells under both conditions that assume (C) ellipsoidal shape and (D) alignment in the direction of flow [59].

Yin et al [61] exposed platelets to different dynamic shear stress waveforms with or without the presence of confluent ECs (Human Coronary Artery Endothelial Cells, HCAECs), using a programmable cone and plate shearing device. The shear stress waveforms included a normal pulsatile one, mimicking shear stress in a healthy left coronary artery, a low pulsatile one, mimicking a recirculation zone, and an elevated one, representing a stenotic condition. It was shown that, in presence of confluent HCAECs, dynamic shear stress had a significant effect on platelet surface P-selectin expression, i.e. platelet activation. Pathological pulsatile shear conditions did not cause a change in EC surface ICAM-1, but induced a significant increase in soluble vWF generation. The increase in soluble vWF may have enhanced platelet activation, indicating that ECs might play a role in the increased sensitivity of platelets to dynamic shear stress. Moreover, due to the stagnant flow in the recirculation zone, platelets get trapped and exposed to low pulsatile shear stress for elongated durations and eventually become activated, increasing the possibility of thrombosis.
Moreover, Czervionke et al. [62] investigated the ability of platelets to ad-

here to the intact endothelium. They incubated platelets suspensions with HUVEC monolayers, both in presence and absence of thrombin and demonstrated that thrombin had the potential to cause platelets to adhere to the undamaged endothelium. Evidence of adherence of platelets to intact endothelium was provided by SEM imaging. Platelet aggregates, as shown in figure 2.14, remained attached to the endothelial monolayer.

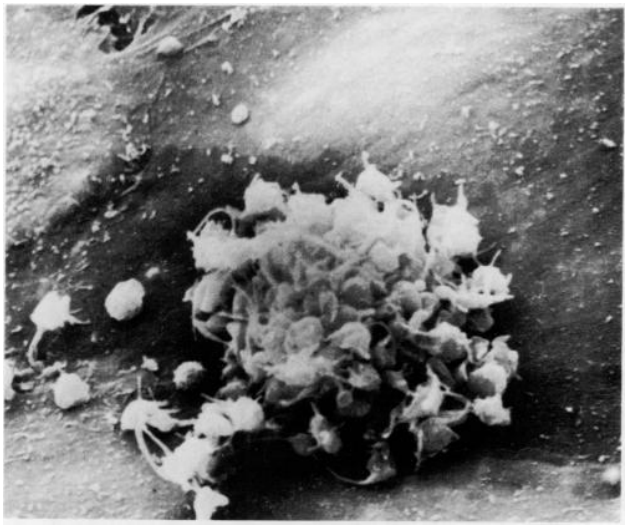

Figure 2.14: Scanning electron micrograph of a thrombin-induced platelet aggregate which was adherent to the monolayer of the cultured endothelial cells (magnification 2600 X) [62]

Although it has been reported that activated platelets can adhere to intact endothelium, the involved receptors have not been fully characterized. Thus, Bombeli et al. [63] incubated unstimulated HUVEC monolayers with thrombin-activated human platelets, in order to clarify the role of the different receptors implicated in the adherence interactions of platelets with ECs. The evaluation of the HUVEC receptors revealed predominant involvement of ICAM-1 and $\alpha_v\beta_3$ integrin. The adhesion is mediated by different adhesive proteins such as fibrinogen, vWF and fibronectin, as shown in figure 2.15.

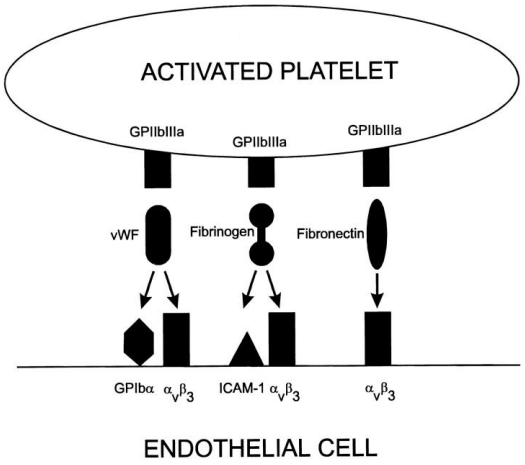

Figure 2.15: Proposed model of adhesion of activated platelets to HUVECs [63]

So far, several studies in literature investigated the role of shear-mediated platelet activation in thrombus formation in LVAD recipients. It was demonstrated that the supra-physiological levels of shear stress exerted by LVADs expose circulating platelets to severe loading regimens, leading to platelet activation and, eventually, to the development of thromboembolic complications. In particular, two main aspects were deeply analysed:

- the increase in platelet damage due to repetitive passes through a device (accumulation of cyclic shear stress exposure).
- the sensitizing effect of shear stress on platelets, so that platelets subjected to hyper-shear conditions continue to activate despite subsequent exposure to low shear stress.

However, another important aspect of thrombus formation in LVAD recipients is the presence of endothelial inflammation, degenerating in endothelial injury. Even if thrombogenesis is likely promoted in heart failure due to endothelial damage, endocardial dysfunction as consequence of disturbed flow conditions in LVAD recipients was poorly investigated so far.
In addition, the interactions between circulating activated platelets and inflamed ECs are known to play critical roles in pathogenesis of thrombosis, but a clear understanding of the responsiveness of circulating activated platelets to the presence of an inflamed endothelium is lacking.
The purpose of the present study is to provide further insights into the mechanisms leading to thrombotic events in LVAD recipients. In the context of this research area, our study aims at characterizing the mutual interaction

between shear activated platelets and inflamed ECs. In particular, the purpose is to investigate the mechanism of platelet adhesion to endothelium, which is the first step of thrombus formation in-vivo, in order to characterize the role of platelets-ECs interaction in thrombosis.

Chapter 3

Materials and Methods

The main purpose of the present study is the in-vitro characterization of the interaction between platelets and ECs that takes place in vivo in LVAD recipients at the LV apex-LVAD inflow cannula interface. In partcular, the adhesion mechanism that leads to thrombus formation in vivo was investigated.
Since it is known that, in LVAD recipients, platelets are activated when exposed to hyper shear conditions within the LVAD artificial pump and that ECs are exposed to pro-thrombotic flow conditions, we aimed at investigating the interaction between the two cellular types in these particular conditions (i.e. hyper-sheared platelets and inflamed ECs). Indeed, platelets-ECs mutual interaction phenomena and their contribution on thrombosis in LVAD recipients was poorly investigated.
In order to face this complex phenomena, it was deconstructed in the following steps:

- characterization of the interaction between non-activated platelets and non-activated ECs;
- characterization of the interaction between activated platelets and non-activated ECs;
- characterization of the interaction between non-activated platelets and activated ECs;
- characterization of the interaction between activated platelets and activated ECs.

In order to characterize these four conditions, three steps were followed:

1. Characterization of the effect of TNF-α on HUVECs (paragraph 3.2.4), in terms of cytotoxicity (i.e. Alamar Blue) and inflammation potential

(i.e. ELISA and flow cytometry). In this way, the conditions *non-activated ECs* and *activated ECs* were characterized.

2. For each of the four conditions, two characterization techniques were used to investigate variabilities in the activation level of the two cell types due to the interaction platelet-ECs. In particular, PAS assay and flow cytometry on platelet sample (i.e. Annexin V and P-Selectin) were used to verify the platelet activation before (characterization of the conditions *non-activated platelets* and *activated platelets*) and after incubation with HUVECs. Flow cytometry on HUVEC sample (i.e. ICAM-1, VCAM-1 and E-Selectin) was used to verify the HUVECs activation level after incubation with platelets.

3. In order to characterize the adhesion mechanism in the four conditions, two analysis techniques were used: SEM images acquisition to visualize the actual adhesion of platelets on ECs and flow cytometry on HUVEC sample after incubation with platelets to determine the expression of the endothelial integrin $\alpha_V\beta_3$.

In the following sections the experimental set up and protocols are deeply described. In particular, details about human platelets extraction and EC culture procedures are given. Next, the activation of both platelets and endothelium is detailed: mechanical (i.e. shear) for platelets and chemical (i.e. TNF α exposure) for ECs. The experimental protocols used to characterize the interaction between platelets and ECs in the four conditions are presented. Finally, the analysis techniques protocols (e.g. assays, imaging, himmunohistochemical tools) are illustrated.
As anticipated in chapter 1, the developed experimental platform could be further improved, substituting the chemical activation of ECs with a shear-conditioning protocol, obtained through the dynamic perfusion of the cellular monolayer. In the final section of this chapter, the shear waveform that might be used to dynamically stimulate the cells is shown. In particular, a CFD study was conducted to model the ventricular chamber with/without the LVAD inflow cannula. In a post-processing step, WSSs in the apical region of the ventricular wall were extracted.

3.1 Platelets extraction and activation

In order to perform experiments involving platelets, GFP was collected starting from whole blood. The collected sample was later activated, both mechanically and chemically. In the following sections, the used protocols are detailed.

3.1.1 Gel Filtered Platelets collection

To collect GFP, the following protocol was adopted:

- 45 cc of blood are withdrawn from healthy donors (donor pool composed of both male and female, between 20 and 30 years old).
- Blood is mixed with 10% ACD-A to prevent clotting and then centrifuged at 1300 rpm for 15 minutes.
- PRP is collected using Pasteur pipet into 15 ml tube.
- Gel column of Sepharose 2B is prepared, i.e. the column is flushed with platelet buffer 1X pH 7.4, thanks to a roller pump which moves the buffer on the top of the column. A refractometer is employed to check if the entire column has been flushed with platelet buffer, measuring the index of refraction of a drop collected at the bottom of the column. Note that the column should be prepared in advance (the flushing process takes $\simeq$ 2 h), to avoid that PRP rests on the workbench.
- PRP sample is gently layered on top of the gel.
- GFP is collected directly from the outlet tubing of the column.
- GFP is analyzed with the particle counter to determine platelet concentration, i.e. 10 μl of GFP sample are gently mixed with 10 ml of isotonic buffer and then counted.
- Based on the averaged count, GFP is diluted in Platelet Buffer 1X in order to obtain a concentration equal to 20'000 pl/μl.
- 50 mM $CaCl_2$ are added to the diluted GFP to reach a $CaCl_2$ concentration equal to 60 μl/ml.

3.1.2 Gel Filtered Platelets activation

Once the GFP sample is ready, depending on the experiment purpose, it could be necessary to activate platelets. Platelets can be activated both chemically and mechanically. Concerning the chemical activation, Arachidonic Acid (AA) is the chemical agonist that was employed in the present study (i.e. known positive control). For the mechanical activation, HSD was used to apply a constant shear waveform to platelets. The three levels of stimulation taken into account in this study are 30, 50, 70 dyne/cm^2 for 10

minutes. In order to activate GFP through HSD, the following protocol was adopted:

- 5-10 minutes prior to the experiment, a small volume of Sigmacote is applied on a kimwipe and spread to all platelets-contacting surfaces of the cone, UHMWPE plate and ring.
- The height of the cone (z-direction) is set and the cone is centered (x-y directions) through the aid of micrometer screws.
- 4 ml of GFP are placed with a Pasteur pipet on the center of the plate.
- MINT Workbench software is used to open the desired project (.wbx) and waveform file (.mnt).
- In the *program* toolbar, *compile and download* option is selected and the program is run clicking F5.
- After 10 minutes stimulation, shear-conditioned GFP is collected through a syringe port and used for further analysis.
- Plate, cone and ring are washed with distilled water and clean with Sodium Dodecyl Sulfate (SDS).

3.2 Endothelial cell culture and activation

The cell line used in this study is HUVEC line. Since the experimental part of the thesis was developed at both Politecnico di Milano and University of Arizona, even if the cell line was the same, since the providers for both cells and culture media were ATCC (American Type Culture Collection) in Milan and PromoCell in Arizona, cultured cells maintenance procedures were slightly different. In the following sections they are deeply detailed.

3.2.1 Culture medium preparation

At Politecnico di Milano, Department of Chemistry, Materials and Chemical Engineering "G.Natta", cryopreserved HUVECs ATCC-CRL 1730^{TM} were used.
In order to prepare the culture medium, the ATCC guidelines were followed. The base medium for this cell line is ATCC-formulated F-12K Medium (Kaighn's modification of Ham's F-12). To obtain the complete growth medium, the following components are added:

- 0.1 mg/ml heparin (filtered before being added to the medium);
- Non filtered Fetal Bovin Serum (FBS F7524) to obtain a final concentration of 10 %;
- Penicillin/Streptomycin (P/S) solution to obtain a final concentration equal to 1%;
- 0.03-0.05 mg/ml Endothelial Cell Growth Supplement (ECGS) prepared from bovine neural tissue (Sigma Catalog no. E-2759).

Falcon tubes containing 45 ml of complete medium without ECGS were prepared. ECGS concentration equal to 0.05 mg/ml was chosen (upper limit of ATCC guidelines). Aliquots of ECGS were prepared and stored apart at -20^{o}C. In this way, pre-filtered growth medium can be supplemented with the correct concentration of ECGS adding the aliquot to the 45 ml falcon just before the use. The preparation of the ECGS aliquots requires the dilution of the ECGS stock (15 mg) in 5 ml of filtered sterile balanced salt solution. For use, the 45 ml aliquots of complete medium were pre-warmed at 37^{o}C.

At the University of Arizona, Sarver Heart Center, cryopreserved HUVECs PromoCell C-12203 were used.
PromoCell provides 500 ml of EC basal media and one vial of supplement mix (catalog no. C-22010). In order to prepare the Endothelial Cell Complete Growth Medium (ECGM), the supplement mix was thawed and added to the basal medium, together with 5 ml of Penicillin/Streptomycin (P/S) solution (final concentration equal to 1%). The complete medium was filtered and aliquoted in 45 ml falcons.
The final concentrations of the complete growth medium are the following:

- Fetal Calf Serum (FCS) 0.02 ml/ml;
- EC Growth Supplement 0.004 ml/ml;
- Epidermal Growth Factor 0.1 ng/ml;
- Basic Fibroblast Growth Factor 1 ng/ml;
- Heparin 90 μg/ml;
- Hydrocortisone 1 μg/ml.

As before, the complete medium was stored at 4^{o}C and the 45 ml aliquots were pre-warmed at 37^{o}C for use. Since the complete medium was characterized by low FCS concentration, it was necessary to prepare additional

Serum-Supplemented Endothelial Cell Growth Medium (SSECGM) aliquotes to be used during the spitting procedure, that is described in section 3.2.3, in order to inactivate trypsin. In particular, 45 ml aliquote of FCS was thawed in a 42^{o}C water bath, centrifuged at 2300 rpm for 8 minutes and then filtered. Finally, 10 ml of FCS were added to 40 ml of complete growth medium to obtain SSECGM with a final serum concentration equal to 20 %.

3.2.2 Endothelial Cell thawing procedure

Cells are stored in a dewar with a storage temperature equal to liquid nitrogen vapor phase, frozen in a complete growth medium supplemented with 5% v/v Dimethyl sulfoxide (DMSO), a cryoprotective agent which lowers the freezing point.
At Politecnico di Milano, we started the cell culture from a cryovial containing 500x10^3 cells (HUVECs - ATCC-CRL 1730^{TM}, lot number 62313032) with reported post-freeze viability 88.5%, passage number equal to 15. Before the thawing procedure, in order to avoid excessive alkalinity of the medium during recovery of the cells, the culture vessel containing complete growth medium was placed into the incubator for 15 minutes to allow the medium to reach a pH equal to 7.4. In order to thaw the cells, the vial was kept at room temperature for few minutes. As soon as the last ice crystal was melted, 1 ml of cell suspension was diluted into 9 ml of pre-warmed complete medium. The suspension was centrifuged (130 g, 7 min, 25^{o}C) and the supernatant excluded. Finally, the pellet was re-suspended in 10 ml of medium. The cell suspension was added to a T75 flask with 6 ml of fresh medium.
At the University of Arizona, the 1 ml cryovial that was initially thawed had a reported passage number equal to 2. When the suspension was melted, it was placed in a T75 flask with 11 ml of fresh medium. Medium renewal was performed between 6 and 24 h after the thawing, since DMSO is cytotoxic.

3.2.3 Endothelial Cell culture and maintenance

In order to maintain the cells in culture and to let them proliferate, the flasks are kept in controlled atmospheric conditions (37^{o}C, 95% humidity, 5% CO_2). Approximately every two days, medium renewal was performed, with the following procedure:

- Supernatant is removed.
- The flask is washed with Phosphate Buffered Saline (PBS) (with 2 ml for T25 flaks and 5 ml for T75 ones).

- Pre-warmed fresh medium is added. The volume of medium depends on the dimension of the cultured flask (e.g. 12 ml for the T75, 5 ml for the T25).

When the cells reached 80-90% of confluence, cell splitting procedure was performed. In Politecnico di Milano, where the complete growth medium was serum supplemented, the splitting procedure was the following:

- Medium is removed.
- The flask is washed twice with PBS.
- Trypsinn is added (e.g. 2 ml for T75 flask, 0.5 ml for T25) in order to detach all the adhered cells and the culture flask is placed into the incubator for 5 minutes.
- Cells are re-suspended in fresh medium.
- Cells are counted to determine the cell seeding density: 20 μl of cell suspension are placed in an eppendorf tube with 20 μl of Trypan blue; then, 20 μl of this mixture is collected and put into a Neubauer chamber, which is observed under an inverted optical microscope, to estimate the number of cells present in the suspension.
- Cell suspension is splitted to new flasks, already containing fresh medium (cell suspension and fresh medium volumes are determined through the count).

Since at the University of Arizona low serum medium was employed, an additional step in the just described splitting procedure was required. In particular, after cell detachment with trypsin, cell re-suspension was performed with SSECGM (10 ml to re-suspend cells from a T75 and 4.5 ml for T25) in order to inactivate trypsin. Cell suspension was centrifuged (1300 rpm, 8 minutes) and the pellet re-suspended in a proper volume of ECGM to perform cell count. The subsequent steps are performed according to the protocol just described.

3.2.4 Endothelial cell activation

In order to characterize the in vitro inflammation potential of HUVECs induced by TNFα, a preliminary experimental campaign was performed at Politecnico di Milano.
Two variables were considered:

- TNFα concentration;
- TNFα exposure time.

Indeed, as described in chapter 2, the effect of TNFα upon EC activation is time and concentration dependent.
First, the cell viability was tested in presence of TNFα (i.e. Alamar Blue Assay), in order to assess concentrations and exposure times that could be toxic for the cells, thus compromising the experiments. Second, the samples were assayed in order to evaluate the expression of activation markers (i.e. VCAM-1, ICAM-1 and E-Selectin through ELISA), as modulated by TNFα.
Six concentrations were evaluated: 0, 0.1, 1, 10, 100, 1000 [ng/ml]
Five exposure times were evaluated: 0, 2, 4, 8, 24 [h]
The two variables were matched, obtaining 25 experimental conditions (4 replicates for each condition, obtaining 100 samples).
The HUVEC chemical activation experimental protocol lasts three days:

- Day 1
  A confluent T175 Flask is splitted with 1:2 ratio. This procedure is called *pre-splitting*, which allows to have all the cells at the same proliferation status (i.e. same phase of the cell cycle).

- Day 2
  5 multiwells, 48 wells each (MW48), are seeded with HUVECs with a surface density equal to 10x10^3 cells/cm^2, in a volume equal to 0.25 ml/well.
  Each of the five 48MW corresponds to one of the defined exposure time intervals.
  In the first MW48, only 4 wells are seeded (4 replicates for the condition t=0 and null TNFα concentration, i.e. control sample); in the other four 48MW, 24 wells are seeded (4 replicates for each of the 6 considered concentrations). The schematic representation of the seeded wells is shown in figure 3.1. In particular, the wells with the same color are stimulated in the same way (4 replicates of the same condition):
  - Yellow wells contain unstimulated cells;
  - Red wells contain the cells stimulated with 0.1 ng/ml of TNFα;
  - Purple wells contain the cells stimulated with 1 ng/ml of TNFα;
  - Blue wells contain the cells stimulated with 10 ng/ml of TNFα;
  - Green wells contain the cells stimulated with 100 ng/ml of TNFα;
  - Brown wells contain the cells stimulated with 1000 ng/ml of TNFα.

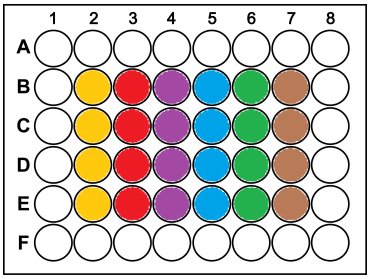

Figure 3.1: Scheme of the 48MW. Each color corresponds to a different TNFα concentration. Each so-organized 48MW corresponds to a TNFα exposure time interval.

- Day 3
  After 24 hours of incubation to allow the cells to adhere to the wells surface, a proper volume of diluted TNFα was added to the wells.
  TNFα (recombinant human TNFα, 210-TA, R&D Systems) was supplied as a powder (20 μg) that was reconstituted at 100 μg/ml in sterile PBS before use. For our purposes, subsequent serial dilutions were performed in order to obtain the following concentrations: 10, 1, 0.1, 0.01, 0.001 [μg/ml]. The diluted solutions were stored at 2^o C, while the stock at -20^o C.
  To obtain the desired concentrations, the volumes of diluted TNFα to add to the wells (3^{rd}, 4^{th} and 5^{th} columns in table 3.1), were calculated according to equation 3.2.1:

$$V_{dilutedTNF} = \frac{C_{prescribed} * V_{well}}{C_{dilutedTNF} - C_{prescribed}} \tag{3.2.1}$$

  where V_{well} is the volume of medium in each well (in this experiment it was equal to 0.25 ml, but it could varies depending on the MW used), $C_{prescribed}$ is the desired TNFα concentration (i.e. first column in table 3.1), $C_{dilutedTNF}$ is the TNFα concentration of the volume $V_{dilutedTNF}$ of the diluted solution (i.e. second column in table 3.1) that was added to the well. The wells containing the unstimulated cells (i.e. 0 ng/ml of TNFα), was supplemented with 27.78 μl of sterile PBS in order to have the same volume as the ones containing the stimulated cells.

  At each of the pre-determined time points (t=2, 4, 8, 24 [h]), the corresponding 48MW was assayed.

Desired TNFα [ng/ml]	Diluted TNF [μg/ml]	Diluted TNF to add [μl] to 0.25 ml	Diluted TNF to add [μl] to 0.5 ml	Diluted TNF to add [μl] to 0.8 ml
0.1	0.001	27.78	56.6	88.88
1	0.01	27.78	56.6	88.88
10	0.1	27.78	56.6	88.88
100	1	27.78	56.6	88.88
1000	10	27.78	56.6	88.88

Table 3.1: Calculation of the diluted TNFα amount that was added to obtain the desired concentrations, considering the medium volume for a 48 MW (0.25 ml, 3^{rd} column), 24 MW (0.5 ml, 4^{th} column) and 12 MW (0.8 ml, 5^{th} column)

The content of the 48MW was withdrawn, centrifuged (optimized centrifuge rotational speed equal to 700 g, 5 minutes, 22^{o}C in an eppendorf micro centrifuge) and stored at -20^{o}C (supernatants are the samples for ELISA tests). The wells were washed with 100 μl of PBS and then assayed with the AlamarBlue reagent. In particular, 0.2778 ml of fresh medium containing resazurin (9/10 medium, 1/10 resazurin) were added to each well. After 2 hours of incubation, a spectrophotometric reading (excitation wavelength: 595 nm; emission wavelength: 540 nm) was performed. In order to perform the spectrophotometric reading, from each well of the 48MW, 200 μl were withdrawn and splitted in two wells of a 96MW of the reader (readings in duplicate).

The chemical stimulation of HUVECs was repeated, following the same protocol, at the University of Arizona, since the cells response could be different for cells from a different provider. The characterization was repeated, evaluating only the EC activation level after 24 hours of TNF exposure and for TNF concentrations 1, 10 and 100 ng/ml. Both ELISA and flow cytometry tecniques were employed to evaluate, respectively, the release of soluble markers and the expression of surface ones.

3.3 Platelets - Endothelial Cells interaction

With the purpose of evaluating the mutual interaction between activated platelets and activated ECs, four main conditions were investigated at the University of Arizona, as itemized at the beginning of the present chapter. The employed protocols depend on the characterization technique that was finally performed (i.e. PAS assay, flow cytometry for both ECs and platelets and SEM), as it is explained in the following sections.

3.3.1 Interaction between non activated platelets and non activated ECs

The first condition that was taken into account was the one where both ECs and platelets were non activated. In figure 3.2 a flow chart of the experiment is reported.

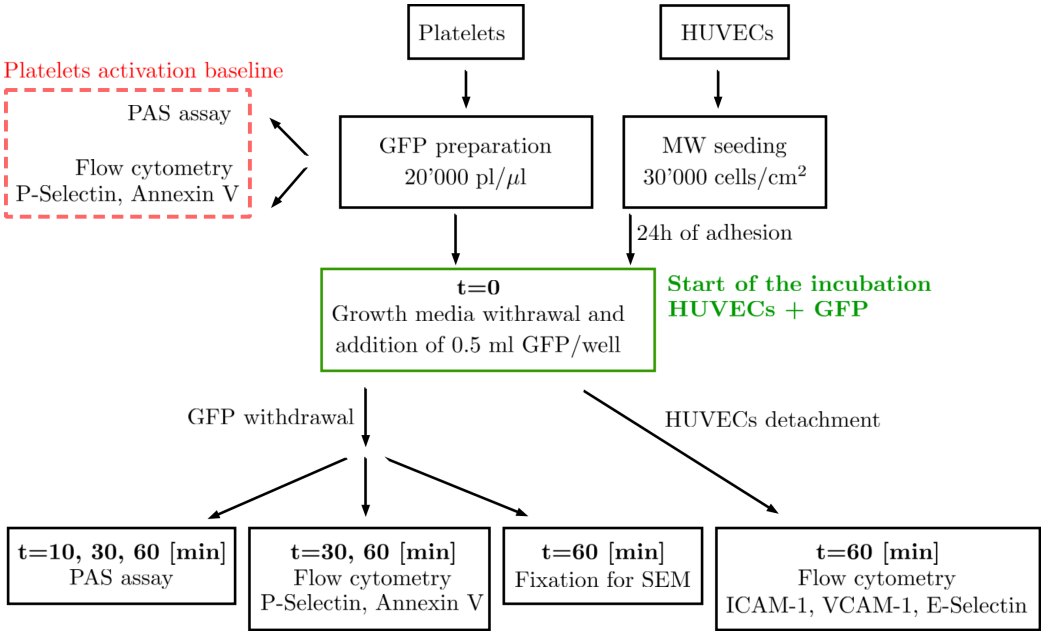

Figure 3.2: Flow chart of the experiment to characterize the interaction between non activated platelets and non activated HUVECs

The experimental protocol depends on the end point variable (EPV):

1. **EPV1**: PAS % value of platelets after incubation with ECs

   If the EPV is the determination of PAS % value of platelets after incubation with non-activated ECs, the protocol is the following:

- HUVECs are seeded on 24 MW (seeding density 30x10^3 cells/cm^2, 0.5 ml of medium per well).
- 24h of incubation in controlled conditions (i.e. 37^{o}C, CO_2 5%, RH 95%) to promote adhesion.
- GFP sample are prepared as described above in section 3.1.1 (20'000 pl/μl).
- PAS % values are calculated for resting GFP (i.e. before the incubation with ECs - red dashed block in figure 3.2).
- Growth media is withdrawn from seeded wells which are washed with sterile PBS 1X (0.5 ml PBS per well repeated twice).
- 0.5 ml GFP are added to each seeded well at room temperature.
- After 10, 30, 60 minutes incubation, GFP is withdrawn and PAS assay is performed (PAS protocol is described in section 3.4.3).

2. **EPV 2**: Determination of the expression of P-Selectin and Annexin V

   If the EPV is the evaluation of platelets activation markers expression (i.e. P-selectin and Annexin V) through flow cytometry before (red dashed block in figure 3.2) and after incubation with non-activated ECs, the protocol is the same just described, exception made for the withdrawal time points, that are only 30 and 60 minutes (sample preparation for flow cytometry is described in section 3.4.2).

3. **EPV 3**: Determination of the expression of ICAM-1, VCAM-1 and E-Selectin

   If the EPV is the evaluation of HUVEC activation markers expression (i.e. ICAM-1, VCAM-1 and E-Selectin) through flow cytometry after incubation with non-activated platelets, the protocol is the same just described, followed by HUVEC detachment at 60 minutes and preparation for flow cytometry analysis (sample preparation is described in section 3.4.2).

4. **EPV 4**: SEM images acquisition

   If the EPV is the visualization of platelets adhesion on ECs for SEM imaging, the protocol is the same just described, exception made for the culture surface support that is 12 MW (medium per well 0.8 ml), since the culture surface of 48 MW is not big enough to contain the glass slide support, mandatory for SEM imaging. In addition, the

withdrawal time point is only 60 minutes (protocol to prepare sample for SEM is described in section 3.4.4).

3.3.2 Interaction between activated platelets and non activated ECs

The next step was the activation of platelets before the incubation with ECs, to evaluate if they modify their activation level after incubation with non activated ECs. In figure 3.3 a flow chart of the experiment is reported.

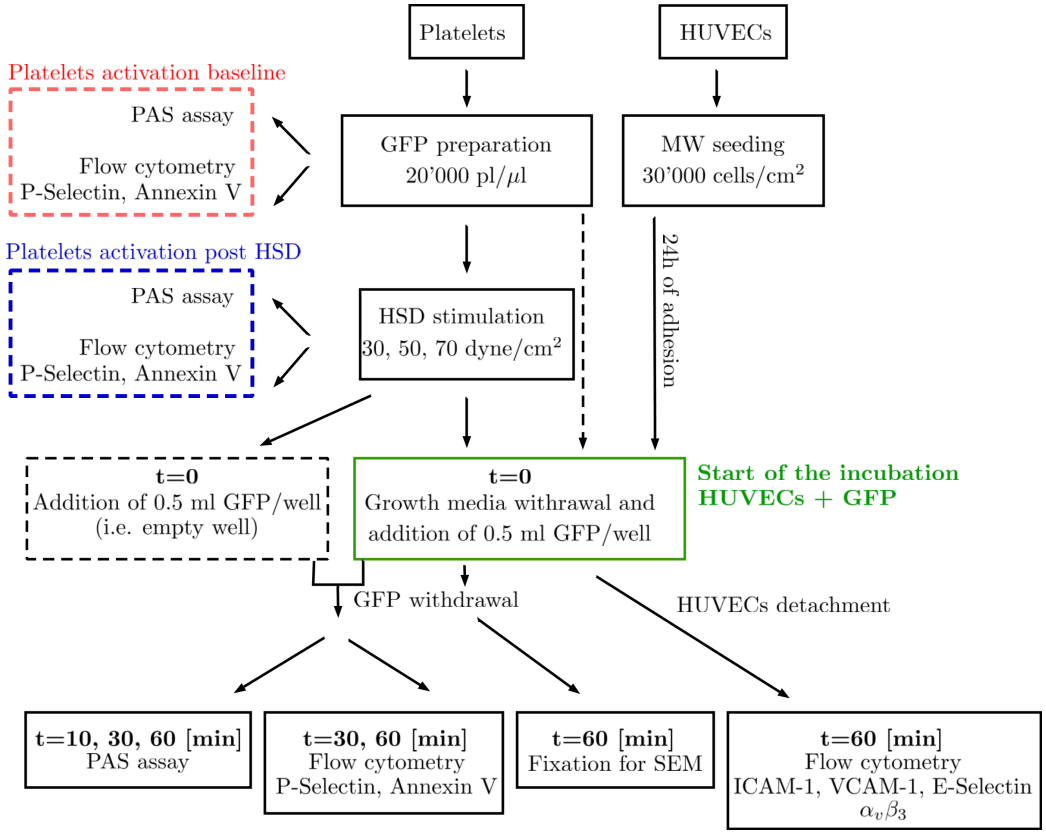

Figure 3.3: Flow chart of the experiment to characterize the interaction between shear activated platelets and non activated HUVECs. Dashed lines represent negative controls

Depending on the EPV, the protocols are the same just described in section 3.3.1, but before incubating GFP with cells, platelets were shear-activated. In particular, 4 ml of GFP 20'000 pl/μl were prepared as described in section 3.1.1 and loaded in the HSD (HSD settings described in section 3.1.2). Three consecutive HSD runs (30, 50, 70 dyne/cm^2, 10 minutes) were per-

formed. PAS% values and P-Selectin and Annexin V expression were calculated (protocols in sections 3.4.3 and 3.4.2) after the HSD run (blue dashed block in figure 3.3), in order to calculate the activation level of platelets before coming in contact with ECs (reference time point t=0). The remaining steps are the same as for non activated platelets.
At the end of the experiment, HUVECs were detached from the MW support and prepared for flow cytometry to evaluate the expression of $\alpha_v\beta_3$ and ICAM-1, VCAM-1 and E-Selectin, to determine if the contact with activated platelets influenced the expression level of this binding integrin and of the surface activation markers.
In addition, three negative controls were studied:

- When activated GFP was placed in the seeded wells, 0.5 ml of the same GFP sample was placed in an empty well (black dashed block in figure 3.3) and analyzed at the analogous time points (i.e. 10, 30, 60 min for PAS; 30, 60 min for flow cytometry). The reason of this additional step was to check if activated platelets do increase or decrease their activation level when incubated alone, in order to compare their temporal activation trend with the one obtained when incubated with ECs.

- The evaluation of $\alpha_v\beta_3$, ICAM-1, VCAM-1 and E-Selectin expression via flow cytometry was performed also detaching a seeded well (i.e. HUVECs at the same passage) where no GFP was added, to determine the baseline expression of these markers.

- The incubation of non activated GFP with HUVECs was always repeated (dashed line in figure 3.3, that links *GFP preparation* and *t=0* blocks, skipping HSD stimulation).

3.3.3 Interaction between non activated platelets and activated ECs

In this case, only ECs are activated. In figure 3.4 a flow chart of the experiment is reported.
Again, depending on the characterization technique, the protocols are the same listed in section 3.3.1, but cells were previously activated. In particular, the preliminary study performed to characterize the activation potential of HUVECs led us to define the following two chemical activation protocols: 10 ng/ml TNF-α for 24h and 100 ng/ml TNF-α for 24h. After having seeded the cells and let them adhere for 24h, TNF-α was added to the medium. The proper volume to add to obtain the three desired concentrations was calculated according to equation 3.2.1. As reported in table 3.1, if PAS

assay or flow cytometry was performed (24 MW), 56.5 μl of the properly diluted TNFα was added to each well, if samples were fixed for SEM (12 MW), 88.8 μl of the properly diluted TNFα was added to each well.
24h after the addition of TNF-α, the protocol to be followed is the same described for the non-activated ECs case.
In addition, when the effect of activated ECs on platelets was evaluated, the negative control with non activated ECs was always added (dashed line in figure 3.4 that links *MW seeding* and *t=0* blocks).

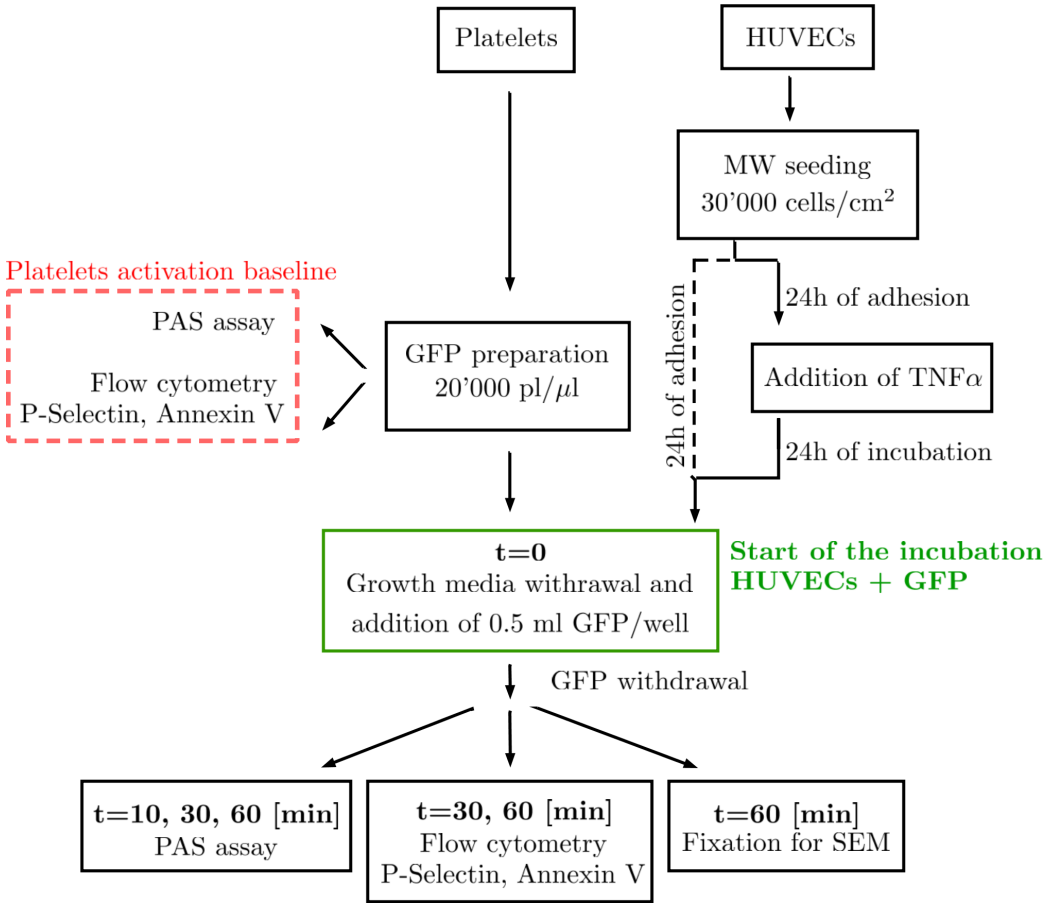

Figure 3.4: Flow chart of the experiment to characterize the interaction between non activated platelets and chemically activated HUVECs. Dashed lines represent negative controls

3.3.4 Interaction between activated platelets and activated ECs

This last condition represents the combination of the previous two experiments. In figure 3.5 a flow chart of the experiment is reported.

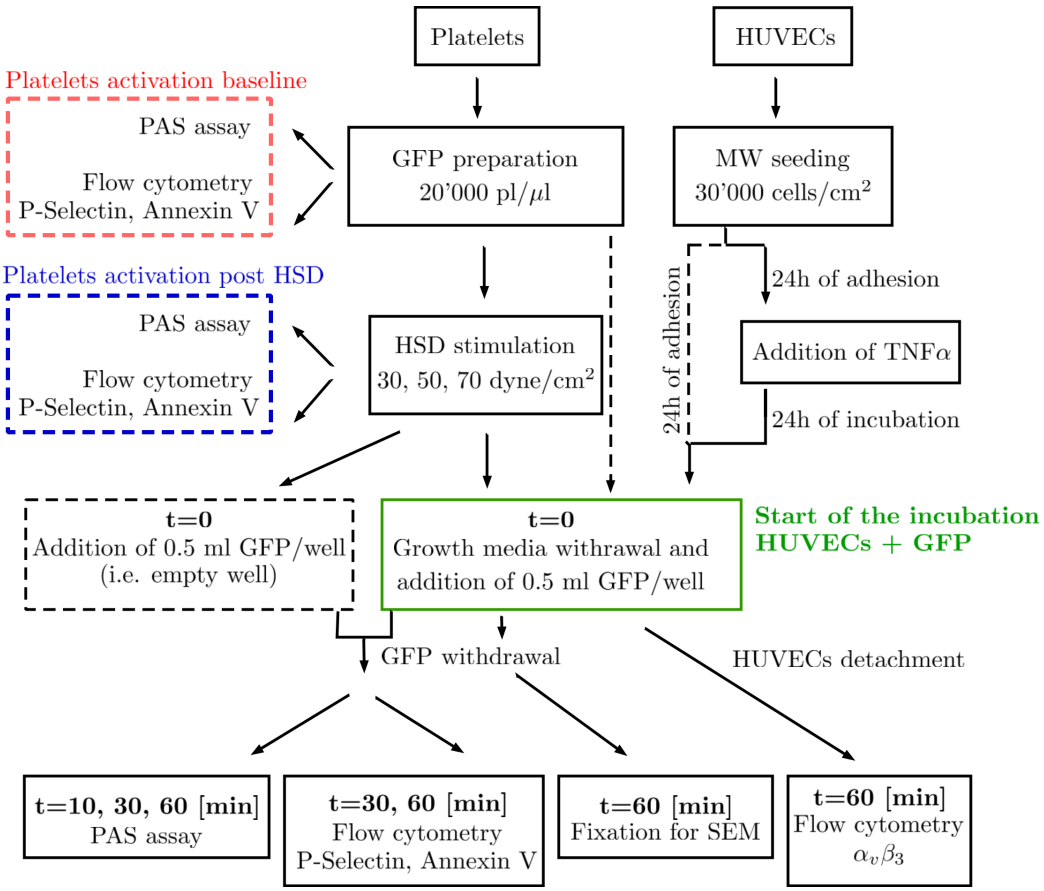

Figure 3.5: Flow chart of the experiment to characterize the interaction between shear activated platelets and chemically activated HUVECs. Dashed lines represent negative controls

Platelets were shear activated via HSD, as described in 3.3.2, and ECs were chemically activated via TNF-α, as described in 3.3.3. Also in this final experiment, the negative controls were evaluated, namely activated platelets incubated in an empty well, activated platelets incubated with non activated ECs, not activated platelets incubated with activated ECs. Even if the conditions tested for the negative controls were a repetition of the previous experiments, they were always performed since HUVECs were at a different passage (i.e. included between passage 3 and 7), characteristic that can affect

their behavior. In addition, since the donor was never the same, the platelets responsiveness could be different.

3.4 Characterization techniques of platelets and ECs activation

As mentioned, since the purpose of the in vitro study was the evaluation of the interaction between platelets and ECs in terms of activation, it was crucial the employment of analysis techniques able to quantify the activation level.
Concerning ECs, ELISA kits were employed for the evaluation of the release of soluble markers (i.e. ICAM-1, VCAM-1 and E-Selectin) and flow cyometry for the expression of surface markers (i.e. ICAM-1, VCAM-1 and e-Selectin). Regarding platelet activation, it was analyzed through flow cytometry (i.e. expression of P-Selectin and Annexin V) and through the PAS assay (i.e. thrombin production rate). In addition, the adhesion of platelets on ECs was investigated through SEM images acquisition. Finally, as an additional proof of platelets adhesion on HUVECs, the expression of the integrin $\alpha_v\beta_3$ was evaluated through flow cytometry on ECs. In the present paragraph, the protocols for samples and reagents preparation, as well as assay procedures, are detailed.

3.4.1 ELISA

In order to evaluate EC activation, three markers, ICAM-1, soluble VCAM-1 (sVCAM-1), soluble E-Selectin (sE-selectin), were detected through quantitative sandwich ELISA technique. Details about the ELISA technique are reported in appendix A. Each microplate provided in the kits was pre-coated with monoclonal antibodies specific for each marker. In particular, three ELISA kits from R&D Systems were employed:

- Human ICAM-1/CD54 Allele-Specific Quantikine ELISA Kit;
- Human sVCAM-1/CD106 Quantikine ELISA Kit;
- Human sE-Selectin/CD62E Quantikine ELISA Kit.

All reagents necessary to perform the assay were prepared an kept at room temperature before use, in particular:

– 20 ml of Wash Buffer Concentrate (25-fold concentrated) are diluted into deionized water to prepare 500 ml of Wash Buffer.

– Substrate solution is prepared mixing color reagent A (stabilized hydrogen peroxide) and B (stabilized chromogen) in equal volumes within 15 minutes of use and protected from light.

– sVCAM-1, ICAM-1 and sE-selectin Standards are reconstituted with 1 ml of deionized water. These reconstitution procedures produce a stock solution of 400 ng/ml sVCAM-1 Standard, 250 ng/ml ICAM-1 Standard, 80 ng/ml sE-selectin Standard. Each stock solution is used to produce a dilution series, as shown in figure 3.6.

Finally, HUVEC supernatant samples are diluted to be assaeyd for E-Selectin and VCAM-1. 1:2 dilution ratio was chosen. ICAM-1 kit required a non-diluted sample. For both standard and samples dilutions, the calibrator diluents provided in the kits are used.

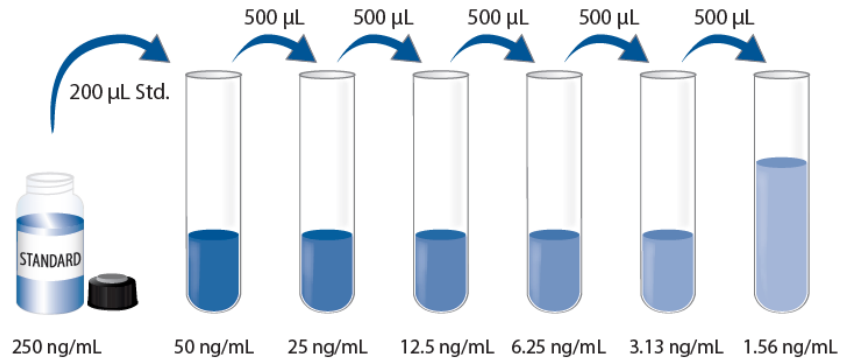

(a)

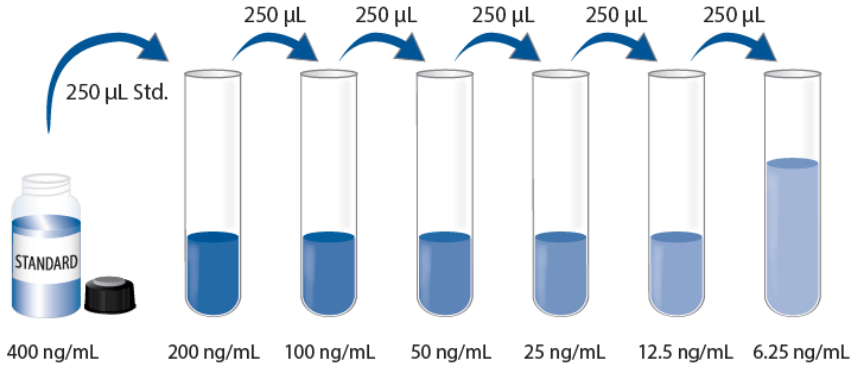

(b)

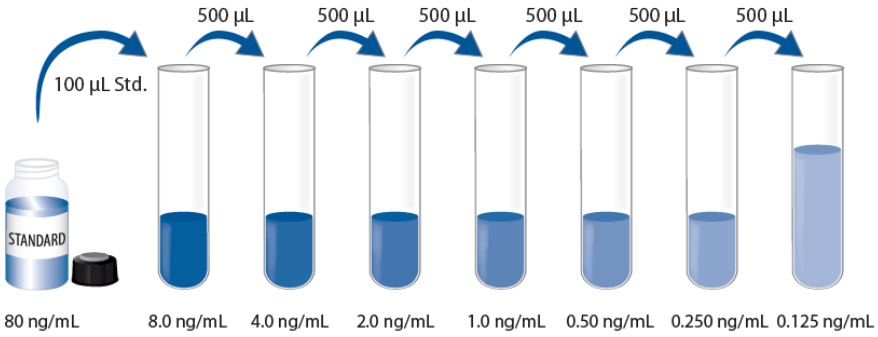

(c)

Figure 3.6: Subsequent dilution of the stock standard to obtain the calibration standard curve for ICAM-1 (a), sVCAM-1 (b) and sE-selectin (c)

The assay procedures were similar for the three kits, in particular:

- sVCAM-1 and ICAM-1 assay procedures
  All samples were brought at room temperature before use. All standards, samples and controls were assayed in duplicate.
  - 100 μl of sVCAM-1 Conjugate or ICAM-1 Conjugate are added to each well.
  - 100 μl of standard, control or sample are added per well. The wells are covered with with the adhesive strip provided and then incubated for 1.5 hours at room temperature.
  - Each well is aspirated and washed, repeating the process three times for a total of four washes. During the washing procedure each well is filled with Wash Buffer (400 μl) using a manifold dispenser. After the last wash, any remaining Wash Buffer is removed by aspirating.
  - 100 μl for sVCAM-1 assay or 200 μl for ICAM-1 assay of Substrate Solution are immediately added to each well. The wells are covered with a new adhesive strip and incubated for 20 minutes for sVCAM-1 assay or 30 minutes for ICAM-1 assay at room temperature, protected from light.
  - 50 μl of Stop Solution are added to each well.
  - The optical density of each well is determined within 30 minutes, using a microplate reader. Two consecutive readings are performed: the readings at 570 nm are subtracted from the readings at 450 nm.

- sE-Selectin assay procedure
  All samples were brought to room temperature before use. All standards, samples and controls were assayed in duplicate.
  - 100 μl of Assay Diluent RD1W are added to each well.
  - 100 μl of Standard, control or sample are added per well. The wells are covered with the adhesive strip provided and then incubated for 2 hours at room temperature.
  - Each well as aspirated and washed, repeating the process three times for a total of four washes. During the washing procedure each well is filled with Wash Buffer (400 μl) using a manifold dispenser. After the last wash, any remaining Wash Buffer is removed by aspirating.
  - 200 μl of sE-Selectin Conjugate are added to each well. The wells are covered with a new adhesive strip and then incubated for 2 hours at room temperature.
  - The aspiration/wash procedure is repeated as in step 3.
  - 200 μl of Substrate Solution are added to each well. The wells are incubated for 30 minutes at room temperature, protected from light.
  - 50 μl of Stop Solution are added to each well.
  - The optical density of each well is determined within 30 minutes, using a microplate reader. Two consecutive readings are performed: the readings at 570 nm are subtracted from the readings at 450 nm.

In order to post-process the results (i.e. optical readings), the steps were followed:

- ODs read at 570 nm is subtracted from the ODs read at 450 nm.
- The mean OD associated with each standard (each standard assayed in duplicate, n=2) is calculated.
- The mean OD of the blank (i.e. well with null protein concentration) is subtracted from the OD of each standard.
- The standard curve is defined: the mean OD read for the standards is plot on the x-axis and the known marker quantity ([ng] of protein loaded in each well) on the y-axis. These points are interpolated with a straight line (i.e. standard curve).

– The marker concentration associated with each sample is calculated, multiplying the absorbance value (i.e. OD_{450nm} - OD_{570nm}) by the angular coefficient of the standard curve and by the sample dilution factor.

– Mean and standard deviation of the concentration of each marker are calculated for each sample (each sample assayed in duplicate, n=2).

3.4.2 Flow cytometry

In the present study, flow cytometry analysis was used to determine the expression of surface activation markers by both ECs and platelets. Details about the flow cytometry technique are reported in appendix A. The flow cytometer that was used is BD FACSCanto II, the one present at the University of Arizona, Cancer Center. It is equipped with 2 lasers (wavelengths equal to 488 and 633 nm), 6 fluorescence channels and 2 channels for forward and side scatter, as it is shown in figure 3.7. The antiboides (abs) that should target the antigen of interest (if present in the sample) are labeled with proper fluorochromes, which emit light at a wavelength detectable by the fluorescence channels.

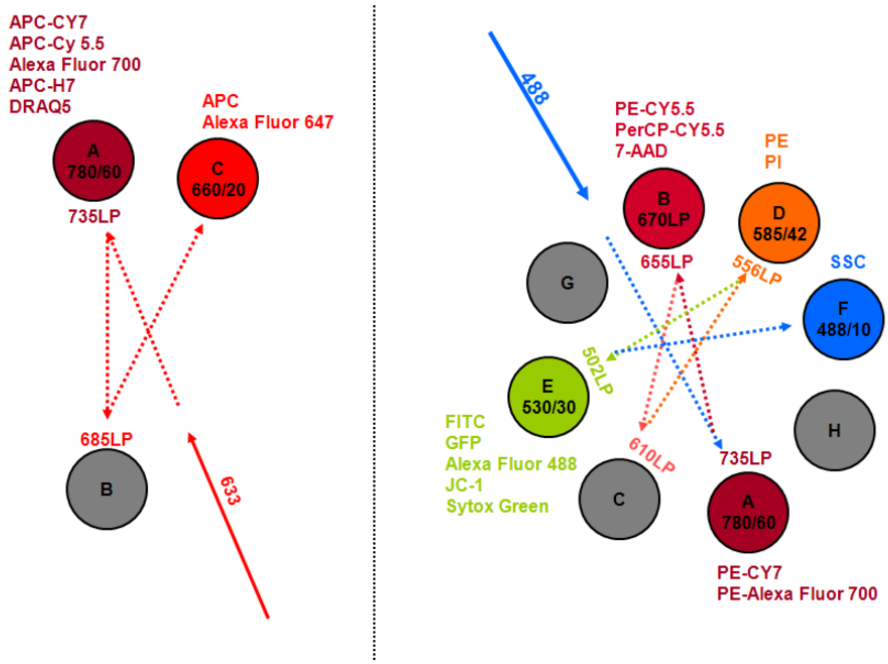

Figure 3.7: Lasers and fluorescence channels schematic of the flow cytometer BD FACSCanto II

In addition, the samples undergo a preparation procedure, according with the datasheet of the commercial antibodies:

- HUVEC sample preparation
  In order to detect the EC expression of the markers of interest (i.e. ICAM-1, VCAM-1, E-Selectin and $\alpha_v\beta_3$) through flow cytometry, the following protocol was followed.
  - ECs are detached from the culture surface through the usual procedure (i.e. trypsinization and centrifugation).
  - After cells count, ECs are re-suspended in sterile PBS 1X in order to obtain a concentration of 10^7 cells/ml.
  - 100 μl of cell suspension are transferred to a 1.5 ml eppendorf tube, where BD Biosciences fluorescently conjugated antibodies are added (20 μl of PE Mouse Anti-Human CD62E, 5 μl of PerCP-Cy^{TM} 5.5 Mouse Anti-Human CD106, 5 μl of APC Mouse Anti-Human CD54, 20 μl FITC Mouse Anti-Human CD51/CD61).
  - After 40 minutes of incubation in ice and darkness, the sample are centrifuged (eppendorf centrifuge, 3000 rpm, 8 min) and re-suspended in PBS twice.
  - The pellet is re-suspended in 500 μl PBS 1X and transferred to flow tubes.

  The same procedure was followed to prepare the flow tube for the control samples, namely statically cultured ECs, without the incubation with fluorochrome-labeled antibodies.

- Platelets sample preparation
  In order to detect the platelets expression of the two markers of interest (i.e. P-selectin and Annexin V) through flow cytometry, the following protocol was followed.
  - GFP sample are diluted in platelet buffer in order to obtain the desired concentration equal to 20'000 platelet/μl.
  - Calcium is added to obtain a final concentration equal to 2.5 mM.
  - 100 μl of GFP sample are transferred to 1.5 ml eppendorf tube. From now on, darkness is required.
  - Fluorochrome-conjugated antibodies (abs) are added to the tube, in particular 5 μl of annexin V ab (eBioscience, rh Annexin V/FITC) and 6.5 μl of pre-diluted (i.e. 1:5 dilution in PBS 1X) P-selectin ab (eBioscience, anti-human/mouse CD62P/APC).

- Sample with abs are incubated for 30 minutes at room temperature followed by the fixation of the sample itself (i.e. addition of 300 μl of 4% paraformaldehyde solution under chemical hood).
- After 20 minutes incubation, the sample are centrifuged (eppendorf centrifuge, 5000 rpm for 5 minutes).
- The pellet is re-suspended in 1 ml of PBS 1X and transferred to flow tube, ready to be analyzed through the flow cytometer.

Again, control flow tube were prepared, following the same procedure, excluding the incubation with labeled antibodies.

Histograms are the best way to visualize flow cytometry results. In order to obtain them, a sufficient number of events is analyzed by the flow cytometer machine (i.e. 10'000 with HUVEC sample, 25'000 with platelet one). After approximately 5 minutes reading, a sufficient number of particles is recorded. A two-variables dot plot is obtained, as shown in figure 3.8 (i.e. figure 3.8a from a cellular sample, figure 3.8b from a platelet one), representing the forward-scatter on the x axis and the side-scatter on the y one, where each dot represents a particle.

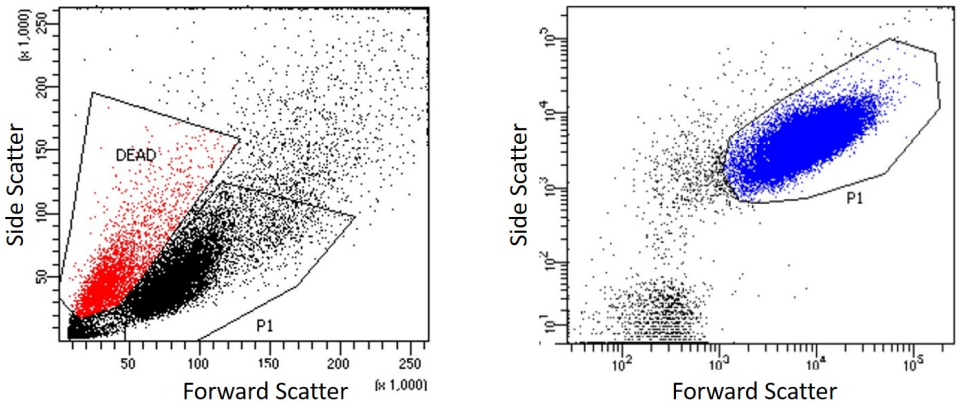

(a) (b)

Figure 3.8: Example of two-variables dot plots, used to select the (a) cellular and (b) platelet populations of interest P1. Red dots in (a), selected by a proper gate, represent dead cells.

It is possible to apply a proper gating in order to select the particles with dimension and granularity characterizing ECs (i.e. exclusion of dead cells, aggregates and debris) or platelets. The selected population is called P1, and only the events belonging to this population are processed. In particular, on the x axis of the histograms the fluorescence intensity of the

marker of interest is reported (i.e. APC-conjugated ICAM-1, PerCP-Cy5.5 -conjugated VCAM-1, PE-conjugated E-Selectin for HUVEC samples and APC-conjugated P-Selectin, FITC-conjugated Annexin V for platelet samples) while the particles count is on the y axis: the higher is the peak, the higher is the number of particles that express that fluorescence intensity; the more the peak is right shifted, the higher is the fluorescence intensity recorded.
In order to define a sub-population that is positive to a certain marker, a fluorescence intensity threshold is applied. In order to define this threshold, a sample of resting cells or platelets without fluorochrome-labeled antibodies is analyzed in order to define the so-called "natural fluorescence" of cells or platelets, that do not depend on the expression of the antigen of interest. The so-obtained threshold are used to compute the ICAM-1, VCAM-1 and E-Selectin (for HUVECs) or P-Selectin and Annexin V (for platelets) positive sub-populations, expressed as % of P1.

3.4.3 PAS

PAS assay was used to quantify the near real time rate of thrombin generation by activated platelets which is used as a measure of their activation level. The required sample is diluted GFP (i.e. 20'000 pl/μl), whose preparation is described in 3.1.1. The reagents that were prepared to perform the assay are the "tubes stock solution" and "wells stock solution": the first one includes all the reagents in which platelets are incubated to allow thrombin generation; the second one contains the stop solution and the dye. The optical density change that takes place in the wells can be quantified through spectrophotometric readings and correlated with the thrombin generation rate. Usually, the number of tubes corresponds to the number of samples (i.e. conditions) that are analyzed and each tube's content is splitted in two wells to assay each condition in duplicate.
In order to prepare the "tubes stock solution", the following regents were mixed (the volumes are referred to 1 tube):

- 50 μl Hepes Buffered Saline with 0.5% Bovin Serum Albumin (HBS:BSA);
- 10 μl 50 mM Calcium Chloride ($CaCl_2$);
- 10 μl 2 μM Acetylated Factor II (aliquotes containing 50 μl Factor II was diluted in 200 μl HBS:BSA + Polyethylene Glycol PEG).

In order to prepare the "wells stock solution", the following regents were mixed (the volumes are referred to 1 well):

– 100 μl HBS:BSA pH 7.4 + 5 mM Ethylenediaminetetraacetic acid (EDTA);

– 50 μl Chromazin - TH (CH-TH).

70 μl of tube stock solution are aliquoted in 1.5 ml eppendorf tubes and 150 μl of wells stock solution into 96-wells plate. Additionally, Factor Xa is diluted (i.e. 10 μl Factor Xa with 490 μl HBS:BSA+PEG).
The assay protocol is the following:

- A tube containing 70 μl of tube solution (i.e. prothrombinase tube) is incubated in a 37^{o}C water bath for 10 minutes.
- 25 μl of platelet sample is added to the tube with 5 μl Factor Xa and incubated (37^{o}C, 10 minutes).
- 10 μl from the prothrombinase tube is added to a well (2 wells per tube).
- Spectrophotometric reading is performed (i.e. kinetic assay, 405 nm, 7 minutes, 13 seconds interval, shaking before reading), obtaining 33 readings (one each 13 seconds).
- I33 readings are interpolated with a straight line: the PAS value corresponds to the slope of the linear fitting of the absorbance-time data points over the 7-min kinetic reading.

PAS values were normalized against those obtained by sonicating non stimulated platelets at 10 Watts for 10 seconds using the Branson sonifier. The sonication step is meant to yield platelets with maximal prothrombinase activity. The protocol to assay the sonicate sample is the same just described. The normalized PAS values (expressed in percentage, PAS %) are calculated as follows:

$$PAS\% = PAS_{sample}/PAS_{sonication} \tag{3.4.1}$$

PAS % represents the bulk activity as a fraction of the thrombin generation rate of sonicated platelets (100%). In this way, the inter-donor variability is eliminated.

3.4.4 SEM

Aiming to visualize EC and platelet samples, SEM images were acquired. Details about the SEM technique are reported in appendix A. In order to acquire SEM images of cultured cells, ECs were seeded on a substrate that

is transferable to SEM mount. In particular, glass slides were used. Glasses were sterilized, dipping them before in 70% ethanol and then in sterile water, followed by 15 minuted of UV light. In order to let the cells adhere on this substrate, poly-lysine coatings (Sigma P 4707 Poly-L-lysine solution) were performed before seeding. In particular, poly-lysine was added to ensure an even coating of the culture surface (i.e. 1 ml/25 cm^2). After five minutes, the solution was removed and the surface rinsed with sterile tissue culture grade water. At least two hours are necessary to let the surface dry before adding cells and media. In addition, cellular samples were fixed (under chemical hood). In order to fix the sample, the media was removed and the cell sample covered with 100% fixator solution, which is 2 % V/V of Glutaraldehyde (Fisacher Sci, G151) in 1X PBS. After 15-20 minutes incubation with the fixator, the sample was covered with the following solutions and let it sit at each stage for 5 minutes:

- 3:1 (100% fixator : distilled water), 1:1, 1:3, 100% distilled water
- 3:1 (distilled water : ethanol), 1:1, 1:3, 100% ethanol
- 3:1 (ethanol : Hexamethyldisilazane - HDMS), 1:1, 1:3, 100% HDMS

At the end of the last series, the HDMS was removed and the sample dried overnight. The dry samples were mounted on an aluminum stub (i.e. a round and flat piece of metal with a stem) with double-sided carbon tape. Non-conductive material samples require metal coating prior to SEM imaging. In particular, a sputter coating, which is the process of applying an ultra-thin coating of electrically-conducting metal (e.g. gold), was performed. After the coating, the fixed samples were analyzed through SEM imaging.

3.5 Statistical analysis

With the purpose to compare the outputs of the just described experiments, a statistical test was exploited, namely the Analysis of Variance (ANOVA). It was used to evaluate the outputs of both PAS assay and flow cytometry. In particular, aiming to compare more than two populations, the ANOVA test is able to determine whether there are any statistically significant differences between the means of these unrelated groups. In the present study, one-way analysis of variance was used, since there is only one property describing the population, i.e. PAS% value or % sub-population which are positive to the marker of interest.
ANOVA tests the non-specific null hypothesis that all population means are equal, i.e. H_0: $\mu_1=\mu_2=\mu_k$, where μ=group mean and k=number of groups.

When the null hypothesis is rejected, the conclusion is that at least one population mean is statistically significantly different from at least one other mean.
There are three main assumption: i) the independent variable is normally distributed in each group that is being compared, i.e. Y_{i1}, Y_{i2},...Y_{in_i} all have N(μ_i, σ); ii) there is homogeneity of variance, i.e. the population variances in each group are equal; iii) there is independence of observations.
The analysis is performed as follows. Data are obtained so that a factor A varies at k different levels A_1, A_2,..A_k. At level A_i, n_i data values, y_{i1}, y_{i2},... y_{in_i}, are collected. Data collection is reported in table 3.2. Note that the mean, e.g. y_1, is computed as follows: $y_1 = 1/n_1(y_{11} + y_{12} + ... + y_{1n_1})$ and that the sample variance, e.g. s_1^2, is computed as follows: $s_1^2 = 1/(n_1 - 1)\sum_{j=1}^{n_1}(y_{1j} - y_1)^2$. The grand mean is defined as follows: $Y = 1/N\sum_{i=1}^{k}\sum_{j=1}^{n_i} y_{ij}$.

Level	Observations	Mean	Sample variance
A_1	y_{11} y_{12} ... y_{1n_1}	y_1	s_1^2
A_2	y_{21} y_{22} ... y_{2n_2}	y_2	s_2^2
A_k	y_{k1} y_{k2} ... y_{kn_k}	y_k	s_k^2

Table 3.2: One way ANOVA: data table

ANOVA is able to estimate three sample variance:

- a *total variance*, based on all the observation deviations from the grand mean, written as:

$$\sum_{i=1}^{k}\sum_{j=1}^{n_i}(y_{ij} - Y)^2 \tag{3.5.1}$$

  In this case, the degrees of freedom (df) are N-1, where $N=n_1+n_2+...n_k$, i.e. the total number of samples.

- an *error variance*, based on all the observation deviations from their appropriate treatment means (y_i), which measures the variation within

samples, written as:

$$\sum_{i=1}^{k}\sum_{j=1}^{n_i}(y_{ij}-y_i)^2=\sum_{i=1}^{k}s_i^2(n_i-1) \tag{3.5.2}$$

In this case, df=N-k and the mean sum of square (MSS) is equal to *error variance*/df.

- a *treatment variance*, based on the deviations of treatment means from the grand mean, which measures the variation between samples (i.e. the dispersion of the means), written as:

$$\sum_{i=1}^{k}n_i(y_i-Y)^2 \tag{3.5.3}$$

In this case, df=k-1 and the MSS is equal to *treatment variance*/df=σ^2.

The two means sums of squares (MSS) are compared by aid of their ratio, so that the test statistic is taken as:

$$F_A=\frac{\sum_{i=1}^{k}n_i(y_i-Y)^2/(k-1)}{\sigma^2}=\frac{MSS_{between}}{MSS_{within}} \tag{3.5.4}$$

It can be shown that F_A has an F-distribution, if H_0 is true. The hypothesis H_0 is rejected if $F_A > F_p(k-1, N-k)$, where p gives the level of significance. The critical value F_p(k-1,N-k) can be found in a table for percentiles of the F-distribution.
In the present study, a Matlab function was implemented to perform the ANOVA test on input variables. As output, it gives a binary value, which indicates if the populations means are statistically significantly different (p-value < 0.05) or not (p-value > 0.05).

3.6 Computational study

As mentioned at the beginning of the chapter, with this thesis project we also settled the basis for a possible improvement of the experimental platform, namely a shear stress conditioning of HUVECs via dynamic perfusion protocols in microfluidic channels, to better replicate the in-vivo hemodynamics-driven inflammation condition at the LV apex-LVAD inflow cannula interface. In particular, it was crucial to define the shear trends that ECs experience in the apical region of the ventricular chamber.
For this aim, a CFD study modeling the LV-LVAD hemodynamics was developed.
Two classes of models were developed:

– *Paradigmatic* models, where the ventricular chamber was simplified (i.e. an ellipsoid);

– *Patient-specific* models, where the geometries were reconstructed from 3D-TT-ECHO images.

The first set of models (i.e. paradigmatic ones) was used to develop an effective numerical tool, based on finite volume approach, in ANSYS Fluent, able to assign a proper displacement to each node of the ventricular grid to simulate consecutive cardiac cycles. The implemented CFD tool was then adapted to the second class of models (i.e. the patient-specific ones).
For both the classes of models, different conditions were simulated:

– Healthy LV, ejection volume 70 ml;

– HF-LV pre-LVAD implant, i.e. dilated with reduced (ejection volume 35 ml) or negligible (ejection volume 10 ml) contractile capacity;

– HF-LV post LVAD implant, i.e. dilated with negligible contractile capacity in presence of LVAD inflow cannula inserted in the ventricular apex.

In the following sections, the numerical tool will be deeply illustrated, for both paradigmatic and patient-specific models. Finally, the post-processing extraction of the WSS trends in the apical region is presented.

3.6.1 Geometry and Mesh

First, a paradigmatic model of a healthy LV at end-diastolic configuration was developed. The ventricular chamber is represented as a semi-ellipsoid, as shown in figure 3.9a.
The truncated cone represents the valvular plane, whose upper surface mimic the mitral valve and the cylinder represents the first portion of the aorta. A rough mesh, composed by 61157 tetrahedral elements was built. The purpose was to firstly develop our numerical tool for a geometry with few elements, requiring limited computational time.
The patient-specific LV geometry at end-systolic configuration reconstructed from 3D-TT-ECHO images acquired from a healthy volunteer is shown in figure 3.9b. In order to determine the appropriate number of elements to be used to approximate this complex geometry, a mesh sensitivity analysis, that is described in section 3.6.1, was performed for this model.

Since the evaluation of the disturbed hemodynamics of the LV of a VAD recipient was of interest, two paradigmatic geometries representing the pre and

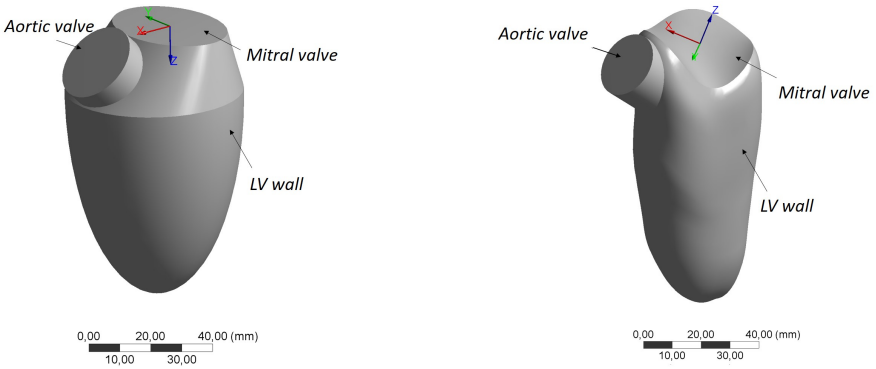

(a) (b)

Figure 3.9: Healthy LV: paradigmatic (a) and patient-specific (b)

post LVAD implant conditions at end-diastolic configurations were developed (figures 3.10a and 3.11a).

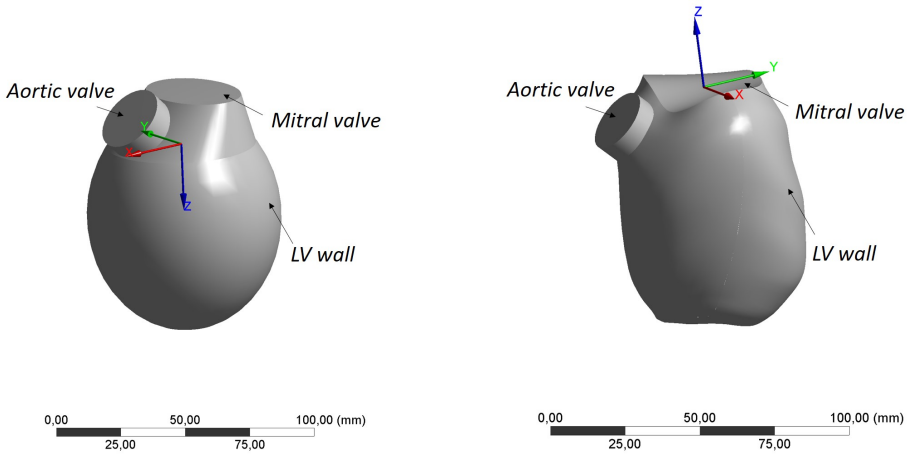

(a) (b)

Figure 3.10: HF LV geometries, pre-implant condition: paradigmatic (a) and patient specific (b)

HF-LV is characterized by a lower contractile capacity of the myocardial fibers and a higher volume with respect to a healthy LV. In order to obtain a dilated ventricular chamber an ellipsoid was realized and properly cut with a plane perpendicular to the major axis to gain the set priming volume of 250 ml. The post-LVAD-implant condition was obtained adding a cylinder (radius equal to 7 mm) inserted in the apex of the dilated LV with a penetration depth equal to 18 mm, mimicking the presence of the HeartMate III

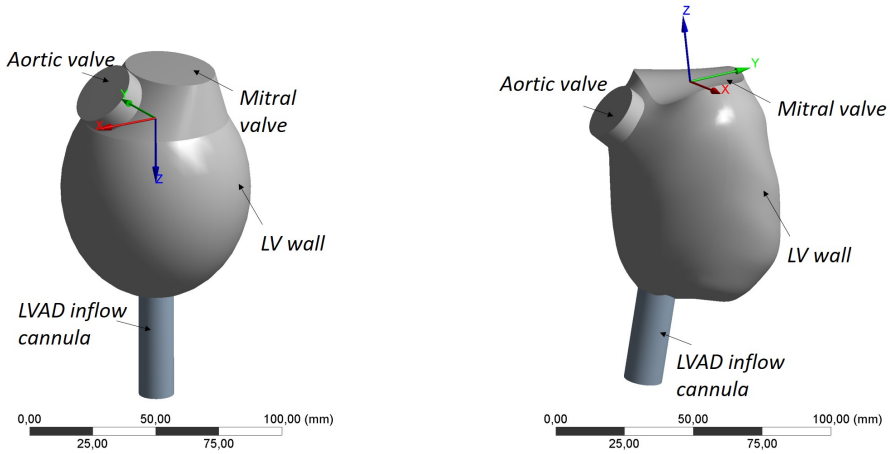

(a) (b)

Figure 3.11: HF LV geometries, post implant conditions: paradigmatic (a) and patient specific (b)

inflow cannula (figure 3.11a).
As in the previous case, rough meshes were built for these models, in order to test the effectiveness of the grid motion. After that, a patient specific LV geometry at end-systolic configuration was reconstructed from 3D-TT-ECHO images acquired at San Raffaele Hospital from a LVAD candidate. The CAD obtained for the HF patient-specific pre-LVAD-implant LV model is shown in figure 3.10b. In order to mimic the post-implant condition, following the same process performed for the paradigmatic case, a cylinder (radius equal to 7 mm and penetration depth equal to 18 mm) was inserted in the ventricular apex. The resulting geometry is shown in figure 3.11b.

Mesh sensitivity analysis

A mesh sensitivity analysis on the two patient-specific LVs was performed in order to determine the optimal spacial grid resolution to mesh these complex geometries.
Concerning the healthy patient-specific geometry (figure 3.9b), six meshed with different number of tetrahedral elements were built. The investigated meshes are collected in table 3.3.
In all models, time step was set equal to 0.001 s. In order to evaluate the solution discrepancy between the meshes, the average velocity magnitude - i.e. the average of the cell center velocity magnitudes - in a region on the ventricular surface 2 cm above the apex was evaluated. This region was defined as the portion included between two edges, as shown in figure 3.12,

Meshes	Mesh 1	Mesh 2	Mesh 3	Mesh 4	Mesh 5	Mesh 6
n^o of elements	71824	234103	341044	445125	618792	771771

Table 3.3: Meshes used for the sensitivity analysis for the healthy patient-specific geometry

which was made of 20 elements for the mesh 1, 250 for the mesh 6.

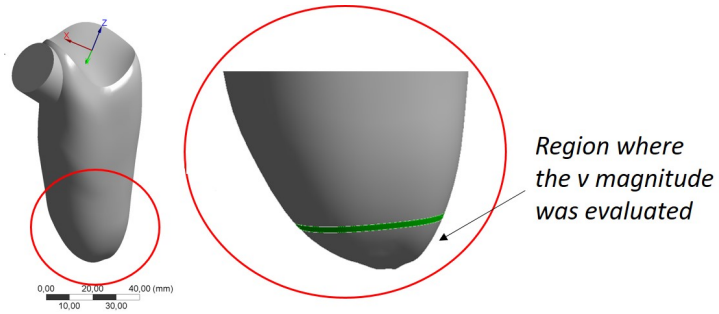

Figure 3.12: Zoom on the apical portion of the LV. The region where the velocity magnitude of each cell center's element was computed to determine the optimal grid resolution is indicated by the arrow.

All the meshes have a refinement on the edge close to the ventricular apex, as it is shown in figure 3.13b. That is why it was not reliable to evaluate the average velocity in the apical region, where all the meshes were similar.
The comparison between the averaged velocity magnitude obtained in the same region considering the six meshes allowed to select the proper grid.
Concerning the pathological patient specific geometry (figure 3.10b), the same procedure just described was followed. In particular, six meshes with different number of tetrahedral elements were built. The investigated meshes are collected in table 3.4.

Meshes	Mesh 1	Mesh 2	Mesh 3	Mesh 4	Mesh 5	Mesh 6
n^o of elements	208679	234103	334815	473428	625575	877896

Table 3.4: Meshes used for the sensitivity analysis for the HF patient-specific geometry

As described for the healthy patient-specific model, the average velocity mag-

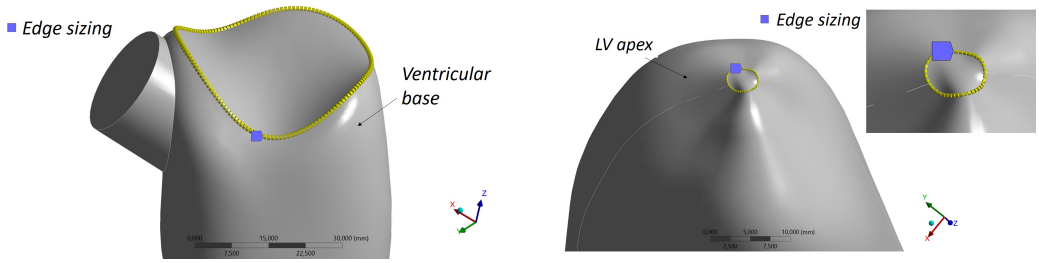

(a) (b)

Figure 3.13: Edge sizing (element size = 0.8 mm) on the ventricular base (a); Edge sizing (number of divisions = 20) on the ventricular apex (b)

nitude in a region on the ventricular wall 2 cm above the apex was evaluated, composed by 32 elements for the mesh 1 and 230 for the mesh 6. The comparison between the averaged velocities in time obtained for the six meshes allowed to select the proper grid.

3.6.2 Grid motion

The cardiac cycle was simulated thanks to the mesh motion, which is obtained implementing specific User Defined Functions (UDFs). These functions are written in C language and assign three values of displacement along the three directions of the Cartesian reference system, u_x, u_y, u_z, to each node of the grid of the ventricle wall. In particular, these UDFs allow to assign two movements that characterize the motion of the LV: compression and twist during systole and dilation and untwist during diastole. In the following sections, the UDFs written for all the models are described.

Healthy paradigmatic LV

The UDF for the motion of the paradigmatic healthy LV was implemented based on the one previously implemented by researchers at the Biomechanics group at Politecnico di Milano, that was further optimized. In particular, this first UDF was suitable to simulate only the systolic phase of the cardiac cycle and the LV movement was limited to the compression.
The UDFs' outputs are the three components of the displacement, which are assigned to the ventricular wall.
In order to simulate the contraction/dilation movement, the displacement was assigned as normal to the LV wall ($u_\perp$) and expressed as the product of three functions:

- $\delta(z)$ is a 6th order polynomial which assigns a specific value of displacement as a function of z coordinate (i.e. along the axial direction of the ventricle). This function was calculated considering the hypotesis of homothetic contraction of the LV with an ejection volume of 70 ml.

- $\sigma(z)$ is a piecewise function (3.6.1) which guarantees a smooth link between the moving LV and the still valvular plane. It is equal to 1 if z $\geq$ 20 mm (approximately below 1/3 of the axial extension of the ventricle), otherwise it corresponds to a parabolic function.

$$\sigma(z) := \begin{cases} 8.14\sqrt{z + 0.0004} - 0.1628 & \text{if } 0 \leqslant z < 0.02 \\ 1 & \text{if } z \geqslant 0.02 \end{cases} \tag{3.6.1}$$

- *f(t)* is a cosines Fourier series which gives the physiological ejection flow rate pattern over time for simulating the systole (figure 3.14a) or it is a sines and cosines Fourier series which gives the physiological filling flow rate over time for simulating the diastole (figure 3.14b).

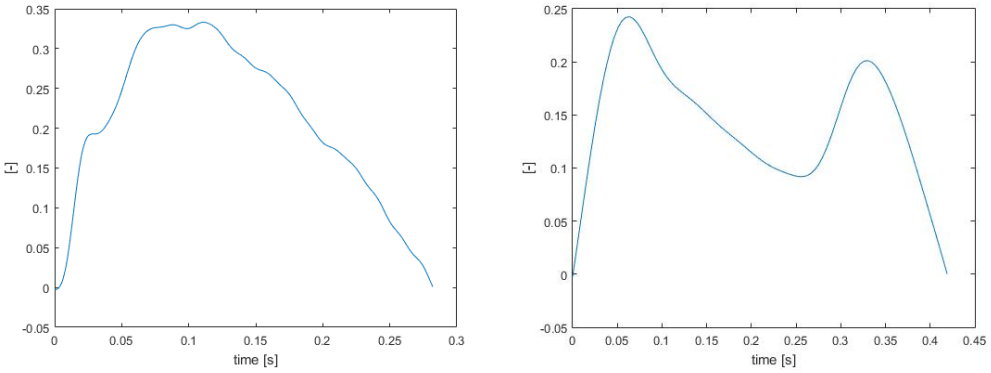

(a) (b)

Figure 3.14: Time function $f(t)$ during sistole (a) and diastole (b)

The displacement is finally multiplied by a coefficient k, which assigns the desired ejection volume (70 ml, physiological value for a healthy LV). Accirdingly, the displacement equations assume the form 3.6.2 for the systolic phase and 3.6.3 for the diastolic one.

$$u_{\perp}(z,t) = k\,\delta(z)\;f(t)\;\sigma(z) \tag{3.6.2}$$

$$u_{\perp}(z,t) = -k\,\delta(z)\;f(t)\;\sigma(z) \tag{3.6.3}$$

In addition, it was necessary to correct the function *f(t)* because it was noticed during the simulation of the diastole that the mitral mass flow rate did not follow the trend shown in figure 3.14b. In fact, the second peak resulted higher than prescribed. This is due to the dependence of the assigned displacement on the current radius of the cross sectional circumference of the ellipsoid, which is bigger in the final part of the diastole. In order to correct this imprecision in the mass flow rate, the function *f(t)* was multiplied by the parabolic function *g(t)* shown in figure 3.15, defined in 3.6.4.

$$g(t) := \begin{cases} 5.7((\frac{1}{k})^{1/8} - 1)t^2 + 1 & \text{during diastole} \\ 12.6((\frac{1}{k})^{1/8} - 1)(t^2 - 0.564t) + (\frac{1}{k})^{1/8} & \text{during systole} \end{cases} \tag{3.6.4}$$

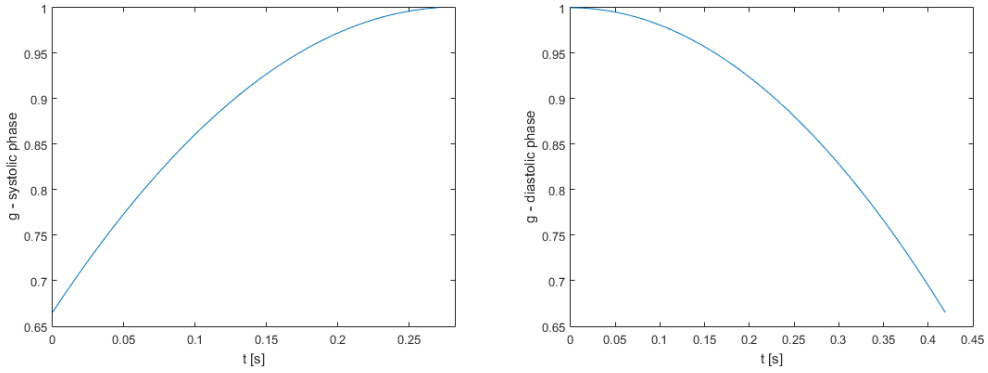

(a) (b)

Figure 3.15: Time function $g(t)$ during sistole (a) and diastole (b) for k=26

The parameters of the diastolic function *g(t)* were optimized through a trial and error approach, evaluating the mitral mass flow rate. In fact, it is known that the E/A ratio (the ratio between the amplitudes of the first peak and the second one in figure 3.14b) has to be $1 < \text{E/A} < 2$, as assessed by Nagueh et al. in [64]. Concerning the systolic phase, the parabolic function was obtained as the symmetric of the diastolic one. Note that *g(t)* depends on k, since the previously described error resulted more evident increasing the contractile capacity of the ventricle, i.e. increasing k.

It is well known that the myocardial fibers of the ventricle contract and twist. This second movement is illustrated in figure 3.16. In particular, during the ejection phase, the torsion consists in a counterclockwise rotation of the apex and clockwise rotation of the base. This movement is followed by the recoil (untwist) during the diastole [65]. In order to simulate the

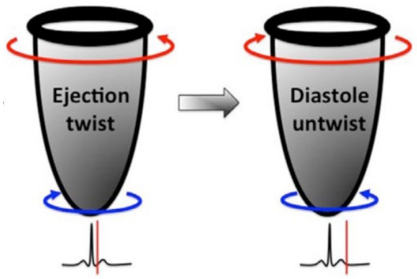

Figure 3.16: Relative rotation of the LV base (red curved arrow) and apex (blue curved arrow) during systole and diastole [65]

twist/untwist movement, the displacement was assigned as tangential to the ventricular wall ($u_{\parallel}$), i.e. tangential to the circumferences in the x-y plane. This displacement is calculated as the product between R and $\Delta\varphi$:

- R is the radius of the circumference (cross section of the ellipsoid in the plane x-y) where the node that must be moved is located, that is simply calculated as $R = \sqrt{x^2 + y^2}$
- $\Delta\varphi$ is defined as the product of three functions:
  - δ_{rot}(z) is the function 3.6.5 that assigns the maximum value of rotation to the apex (z_{max}) and that decreases linearly moving towards the base (z_{min}), up to zero.

$$\delta_{rot} = \frac{z - z_{min}}{z_{max} - z_{min}} \tag{3.6.5}$$

  - f_{rot}(t) for the systolic phase is the sines and cosines Fourier series shown in figure 3.18a. It is the interpolation of the black curve shown in figure 3.17b (the section between the two vertical lines, i.e. systolic phase of the cycle), which gives the temporal sequence of the left ventricular twist rate (°/s). This curve, that was found in literature [65], corresponds to the difference between the apical rotational rate curve (blue curve in figure 3.17b) and the basal one (red curve in figure 3.17b). f_{rot}(t) for the diastolic phase is the sines and cosines Fourier series shown in figure 3.18b, which reproduces the trend of the second part of the black curve in figure 3.17b, that is the twist rate after the closure of the aortic valve (i.e. diastolic phase of the cycle).
  - $\sigma(z)$ is the same previously defined (function 3.6.1.

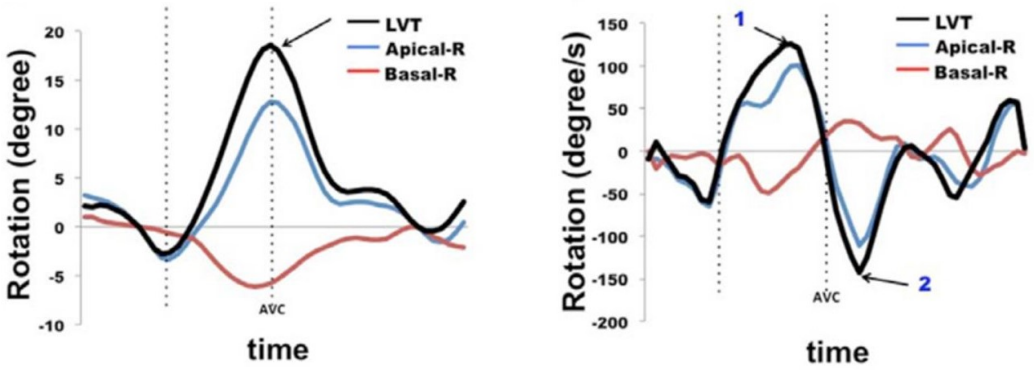

(a) LV rotational curves (b) LV rotational rate curves

Figure 3.17: Temporal sequence of LV twist. Red lines correspond to the base rotation (a) or rotational rate (b), blue to the apex rotation (a) or rotational rate (b), black to the difference between basal and apical rotation (a) or rotational rate (b). The rotational rate trends (b) are obtained deriving in time the rotation trends (a). These values are taken from a healthy subject. The point AVC corresponds to the closure of the aortic valve.

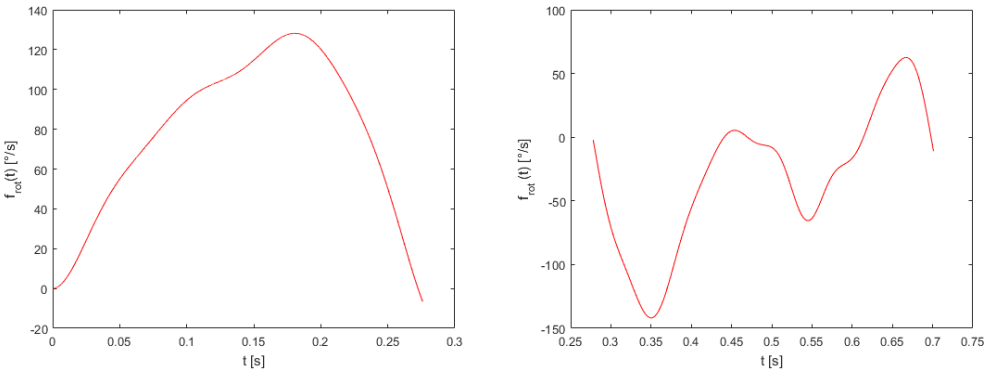

(a) $f_{rot}(t)$ during systole (b) $f_{rot}(t)$ during diastole

Figure 3.18: LV rotational rate curves during systole (a) and diastole (b), obtained through the interpolation of the black curve in figure 3.17b

$\Delta\varphi$ is finally multiplied by the coefficient 0.0174 (i.e. $\pi/180^o$) to convert the twist rate from ^{o}/s to rad/s.

In this way, $u_{\parallel}$ is defined by the expression 3.6.6 during systole and 3.6.7 during diastole.

$$u_{\parallel} = R\ \Delta\varphi = R\ 0.0174\ \delta_{rot}(z)\ f_{rot}(t)\ \sigma(z) \tag{3.6.6}$$

$$u_{\parallel} = R\ \Delta\varphi = -R\ 0.0174\ \delta_{rot}(z)\ f_{rot}(t)\ \sigma(z) \tag{3.6.7}$$

Thanks to the two angles ϑ and φ, shown in figure 3.19 and defined in 3.6.8 and 3.6.9, it was possible to project the two just described displacements $u_{\perp}$ and $u_{\parallel}$ along the 3 directions of the reference system.

$$\varphi = arctg\frac{y}{x} \tag{3.6.8}$$

$$\vartheta = arctg\frac{z - z_p}{\sqrt{x^2 + y^2}} \tag{3.6.9}$$

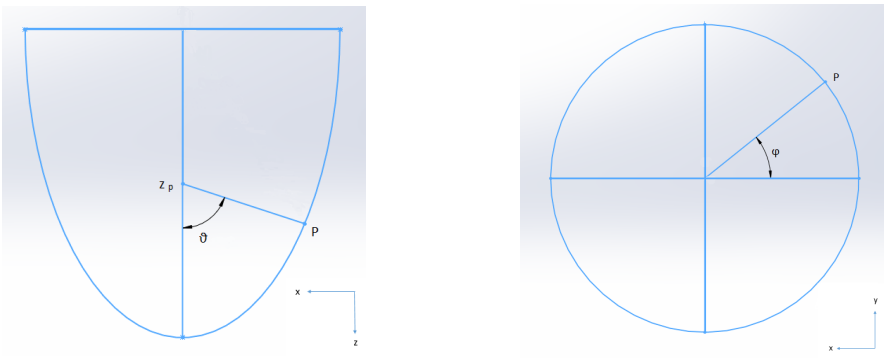

(a) (b)

Figure 3.19: Definition of the angles: ϑ (a) and φ (b)

The function z_p used to define the two angles and reported in 3.6.10, is a function of z which assigns to each node the value of the z-coordinate of the intersection point between the z axis and the axis perpendicular to the semi-ellipsoid passing through that point.

$$z_p(z) = 0.5244\ z + 9e - 16 \tag{3.6.10}$$

The three components of the displacement, projections in the three directions of the reference frame, are reported in 3.6.11 , 3.6.12 and 3.6.13.

$$u_x = -u_{\perp} \cos\vartheta \cos\varphi - u_{\parallel} \sin\varphi \tag{3.6.11}$$

$$u_y = -u_{\perp} \cos\vartheta \sin\varphi + u_{\parallel} \cos\varphi \tag{3.6.12}$$

$$u_z = -u_{\perp} \sin\vartheta \tag{3.6.13}$$

Healthy patient-specific LV

In order to adapt the mesh motion UDF simulating the LV movement along the cardiac cycle for the patient-specific LV model, three main modifications to the UDF implemented for the paradigmatic model were performed.

– *Roto-translation of the reference frame*
It is evident in figure 3.9b that the absolute reference frame does not coincide with the one used for the paradigmatic model. Since it was necessary to refer to a local reference frame whose z axis points to the ventricular apex, the absolute nodal coordinates were transformed to local coordinates through three rotational matrices. The global coordinates of one node of the apex were identified (x_{apex}, y_{apex} and z_{apex}). Then, the passage of the local x-axis through this point was imposed through two subsequent rotations of the reference frame by α and β, reported respectively in 3.6.15 and 3.6.14.

$$\beta = \arcsin \frac{z_{apex}}{\sqrt{x_{apex}^2 + y_{apex}^2 + z_{apex}^2}} \tag{3.6.14}$$

$$\alpha = \begin{cases} \arccos \frac{x_{apex}}{cos\beta\sqrt{x_{apex}^2+y_{apex}^2+z_{apex}^2}} & \text{if } y_{apex} > 0 \\ 2\pi - \arccos \frac{x_{apex}}{cos\beta\sqrt{x_{apex}^2+y_{apex}^2+z_{apex}^2}} & \text{if } y_{apex} < 0 \end{cases} \tag{3.6.15}$$

Substituting in 3.6.15 and 3.6.14 the apex coordinates of the healthy patient specific LV, α resulted equal to 3.0435 rad and β to -1.2053 rad.
With the just defined two subsequent rotations, the local x-axis was forced to pass through the apex. In order to have the local z-axis passing through the apex of the LV, an additional rotation of the reference frame by 90^o was performed.
Finally, a shift of the local reference frame (z_{shift}=1.91 cm) along the z_{local} direction was applied. This shift allowed the moving portion of the LV to start from z_{local}=0, excluding from the movement the portion of the LV that intersects the aorta.
To adapt the UDF to the new geometry, few lines of the UDF code were modified. In particular, the nodal coordinates were converted in the new local frame, according to equation 3.6.16.

$$\begin{bmatrix} x_{local} \\ y_{local} \\ z_{local} \end{bmatrix} = \left[Rot_{90^o}\right] \left[Rot_{\beta}\right] \left[Rot_{\alpha}\right] \begin{bmatrix} x_{global} \\ y_{global} \\ z_{global} \end{bmatrix} + \begin{bmatrix} 0 \\ 0 \\ -z_{shift} \end{bmatrix} \tag{3.6.16}$$

where Rot_{90}, Rot_{α} and Rot_{β} are the three rotational matrices, computed according to 3.6.17.

$$\left[Rot_{\alpha}\right] = \begin{bmatrix} cos\alpha & sin\alpha & 0 \\ -sin\alpha & cos\alpha & 0 \\ 0 & 0 & 1 \end{bmatrix} \quad \left[Rot_{\beta}\right] = \begin{bmatrix} cos\beta & 0 & sin\beta \\ 0 & 1 & 0 \\ -sin\beta & 0 & cos\beta \end{bmatrix}$$

$$\left[Rot_{90^o}\right] = \begin{bmatrix} cos\ 90^o & 0 & -sin\ 90^o \\ 0 & 1 & 0 \\ sin\ 90^o & 0 & cos\ 90^o \end{bmatrix} \tag{3.6.17}$$

The three components of the displacement were finally expressed in the global system through the inverse of the global rotational matrix (the product of the three matrices 3.6.17) to update the global nodal coordinates at each time step.

– *Adaptation of $\delta(z)$*
The function $\delta(z)$ that assigns a displacement value as a function of the z-coordinate was adapted to the new dimensions of the real LV. The ventricular motion was still assumed as an omothetic contraction/dilation.

– *Adaptation of k*
The value of the constant k was changed in order to guarantee an ejected volume equal to 70 ml (k=26).

– *Adaptation of $\sigma(z)$*
The function $\sigma(z)$ was adapted since some points have negative z_{local} coordinates. The resulting piece wise $\sigma(z)$ is the function 3.6.18.

$$\sigma(z) := \begin{cases} 0 & \text{if } z_{local} \leqslant 0 \\ 8.14\sqrt{z_{local} + 0.0004} - 0.1628 & \text{if } 0 \leqslant z_{local} \leqslant 0.02 \\ 1 & \text{if } z_{local} \geqslant 0.02 \end{cases} \tag{3.6.18}$$

HF paradigmatic LV pre-LVAD implant

To move the HF LV model without inflow cannula (pre-LVAD implant model), the UDF implemented for the healthy paradigmatic LV was modified. Since the shape of the dilated ventricle is no more a semi-ellipsoid, in order to achieve an homothetic contraction, a constant in time coordinate $z_{equator}$ was defined, highlighted in figure 3.20.

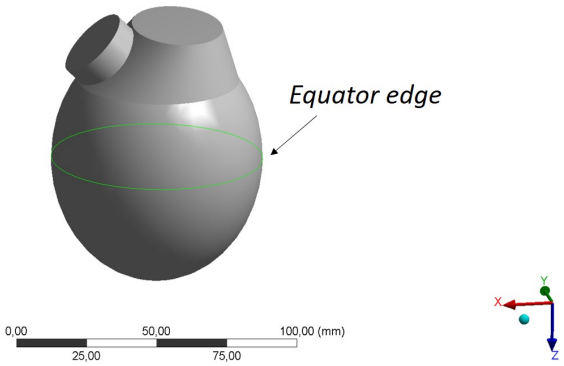

Figure 3.20: Equator edge, corresponding to $z_{equator}$ coordinate

Due to the shift of the reference frame, whose origin now coincides with the center of the ventricular base (see figure 3.10a), $z_{equator}$ corresponds to the distance between the ventricular base (z=0) and the x-y symmetry plane of the ellipsoid.
Thanks to the definition of $z_{equator}$, it was possible to introduce the coordinate $zz = z - z_{equator}$ that allows to discriminate the points below ($zz > 0$) and above ($zz < 0$) the equator. In fact, each node above the equator and the corresponding one below, move in a symmetric way with respect to the equatorial plane. In order to impose this symmetric movement, δ was no more expressed as a function of z but as a function of zz:
if ($zz < 0$), $\delta(zz) = \delta(-zz)$
The displacement components u_x and u_y of each node above the equator are the same as the ones of the corresponding node below the equator, while u_z is the opposite.

HF paradigmatic LV post-LVAD implant

Regarding the post-implant model, two different UDFs, one for the motion of the ventricular wall and one for the motion of the inflow cannula, were necessarily implemented.

1. UDF for the motion of the ventricle

   It was hypothesized that the the portion of the ventricle around the cannula (apex) translates only in z direction, as the cannula itself. In this way, a sort of suture was modeled. Under this assumption, the motion of the nodes of the ventricular wall depends on the region where they are located:

   – The *valvular plane* is still (as before);

– The *apex* translates in z direction;

– The part in between contracts in the three directions and twists.

Given the fact that the apex does not contract in the other two directions (x and y), it has been necessary to add a connection function γ that guarantees the continuity of different displacement functions along the LV wall in order to obtain a smooth deformed wall configuration.
Going into the implementation details, in order to define the just itemized zones (i.e. *valvular plane*, *apex* and part in between) a new time dependent coordinate has been introduced: z_{apex}. It corresponds to the z coordinate of the nodes located on the circumference of contact between the ventricular wall and the cannula (where the cannula is inserted), highlighted in figure 3.21.

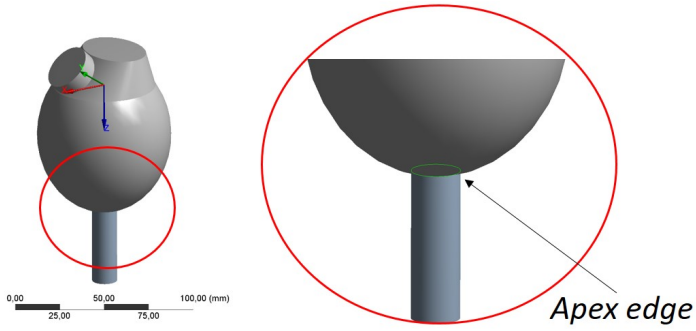

Figure 3.21: Zoom on the region of cannula insertion. The arrow points the so-called apex edge, corresponding to z_{apex} coordinate.

Since the ventricular wall moves over time, a code able to detect the updated coordinates of the apex (z_{apex}) at each time step was implemented and included in the UDF as reported in the algorithm 3.6.1.

The function F_CENTROID(j,f,tf) stores in the vector j the coordinates of the centroid of each cell of the domain (*f_loop(f, tf)* cycles all the cells). The algorithm assigns at each time step to z_{apex} the z coordinate of the cell with the highest value of z.
Thanks to the definition of z_{apex}, $z_{equator}$ and zz, it has been possible to define the piece wise movement of the ventricular wall, as follows:

- $zz < 0$
  $u = k\ \delta(-zz)\ \sigma(z)\ f(t)$
  $u_x = -u \cos\vartheta \cos\varphi - R\Delta\varphi \sin\varphi$
  $u_y = -u \cos\vartheta \sin\varphi + R\Delta\varphi \cos\varphi$

Algorithm 3.6.1: Algorithm to compute z_{apex}

```
1  conta=0;
2  begin_f_loop(f, tf)
3  if conta=0 then
4  |  F_CENTROID(j,f,tf);
5  |  z_apex = j[2] ;
6  |  conta++;
7  else
8  |  F_CENTROID(j,f,tf);
9  |  if j[2] > z_apex then
10 |  |  z_apex=j[2]
11 |  end
12 end
13 end_f_loop(f, tf)
```

$$u_z = u \sin\vartheta$$

- $zz > 0$
  $u = k\ \delta(zz)\ \sigma(z)\ f(t)$

  - $zz < 0.7\ (z_{apex} - z_{equatore})$
    $u_x = -u\cos\vartheta\cos\varphi - R\Delta\varphi\sin\varphi$
    $u_y = -u\cos\vartheta\sin\varphi + R\Delta\varphi\cos\varphi$
    $u_z = -u\sin\vartheta$

  - $0.7\ (z_{apex} - z_{equatore}) < zz < 0.95\ (z_{apex} - z_{equatore})$
    $u_x = (-u\cos\vartheta\cos\varphi - R\Delta\varphi\sin\varphi)\ \gamma(zz)$
    $u_y = (-u\cos\vartheta\sin\varphi + R\Delta\varphi\cos\varphi)\ \gamma(zz)$
    $u_z = -u\sin\vartheta$

  - $zz\ > 0.95\ (z_{apex} - z_{equatore})$
    $u_x = 0$
    $u_y = 0$
    $u_z = -u\sin\vartheta$

Note that, in contrast with δ, σ depends on z and not on zz, since it serves as a connection with the valvular plane, that is located at $z = 0$. $f(t)$ does not change with respect to the healthy condition (as before,

it depends on the phase of the cardiac cycle).
The function $\gamma(zz)$ is reported in 3.6.19. It is a parabolic function that is equal to zero for $zz = 0.95\ (z_{apex} - z_{equatore})$ and equal to one for $zz = 0.7\ (z_{apice} - z_{equatore})$:

$$\gamma(zz) = \frac{\sqrt{0.95\ ((z_{apex} - z_{equator}) - zz)}}{\sqrt{0.25\ (z_{apex} - z_{equator})}} \tag{3.6.19}$$

2. UDF for the motion of the cannula

   As previously mentioned, the cannula translates upward in z direction. In order to obtain a synchronous movement between the ventricular wall and the cannula, it was necessary to define a function (z_{intime}) which gives the temporal variation of the z coordinate of the nodes of the ventricle in contact with the cannula, i.e. apex edge in figure 3.21. Given that the region of contact is a circumference whose points share the z coordinate (i.e. z_{apex}), it was sufficient to select one of them and describe its motion. In particular, a node located on the apex edge (i.e. so-called contact node) with ID equal to 19770 and coordinates $x_{ref} = 7,317e-004$, $y_{ref} = 6,9617e-003$ and $z_{ref} = 7,3085e-002$ was selected.
   Through a Matlab script, the z coordinate of the contact node is updated at each time step, summing to the current value of z the u_z calculated as previously defined for the apex region (piecewise function corresponding to the region $zz > 0.95\ (z_{apex} - z_{equatore})$). Through this procedure, discrete values of z (one for each time step) were obtained and then interpolated using the Matlab function polyfit-polyval with a 15th order polynomial, achieving the temporal variation of the z-coordinate of the contact node.
   Given that, i) the nodes belonging to the apex edge share the z-coordinate and ii) these nodes only translates along z-direction, it is possible to deduce that the temporal variation of the z-coordinate of all the nodes belonging to the apex edge is equal to the contact node's one.
   Note that, in order to obtain the contact node motion during systole, the starting point is the one previously defined (i.e. x_{ref}, y_{ref} and z_{ref}) which was extracted from the end-diastolic configuration mesh; on the other hand, for the diastole, the starting point have the coordinate of that node at the end of the systole (last position of the vector containing the discrete values of z).
   The figure 3.22 shows the interpolation of the z coordinate of the contact node in time for systole (3.22a) and diastole (3.22b).

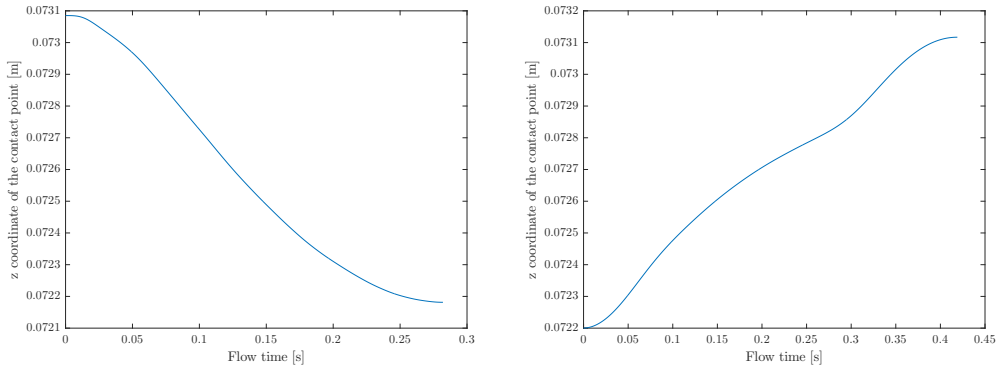

(a) (b)

Figure 3.22: Polynomial z_{intime}, during systole (a) and diastole (b)

Regarding the UDF implementation, the functions depending on z, which are z_p and δ, are expressed as functions of z_{intime}, while ϑ and φ, which depend on the three coordinates, are expressed as function of z_{intime}, x_{ref}, y_{ref}. Note that x_{ref} and y_{ref} do not change in time because the cannula only translates along z, so only the z-coordinate of its nodes changes in time.

For both the HF LV models (i.e. pre and post LVAD implant), the following modifications with respect to the healthy LV model were implemented:

- The polynomial $\delta(z)$ is modified according to the new dimensions of the dilated (i.e. HF) LVs.
- The lower capacity of contraction is given by a lower value of k.
- Concerning the torsional movement, two things change in the definition of $\Delta\varphi$: the function δ_{rot}, that is reported in 3.6.20, is now expressed as a function of z and z_{apex} and an additional multiplying factor (0.56) is introduced, because the twisting capacity is reduced for the dilated LV.

$$\delta_{rot} = \frac{z}{z_{apex}} \tag{3.6.20}$$

In the work by A. Marbrouk et al. [65], it is assessed that the rotational values are decreased for patients with dilated cardiomyopathy with reduced ejection fraction, signifying exhaustion of LV twist mechanism. In these patients the peak rotational rate is equal to 70 °/s (note that for healthy patients it is equal to 125 °/s, as it is shown in figure 3.17b).

HF patient-specific LV pre-LVAD implant

As previously described for the healthy patient-specific LV, also in this case it was necessary to adapt the mesh motion UDF implemented for the paradigmatic model to the patient-specific one. Four main modifictaions were performed:

- *Roto-translation of the reference frame*
  The reference frame was roto-translated using the operation described in 3.6.16, in order to impose the z axis to pass by the ventricular apex and to shift the origin where the moving portion of the ventricle begins. Substituting in 3.6.15 and 3.6.14 the apex coordinate of the patient-specific HF LV, α resulted equal to 4.0007 rad and β to -1.3139 rad. z_{shift} was set equal to 1.55 cm.
  In this way, the so-called local reference frame was obtained.

- *Adaptation of $\sigma(z)$*
  The function $\sigma(z)$ was the one defined in the equation 3.6.18 to link the moving portion of the ventricle with the still valvular plane.

- *Adaptation of $\delta(z)$*
  The function $\delta(z)$ was adapted to the new dimension of the LV.

- *Adaptation of k*
  The constant k was changed, in order to simulate different contractile capacity. In particular, k was equal to 17 to obtain an ejection volume of 35 ml; 5 to obtain an ejection volume equal to 10 ml.

In addition, since the shape of the patient-specific HF LV was no more a truncated ellipsoid, it was not necessary to define in the UDF code the $z_{equator}$ coordinate. Finally, Concerning the twisting movement, it was reduced with respect to the physiological torsion as described for the paradigmatic HF model.

HF patient-specific LV post-LVAD implant

The mesh motion UDF for the HF patient specific LV post LVAD implant have the same implementation details described for the same paradigmatic model:

- Two grid motion UDFs, one for the motion of the ventricular wall and one for the motion of the cannula are defined.

- Regarding the motion of the ventricular wall, it is subdivided in three zones (i.e. still *valvular plane*, translating *apex* and portion in between that contracts and twists).

- The inflow cannula translates in z direction, together with the apical portion of the ventricle.

- Two time-varying z-coordinates are defined: z_{apex} and z_{intime}. z_{apex} is iteratively computed with algorithm 3.6.1. z_{intime} was adapted to the new geometry, as it is described below.

The adaptation of the paradigmatic UDF to the patient-specific model was reached through five main modifications:

- *Roto-translation of the reference frame, adaptation of $\sigma(z)$ and $\delta(z)$*
  These three modifications are the same listed above for the HF-patient specific pre-LVAD implant model: the reference frame was roto-translated through the operation described in 3.6.16; the function $\sigma(z)$ is the piece-wise one defined in the equation 3.6.18 and $\delta(z)$ was adapeted to the HF LV size.

- *Adaptation of k*
  The factor k was set equal to 7 to obtain a difference in volume between end-systolic and end-diastolic configuration of 10 ml.

- *Adaptation of z_{intime}*
  Since the contact edge between the cannula and the ventricular wall is no more a circumference whose points share the z-coordinate, the contact point with the lower z_{local} was chosen to compute z_{intime}.
  The points of the ventricular wall with $z_{local} \geq z_{intime}$ only translated in z_{local} direction. The linking function between the purely translating region ($z_{local} \geq z_{intime}$) and the contracting and twisting one ($0.02 \leq z_{local} \leq 0.5\ z_{apex}$) is defined in 3.6.21, where $c = z_{intime}$, $b = 8c - \sqrt{80c^2 - 8cz_{apex}}$, $a = -b^2/8c$.

$$\epsilon(z_{local}) = \sqrt{\frac{1}{a}(z_{local} + \frac{b^2}{4a} - c)} - \frac{b}{2a} \tag{3.6.21}$$

  The function ϵ was computed such that $\epsilon = 0$ if $z_{local} = z_{intime}$ and $\epsilon = 1$ if $z_{local} = 0.5 z_{apex}$.

3.6.3 Numerical inertia

In our simulations, initially, all the fluid inside the LV was at rest, so the computation of several cycles was required to reach a periodic solution and a full development of the flow. The WSS trend in a region close to the ventricular apex for the healthy patient-specific LV model was evaluated at each cardiac cycle, since it is the variable of interest. The considered region is highlighted in the section 3.6.6 in figure 3.28a. In particular, WSS trends for both systole and diastole were computed and plotted for each cycle and the percentage difference between the time-averaged WSS between each cycle and the previous one was computed, until a reasonable low value was reached.

3.6.4 Boundary conditions

In order to assign proper boundary conditions, it was necessary to create named selections. In particular, for both the paradigmatic and patient-specific healthy and HF pre-LVAD-implant LVs, the following surfaces were named, as shown in figures 3.23 and 3.24: *ventricle*, *aortic_valve*, *mitral_valve*. For the HF LVs post-LVAD-implant, (paradigmatic and patient-specific), since the cannula is present, the following surfaces were named, as shown in figure 3.25: *ventricle*, *aortic_valve*, *mitral_valve*, *wall_cannula* and *velocity_inlet*.

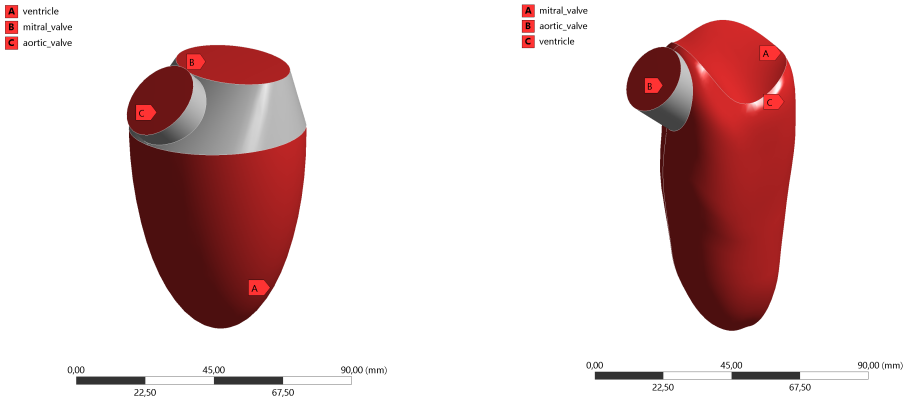

(a) (b)

Figure 3.23: Named selection for the healthy LV models: paradigmatic (a) and patient-specific (b)

For the healthy LVs, it was possible to find in literature (Imanparast et al [66]) the trends of the pressure in time on the valvular orifices, which are shown in figure 3.26a. These curves were interpolated through a sines and

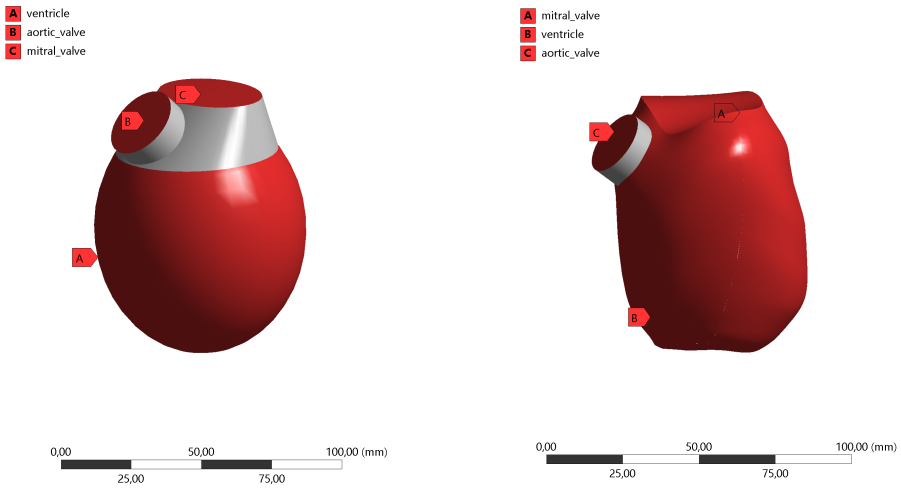

(a) (b)

Figure 3.24: Named selections for HF LV pre-LVAD-implant models: paradigmatic (a) and patient specific (b)

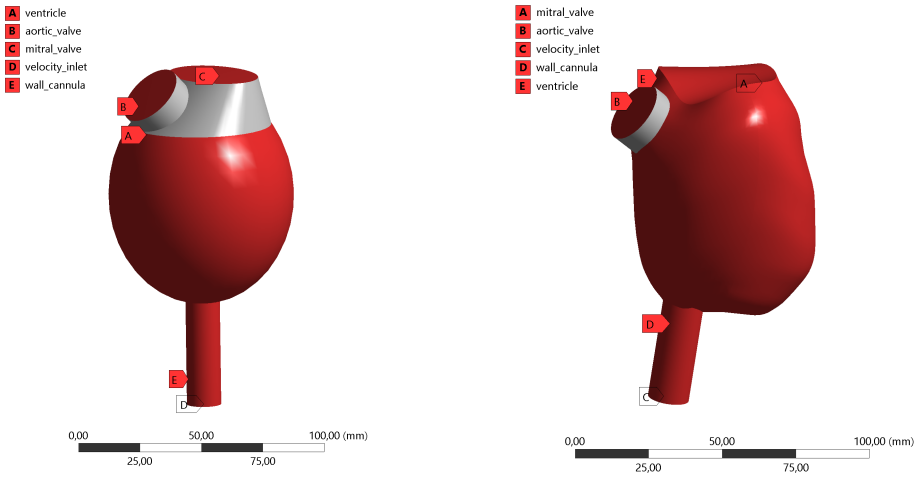

(a) (b)

Figure 3.25: Named selections for HF LV post-LVAD-implant models: paradigmatic (a) and patient specific (b)

cosines Fourier series for the aortic curve and a 10th order polynomial for the mitral curve, as shown in figure 3.26b.

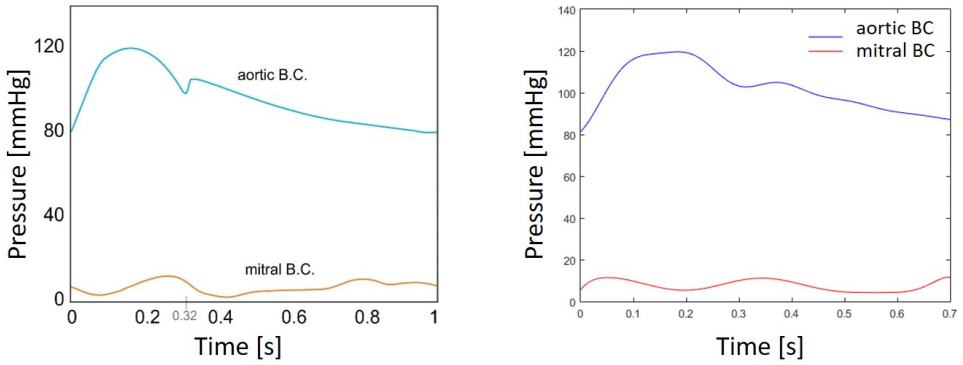

(a) (b)

Figure 3.26: Pressure boundary conditions: trends found in literature [66] (a) and our interpolation (b)

In this way, physiological pressure boundary conditions were assigned on the valvular orifices. Since the valvular pressure trends are not available for the HF LVs, it was necessary to apply zero-pressure boundary conditions on the valvular orifices. Nevertheless, the boundary condition that determines LV's inflow and outflow is the grid motion, so these zero-boundary conditions do not strongly influence the fluid dynamics.

In the following sections, the applied boundary conditions are described.

Healthy LVs, paradigmatic and patient-specific

For the systolic phase simulation, the following boundary conditions were imposed:

- *Moving wall* (motion relative to adjacent zone given by components) for the named selection *ventricle*;
- Pressure assigned through an interpreted DEFINE_PROFILE UDF which assigns the temporal trend of aortic pressure shown in figure 3.26b to the named selection *aortic_valve*;
- *Stationary wall* for the named selection *mitral_valve*.

For the diastolic phase simulation, the following boundary conditions were imposed:

- *Moving wall* (motion relative to adjacent zone given by components) for the named selection *ventricle*;
- Pressure assigned through an interpreted DEFINE_PROFILE UDF which gives the temporal behavior of mitral pressure shown in figure 3.26b for the named selection *mitral_valve*;
- *Stationary wall* on the named selection *aortic_valve*.

HF LVs, paradigmatic and patient-specific - pre and post LVAD implant

For the systolic phase simulation, the following boundary conditions were imposed:

- *Moving wall* (motion relative to adjacent zone given by components) for the named selection *ventricle*;
- *Moving wall* (motion relative to adjacent cell zone given as translational with direction -z) for the named selection *wall_cannula* and *wall_cannula_shadow*. This last zone appears automatically in the boundary condition dialog box on Fluent loading the mesh. It represents the region of the wall of the cannula inside the ventricle that is in contact with the interior of the ventricle.
- Velocity magnitude normal to boundary equal to -0.54 m/s on the named selection *velocity_inlet*. This value has been set in order to guarantee a flow rate of 5 l/min.
- *Stationary wall* on the named selections *mitral_valve*;
- Pressure equal to zero on the named selection *aortic_valve* (*pressure_outlet*).

For the diastolic phase simulation, the following boundary conditions were imposed:

- *Moving wall* (motion relative to adjacent zone given by components) for the named selection *ventricle*;
- *Moving wall* (motion relative to adjacent cell zone given as tranlational with direction z) for the named selection *wall_cannula* and *wall_cannula_shadow*;
- Velocity magnitude normal to boundary equal to -0.54 m/s on the named selection *velocity_inlet*. Note that the value of the velocity at the inlet of the cannula is constant in both the phases of the cycle in order to simulate a continuous flow pump.

- Pressure equal to zero for the named selection *mitral_valve* (*pressure_inlet*);
- *Stationary wall* for the named selections *aortic_valve*.

3.6.5 Numerical method and simulation settings

In order to perform the fluid dynamic simulations (3D, transient), the meshes were imported in ANSYS Fluent 16.2.
Blood was modeled as a Newtonian fluid with viscosity μ=0.003 Pa s and density ρ=1060 kg/m^3.
In the cases of healthy and HF pre-implant LVs, the UDFs for the grid motion are compiled, loaded and assigned to the named selection *ventricle* in the enabled *Dynamic Mesh* dialog box, shown in figure 3.27a. As mesh methods *Spring Smoothing* and *Local Cell*, *Local Face* and *Region Face Remeshing* were set, as shown in figure 3.27b.

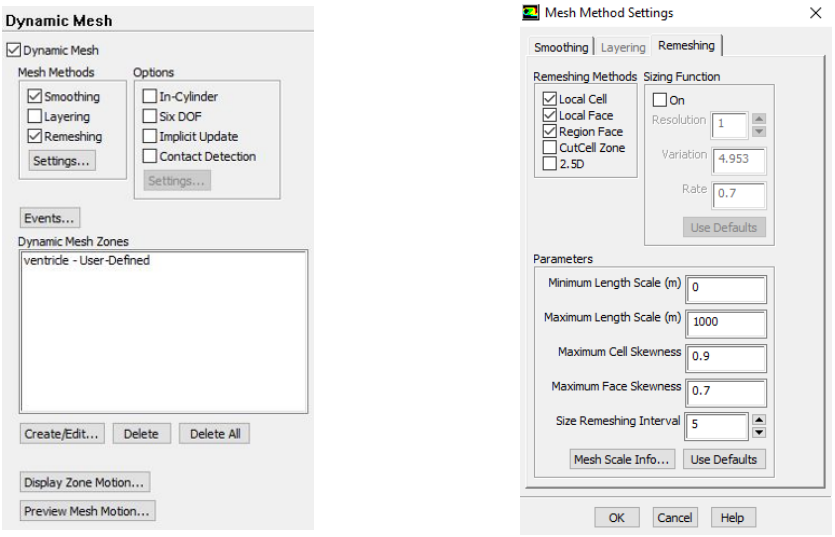

(a) (b)

Figure 3.27: (a) Example of the dynamic mesh dialog box where the UDF for the zone *ventricle* was defined. (b) Mesh method settings dialog box

In the case of HF post-implant LV, the two grid motions for the two fluid domains (ventricular wall and LVAD inflow cannula) are defined through the command DEFINE_GRID_MOTION in the same text file that is compiled and loaded in ANSYS Fluent only once. The ventricle mesh motion is assigned to the named selection *ventricle*, while the cannula mesh motion to the named selections *velocity_inlet*, *wall_cannula* and *wall_cannula_shadow*. In this way, all the elements of the cannula move together. Once all these

dynamic mesh motions are applied, the corresponding zones are listed in the window of the dynamic mesh dialog box (figure 3.27a).
The chosen numerical scheme is the Pressure-Velocity Coupling SIMPLE algorithm, with a 2nd order upwind spacial discretization and 1st order implicit transient formulation. For the under relaxation factors, the following values are set: 0.3 for pressure and 0.7 for momentum.
As a convergence criteria of the solution, the residuals for continuity and x,y,z-velocity are set to 10^{-5}. The calculations are run with a time step equal to 0.001 s and 150 iterations/time step. The number of time steps depends on the phase of the cycle: 282 for the systole and 419 for the diastole. For all the paradigmatic models, the simulations start with the systolic phase (from t=0 s to t=0.282 s) followed by the diastolic one (from t=0.282 s to 0.701 s). Regarding the patient-specific model, since the initial configuration is the end-systolic one, the simulations start with the diastole, followed by the systole.

3.6.6 WSS extraction

During the simulations, the values of WSS modulus and its components are extracted and stored in ASCII files at each time step for the cell center of each element of the LV surface (calculation activities, automatic export). Thanks to a Matlab script, the ASCII files are processed in order to obtain plots that describe the trend in time of the averaged zWSS in the apical regions, shown in figure 3.28.

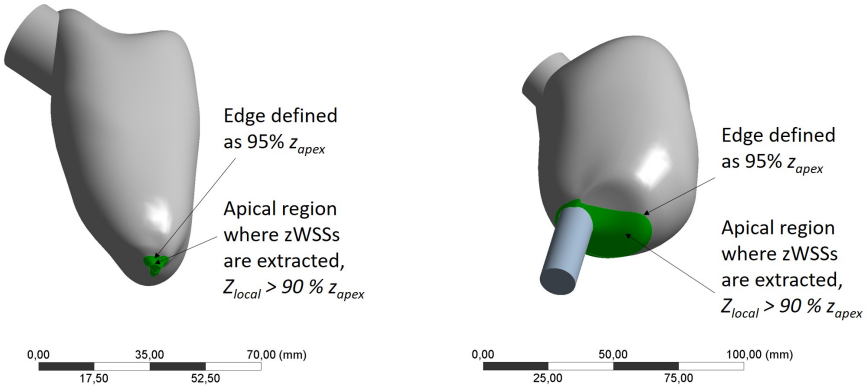

(a) (b)

Figure 3.28: Apical region (in green) where the zWSS were evaluated for the patient-specific healthy (a) and HF post-LVAD implant (b) LVs

These regions are identified as portion of the ventricular wall whose z-coordinate is higher than a pre-defined percentage of z_{apex}, which is iteratively computed at each time step (i.e. the points of the green regions are the ones where z_{local} $> 95\%$ z_{apex}).
The region used for the HF LV pre-LVAD implant model is not reported, since it is the same as the one considered for the post-LVAD implant one (figure 3.28b).

Chapter 4

Results

In the present chapter, the obtained results are reported.
Firstly, the experimental results are presented. As detailed in paragraph 3.3, four main conditions were characterized, namely:

- Interaction between non-activated platelets and non-activated ECs;
- Interaction between activated platelets and non-activated ECs;
- Interaction between non-activated platelets and activated ECs;
- Interaction between activated platelets and activated ECs.

In order to characterize these four conditions, three steps were followed, as detailed in the introduction of chapter 3:

1. Characterization of the effect of TNF-α on HUVECs (paragraph 4.1);
2. Characterization of the activation level of the two cell types due to platelet-EC interaction through PAS assay and flow cytometry (Annexin V and P-Selectin on platelet samples and ICAM-1, VCAM-1 and E-Selectin on HUVECs, paragraph 4.2);
3. Characterization of the adhesion mechanism through SEM images acquisition and flow cytometry for $\alpha_V\beta_3$ on HUVEC sample after incubation with platelets (paragraph 4.2).

Then, the results related to the CFD study are illustrated (paragraph 4.3).

4.1 TNF-α effect on endothelial cells

A preliminary study performed at Politecnico di Milano, Departament of Chemistry, Materials and Chemical Engineering "G.Natta", was conducted with the aim of characterizing, in vitro, the inflammation potential of HUVECs. For this aim, HUVECs were exposed to different TNF-α concentrations for different exposure time, as described in paragraph 3.2.4. Firstly, the cytotoxicity of the TNFα was characterized (i.e. Alamar Blue assay), followed by the evaluation of HUVEC inflammation (i.e. ELISA). The experimental campaign was partially repeated at the University of Arizona, where the HUVEC inflammation was characterized through both ELISA and flow cytometry.

4.1.1 TNFα cytotoxicity - Alamar Blue

The Alamar Blue assay was carried out following the procedure described in paragraph 3.2.4. The purpose was to evaluate the viability of the cells, after exposure to varying TNFα concentrations for different exposure time. The output of the assay were the values of optical density (OD) read by the spectrophotometer. For each reading, also a measurement on a blank sample was performed, i.e. a well containing just the solvent (i.e. cell medium with resazurin), which was used as a control. In this way, the absorbance of the solvent was known and any change in the absorbance when measuring the sample was attributable to the metabolic activity of the cells. In addition, since each studied condition (i.e. combination of TNFα exposure time and concentration) was replicated four times, mean values and standard deviations (SDs) of OD values were calculated.
The trends of the mean values of the optical densities (i.e. OD-OD_{blank}), varying TNFα exposure time and concentration, are shown in figure 4.1.
The % viability was calculated as $OD_{sample}/OD_{control}$. $OD_{control}$ corresponds to the OD measured for the cells incubated with a null concentration of TNFα for the same period of time. The trend in time of the mean $OD_{control}$ is represented by the blue curve (i.e. C = 0 ng/ml) in figure 4.1a. The trends of the mean % viability, with corresponding SDs, varying exposure time and concentration, are shown in figure 4.2.
According to our results (figure 4.1a), it is evident that the OD increases in time for all the samples. Comparing the curves corresponding to different concentrations, it is possible to recognize two different behaviours: i) the OD curves of the samples with a low TNFα concentration (i.e. C = 0.1 and 1 ng/ml) are steeper than the reference curve (i.e. C = 0 ng/ml) up to 8 hours of TNFα exposure, after that point the slope progressively decreases;

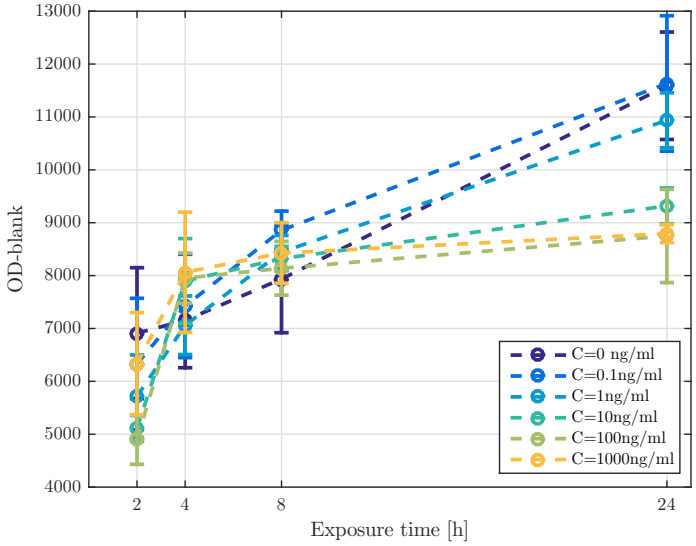

(a)

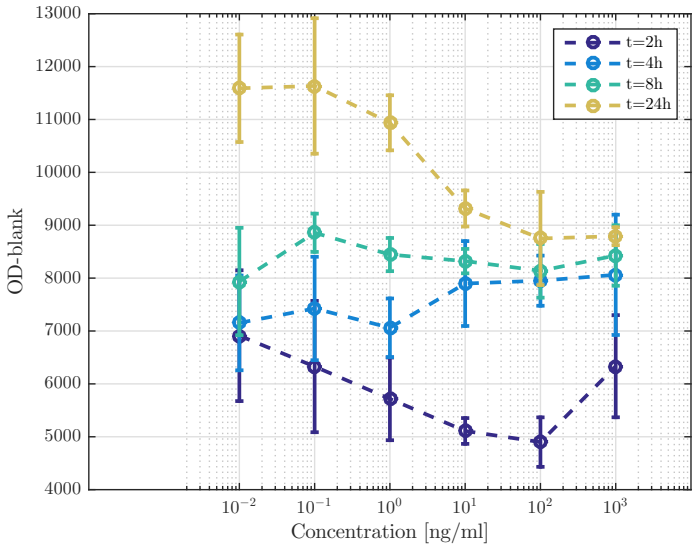

(b)

Figure 4.1: Parametric plots of the samples' OD (mean ± SD, n=4), varying the TNFα concentration (a) and the TNFα exposure time (b). In the legends, C indicates TNFα concentration and t TNFα exposure time.

ii) the OD curves of the samples with a high TNFα concentration (i.e. 10, 100 and 1000 ng/ml) are steeper than the reference curve up to 4 hours of TNF exposure, then decreasing over time. This observation is confirmed by

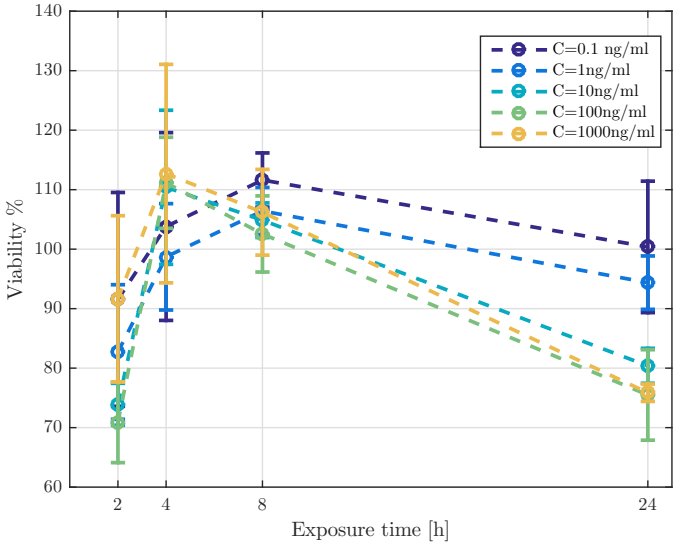

(a)

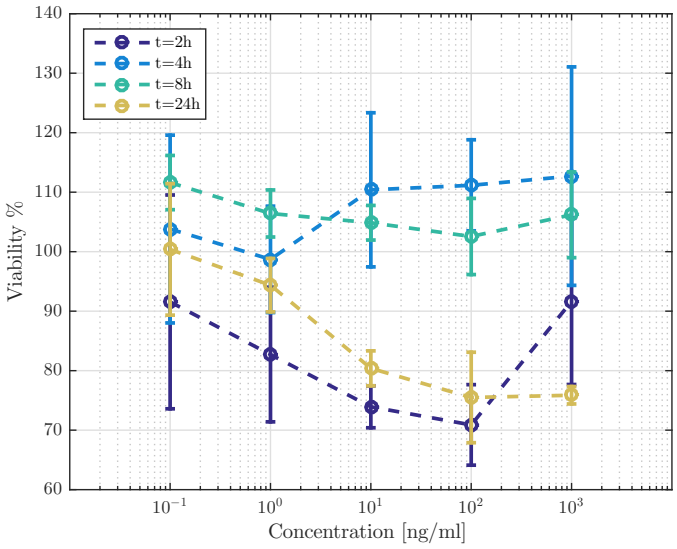

(b)

Figure 4.2: Parametric plots of the samples' % viability (mean ± SD, n=4), i.e. ratio between the OD of the sample and the OD of the control, varying the TNFα concentration (a) and the TNFα exposure time (b). In the legends, C indicates TNFα concentration and t TNFα exposure time.

the the % viability trends in figure 4.2a: the viability increases up to 8 hours for samples with low TNFα concentration and then it reverses its trend; the

same reversal of this tendency happens at 4 hours for the samples with high TNFα concentration. A possible explanation of this behavior is that the effect of TNFα, that affects the cells viability, becomes more evident after 4 hours of TNFα exposure if the concentration is sufficiently high, otherwise the effect becomes evident after 8 hours. Observing the plots in figure 4.1b, it is possible to notice that the OD decreases with increasing TNFα concentration. The curve that better fits this TNFα concentration-dependent behavior is the one for the samples incubated for 24 h (yellow curve in figure 4.1b). It could be explained by the fact that the longer is the exposure time, the more the cells are sensitive to that concentration.
Nevertheless, the % viability remains high, i.e. above 70%, for all the considered TNF-α concentrations and exposure times (figure 4.2).

4.1.2 TNFα inflammation potential - ELISA

The supernatants of HUVECs incubated with TNFα were assayed using the ELISA kits in order to evaluate the expression of soluble inflammation markers, i.e. ICAM-1, VCAM-1, E-selectin.
The output of each ELISA are OD values associated with each well, read by the spectrophotometer at two different wavelengths (i.e. 450 nm and 570 nm). The post-processing procedure of the results is described in paragraph 3.4.1.
The concentration of each of the three markers related to each sample was obtained. Since each sample is associated to a precise TNFα concentration and a specific incubation time interval, the correlation between TNFα concentration/TNFα exposure time and ICAM-1/VCAM-1/Eselectin concentration was achieved.
For each marker, the concentration trend in time associated with each TNFα concentration is reported in figure 4.3.
HUVEC inflammation resulted modulated by TNFα concentration:

- Null TNFα concentration
  HUVECs incubated without TNFα do not release any soluble marker;

- Low TNFα concentration
  Low TNFα concentrations (0.1 and 1 ng/ml) do not have any effect on soluble markers expression, regardless of the exposure time (figures 4.3a, 4.3c and 4.3e);

- High TNFα concentration
  High TNFα concentrations (10, 100 and 1000 ng/ml) induce an evident increase of the concentration of the soluble markers at 24h of exposure.

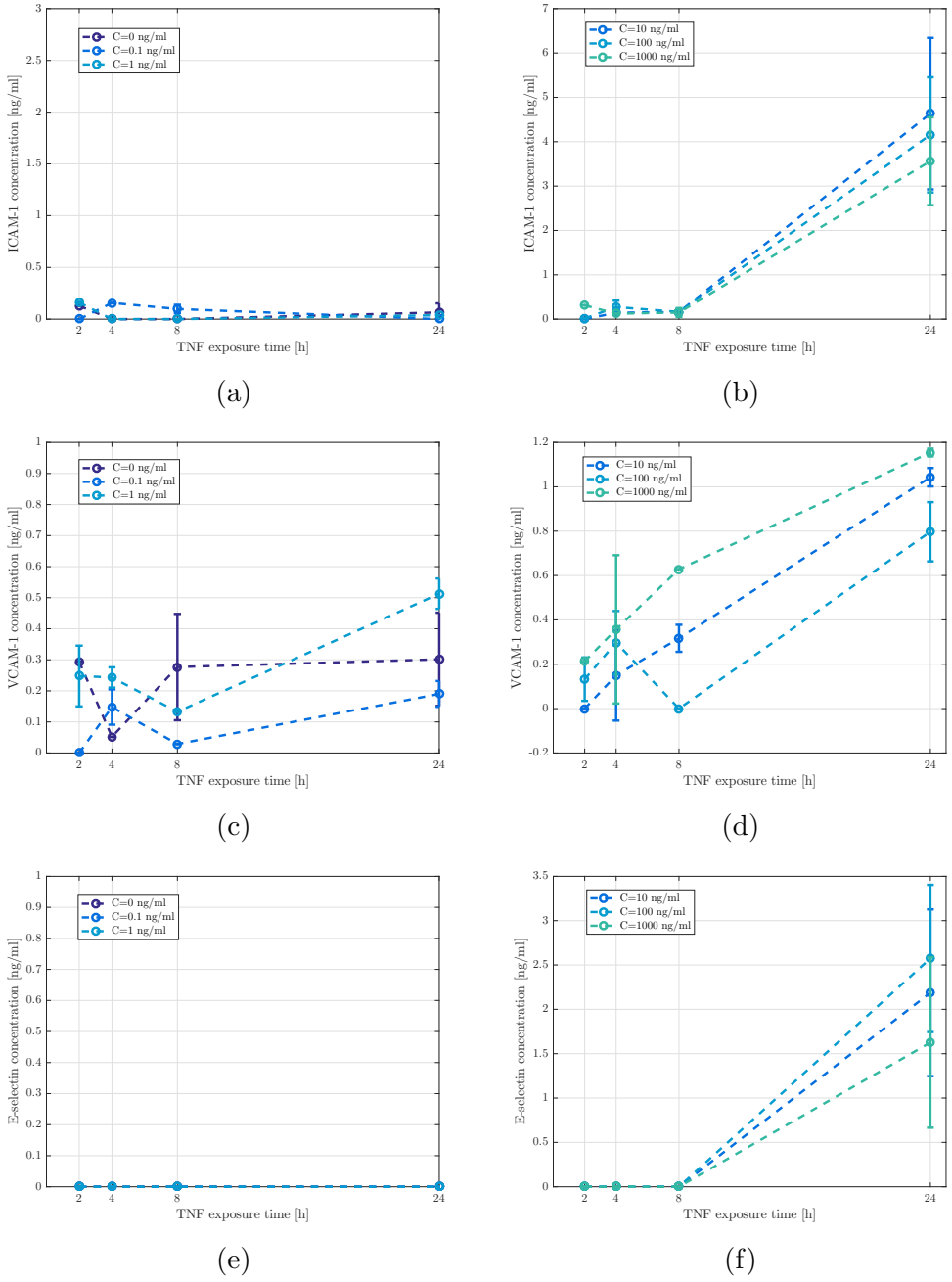

Figure 4.3: Soluble markers concentrations trend in time (mean ± SD, n=3 replicates from the same sample) related to different TNF-α concentrations exposure: (a-b) ICAM-1, (c-d) E-Selectin, (e-f) VCAM-1. Plots in figures (a) (c) (d) are related to low TNF-α concentrations, (b) (d) (f) to high ones.

As previously mentioned, the chemical stimulation and the subsequent characterization of HUVEC activation was repeated at the University of Arizona, since the available cell line was different with respect to the one used at Politecnico di Milano.
In this case, only 24h TNFα exposure time was considered with TNFα concentrations equal to 1, 10, 100 ng/ml. Unstimulated HUVECs were considered as negative control.
ELISAs were performed to obtain the concentrations of the soluble markers after 24h of TNFα exposure, which are reported in table 4.1, compared to the values obtained at Politecnico di Milano.

HUVEC supernatant	ICAM-1 [ng/ml]	E-Selectin [ng/ml]	VCAM-1 [ng/ml]
100 ng/ml TNFα	26.78 ± 0.46^a 4.15 ± 1.3^b	10.25 ± 0.05^a 2.57 ± 0.83^b	29.45 ± 2.46^a 0.79 ± 0.13^b
10 ng/ml TNFα	21.56 ± 1.01^a 4.63 ± 1.7^b	6.01 ± 0.07^a 2.18 ± 0.94^b	22.08 ± 2.27^a 1.04 ± 0.04^b
1 ng/ml TNFα	4.26 ± 0.23^a 0.038 ± 0.01^b	0.68 ± 0.01^a 0.05 ± 0.02^b	2.61 ± 0.35^a 0.51 ± 0.05^b
Unstimulated	4.99 ± 1.19^a 0.064 ± 0.08^b	1.22 ± 0.08^a 0.27 ± 0.031^b	0.76 ± 0.04^a 0.30 ± 0.15^b

Table 4.1: Soluble markers (i.e. ICAM-1, VCAM-1, E-Selectin) concentrations (mean $\pm$ SD, n=2) detected by ELISA after HUVEC chemical activation at 24h TNF-α exposure, obtained at a=University of Arizona and b=Politecnico di Milano

It is evident that the exposure of HUVECs to 10 and 100 ng/ml of TNF-α produced a high expression of ICAM-1, VCAM-1 and Eselectin after 24h. A TNF-α dose-dependent expression of the three markers is highlighted. 24h incubation with 1 ng/ml TNFα does not produce any effect on markers expression, which is comparable to the one obtained with unstimulated HUVECs, confirming the trends reported in figures 4.3.
In figure 4.4, the soluble markers expression obtained at the University of Arizona and Politecnico di Milano are compared. It is evident that the markers concentrations detected at the University of Arizona are considerably higher. It could be ascribed to the different cellular providers, that could imply cellular lines with different characteristics. Additionally, at the University of

Arizona, HUVECs from passage 2 and 7 were used. At Politecnico di Milano, we used HUVECs at higher passage (e.g. passage 16).

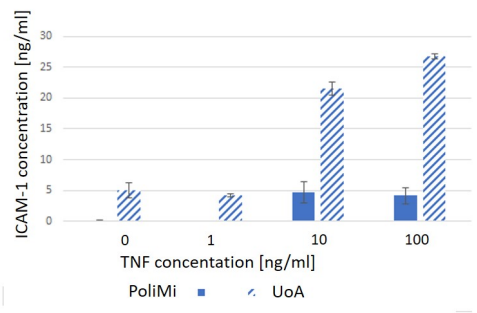

(a)

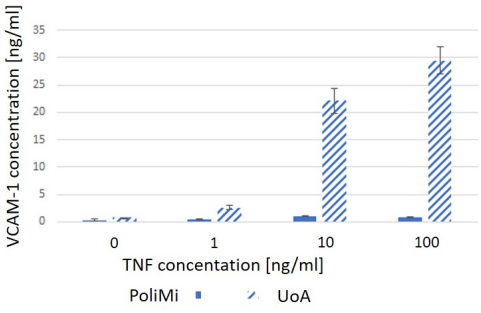

(b)

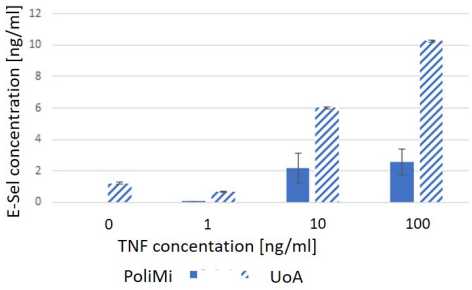

(c)

Figure 4.4: Histograms representing the comparison of markers expression by HUVECs, after 24h TNF-α exposure at different concentrations, obtained at Politecnico di Milano - PoliMi in the legend- and at University of Arizona - UoA in the legend: (a) ICAM-1, (b) VCAM-1 and (c) E-Selectin.

4.1.3 TNFα inflammation potential - Flow cytometry

In addition to ELISA, also a flow cytometric analysis was performed at the University of Arizona, in order to evaluate the expression of the surface markers ICAM-1, VCAM-1 and E-Selectin by TNF-α activated and non-activated (i.e. negative control) HUVECs. The resulting histograms for the negative control and for 100 ng/ml TNF-α are shown in figure 4.5.
The positive populations to each markers (i.e. % of P1), calculated as described in paragraph 3.4.2, are reported in table 4.2, based on the results of N=2 experiments.

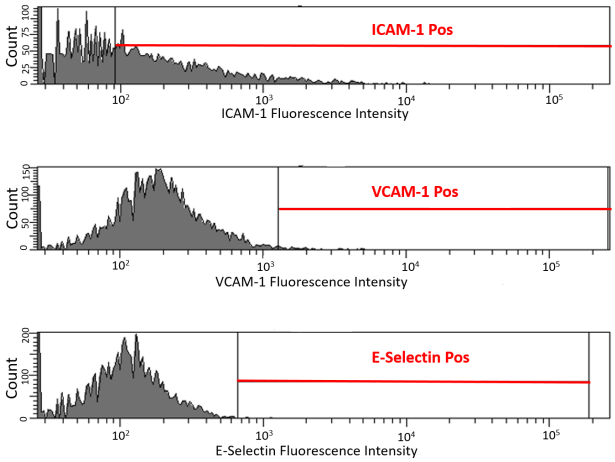

(a) Negative control - TNF α concentration 0 ng/ml

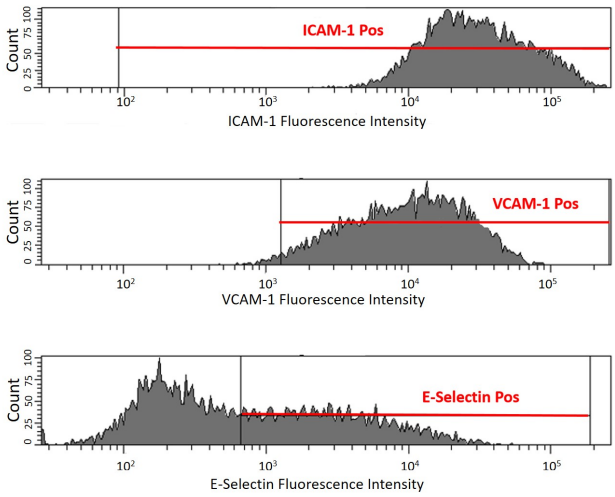

(b) TNF α concentration 100 ng/ml

Figure 4.5: HUVECs surface markers (from the top to the bottom ICAM-1, VCAM-1, E-selectin) expression after TNF-α exposure: (a) 0 ng/ml - negative control, (b) 100 ng/ml for 24 h

Flow cytometry results confirmed the ones obtained with ELISA, i.e. the surface markers expression is TNF concentration dependent. Additionally, surface markers and soluble markers are shown to have an analogous concentration-dependent response. Considering the outputs of both the techniques, it is evident that with a TNFα concentration equal to 1 ng/ml, the ECs are not activated (i.e. markers expression comparable to the one obtained with unstimulated ECs), that is why the selected inflammation protocols for the

HUVEC sample	ICAM-1 positive [%]	VCAM-1 positive [%]	E-Selectin positive [%]
100 ng/ml TNFα	100	93.45 ± 5.02	63 ± 21.21
10 ng/ml TNFα	99.5 ± 0.70	85.35 ± 12.2	42.25 ± 7.99
1 ng/ml TNFα	45.60 ± 0.84	2.40 ± 0.14	2.65 ± 2.47
Unstimulated	40.35 ± 4.03	1.6 ± 0.84	1.25 ± 0.63

Table 4.2: HUVEC sub-populations (mean ± SD, N=2), expressed as a % of the total cellular sample P1, positive to the activation markers after chemical activation through TNF-α at different concentrations

subsequent experiments are i) 10 ng/ml TNF-α for 24h and ii) 100 ng/ml TNF-α for 24h.

4.2 Platelets-Endothelial Cells interaction

With the aim of characterizing the interaction between activated platelets and activated ECs, 4 different experiments were performed, as described at the beginning of this chapter. The experimental layout was designed in order to deconstruct the entire phenomenon in steps. In the following sections, the results of each analyzed condition are reported. In particular, the results are organized as detailed at the beginning of this chapter:

- PAS assay and flow cytometry (Annexin V, P-Selectin, ICAM-1, VCAM-1, E-Selectin) to investigate activation markers expression;
- SEM and flow cytometry ($\alpha_V\beta_3$) to characterize the adhesion mechanism.

4.2.1 Interaction between non-activated platelets and non-activated ECs

The focus of the first experiment, was to characterize the interaction between resting platelets and non-activated ECs, through different techniques.

1. Characterization of markers expression

- Regarding the PAS assay, platelets were collected after 10, 30 and 60 minutes of incubations with HUVECs and then assayed. The outputs were 33 values of absorbance (one reading every 13 seconds for 7 minutes) read by the spectrophotometer (basic kinetic protocol, wavelength equal to 405 nm). The slope (PAS value) of the linear interpolation curve of these 33 values was automatically computed by the software Soft Max 6.3. Two values of PAS were associated to each sample, since each one was assayed in duplicate. A mean sonication PAS value was calculated. Then, two values of PAS % (percentage of sonication, calculated according to equation 3.4.1) were obtained for each time point.
  Since this experiment was repeated three times (N=3), 6 values of PAS % (N=3, n=6) were obtained for each time point. Mean and SD of these six values were calculated. The obtained trend in time of the PAS % is showed in figure 4.6.

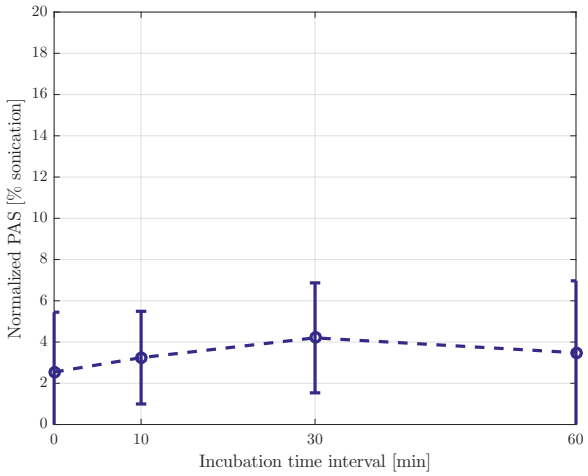

Figure 4.6: Trend of PAS % in time (mean ± SD, N=3 experiments, n=6) obtained incubating non-activated HUVECs with non-activated platelets

  It is possible to notice that resting platelets do not increase their PAS % value (i.e. they don't activate) after incubation with non-activated ECs, since PAS % remains significantly constant over the entire incubation period (p-value > 0.05 over time).

- Regarding the flow cytometry, platelets were incubated with non-activated HUVECs and then collected after 30 and 60 min and prepared for flow cytometry in order to characterize the expression level of the activation markers P-Selectin and Annexin V. The

positive controls are platelets incubated with arachidonic acid, a known platelets activator, and sonicated platelets.
The resulting histograms, obtained through the procedure described in paragraph 3.4.2, are shown in figure 4.7, representing platelet activation markers expression without incubation with HUVECs, i.e. negative control (figure 4.7a); after 1h incubation with HUVECs (figure 4.7b); in presence of arachidonic acid (figure 4.7c) and sonicated (figure 4.7d) i.e. positive controls.

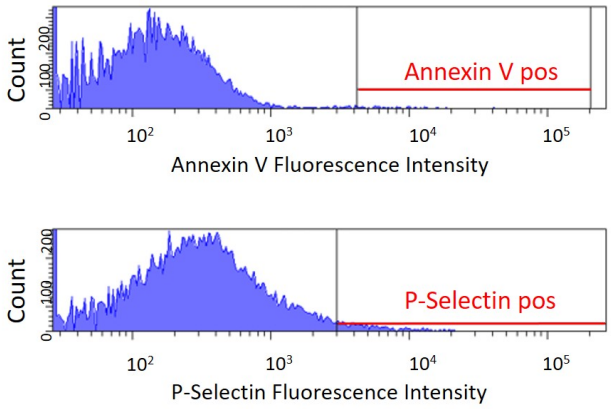

(a) Resting platelets - without incubation with HUVECs

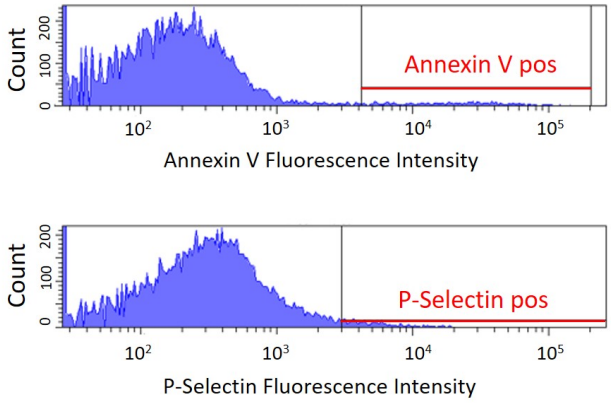

(b) Resting platelets - after 1h incubation with HUVECs

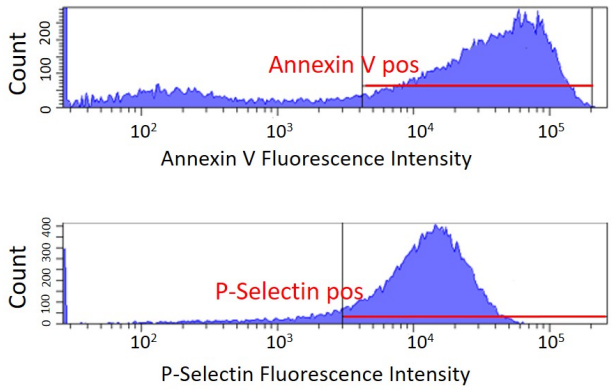

(c) Chemically activated platelets (arachidonic acid)

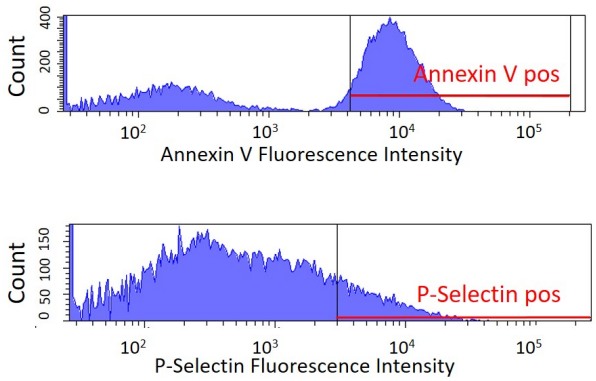

(d) Sonicated platelets

Figure 4.7: Flow cytometry histograms for non activated platelets expression of Annexin V (FITC conjugated) and P-selectin (APC conjugated), including the two positive controls, chemical activation (c) and sonication (d)

The results obtained after 30 minutes of incubation are not reported, since they are comparable to the ones after 60 minutes.
The regions of positiveness to the two markers are red highlighted in figure 4.7 and the % values (percentage of positive events with respect to the entire population P1) are reported in table 4.3, based on the results of two experiments (N=2) performed in duplicate (n=4).
Non-activated platelets incubated with non-activated ECs do not express the two activation markers P-selectin and Annexin V, which are strongly expressed by the chemically activated and sonicated platelets instead.

Resting platelets	Annexin V positive [%]	P-Selectin positive [%]
No EC incubation	0.95 ± 0.07	2.75 ± 0.35
After 1 h EC incubation	2.05 ± 1.34	2.35 ± 0.21
Chemically activated	79.6 ± 14.42	76.1 ± 15.98
Sonicated	53.05 ± 0.91	11.55 ± 0.91

Table 4.3: Non-activated platelets sub-populations (mean ± SD, N=2, n=4), expressed as a % of the total platelet population P1, positive to the markers of interest

To determine if the incubation with non-activated HUVECs produces any change in non-activated platelet expression of Annexin V or P-Selectin, ANOVA test was carried out to verify the equality of the considered populations, i.e. i) resting platelets; ii) resting platelets 30 min incubated with non-activated HUVECs and iii) resting platelets 60 min incubated with non-activated HUVECs. According to our results, data are comparable (p-value > 0.05), i.e. there is not any statistically significant difference among data. In other words, there is no difference in markers expression by resting platelets with or without incubation with non-activated HUVECs.

- Finally, it was of interest to evaluate if the exposure to non-activated platelets lead HUVECs to express their marker of activation. With this purpose, flow cytometry for ICAM-1, VCAM-1 and E-Selectin was performed on ECs after 1 h incubation with resting platelets. HUVECs that were not incubated with platelets were used as control sample. As previously described, only events belonging to P1 were used to obtain the histograms (not shown), from which the sub-populations positive to the three markers were deducted. In table 4.4 the values of the % sub-populations are reported.
  The first row in table 4.4 (control) represents the same condition reported in the last row in table 4.2 (unstimulated HUVECs). The expression levels of ICAM-1 and VCAM-1 are slightly different in these two cases. This can be ascribed to the different passage of the cells that could affect markers expression.

HUVECs	ICAM-1 positive [%]	VCAM-1 positive [%]	E-Selectin positive [%]
No platelets incubation	70 ± 0.71	5.65 ± 0,07	1.4 ± 0.56
1h with resting platelets	67.05 ± 3.88	5.75 ± 0.49	1.4 ± 0.01

Table 4.4: HUVEC sub-populations (mean ± standard deviation, N=2, n=4), expressed as a % of the total cellular sample P1, positive to the activation markers after incubation with non activated platelets

From these data, it is possible to deduce that EC activation is not induced by the exposure to resting platelets, since no EC activation markers increase was highlighted after incubation with resting platelets. Three ANOVA tests were performed to verify the equality of the considered populations, i.e. i) HUVECs not incubated with platelets; ii) HUVECs 1h incubated with resting platelets. According to our results, data are comparable ($p > 0.05$), i.e. there is not any statistically significant difference among data, therefore the expression level of the ECs' markers of activation does not change after incubation with resting platelets.

2. Characterization of adhesion mechanism
   Concerning SEM imaging acquisition, the obtained images after incubation of resting platelets with non activated HUVECs are shown in figure 4.8.
   In order to estimate the number of adhered platelets, the images were always acquired with the same magnifications, i.e. 3000X (figure 4.8a) and 20'000X (figure 4.8b).
   In the case of non activated platelets incubated with non activated HUVECs, it is possibile to estimate, based on the image 4.8a, an average number of 4 platelets in 10'000 μm^2.
   In addition, the image 4.8b points out that platelets have a rounded shape, typical of non activated platelets.

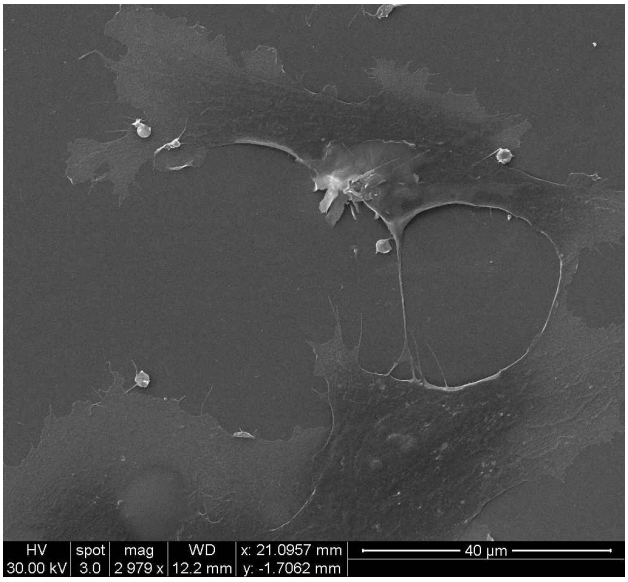

(a) Magnification 3000X

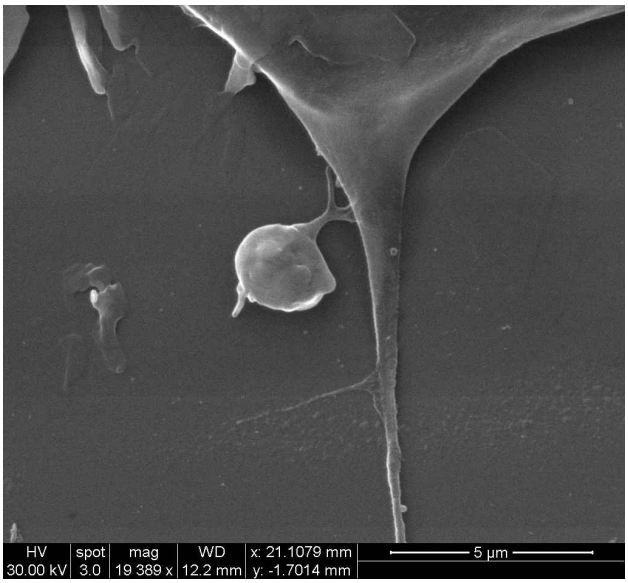

(b) Magnification 20'000X

Figure 4.8: SEM images acquired for non activated platelets incubated with non activated ECs

4.2.2 Interaction between activated platelets and non-activated ECs

In order to characterize the interaction between activated platelets and non-activated ECs, shear activated platelets were incubated with cultured HUVECs. Platelets were sheared through the HSD. Three different time-constant stimulations were considered: 30, 50 and 70 dyne/cm^2 for 10 minutes. Activated platelets were incubated also without cultured HUVECs as a negative control.

1. Characterization of markers expression

   - Regarding the PAS assay, platelets were collected after 10, 30 and 60 minutes of incubation with/without HUVECs and then assayed. The procedure described in the paragraph 4.2.1 was followed to obtain the trends in time of the mean PAS %, for both platelets incubated with HUVECs (N=3 experiments) and platelets incubated alone (i.e. negative control, N=2 experiments). Figure 4.9 shows the curves related to platelets incubated with ECs.

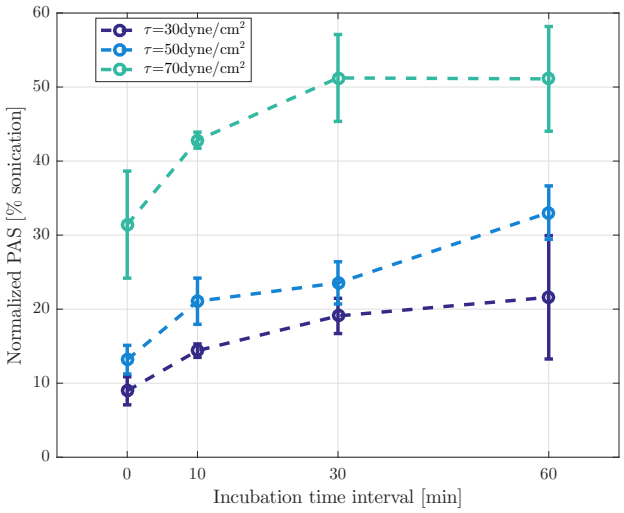

Figure 4.9: Trend of PAS % in time (mean ± SD, N=3, n=6) obtained incubating not activated HUVECs with shear activated platelets. Each curve is associated to a different shear stimulation.

The obtained PAS % trends increase over time, starting from t=0, i.e. platelets assayed right after HSD run, up to 60 minutes incu-

bation. In particular, the PAS% values increase from t=0 to t=60 min as follows:

- From 5 to 13 % for 30 dyne/cm^2 activated platelets (2.6 times higher)
- From 8 to 18 % for 50 dyne/cm^2 activated platelets (2.2 times higher)
- From 28 to 45 % for 70 dyne/cm^2 activated platelets (1.6 times higher)

Figure 4.10 shows the comparison between the PAS % trend in time of platelets incubated with ECs and platelets incubated without ECs (i.e. alone).

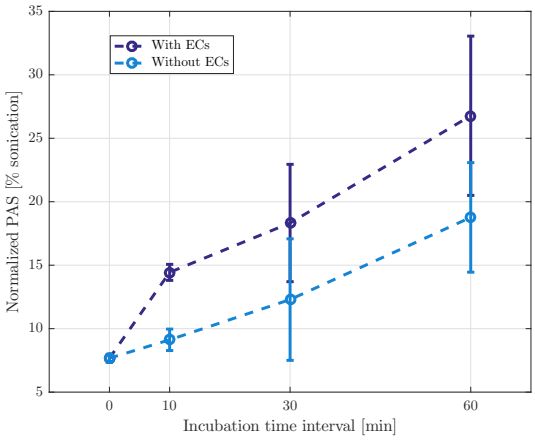

(a)

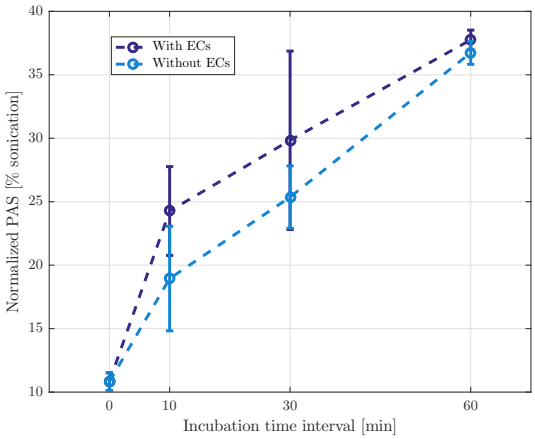

(b)

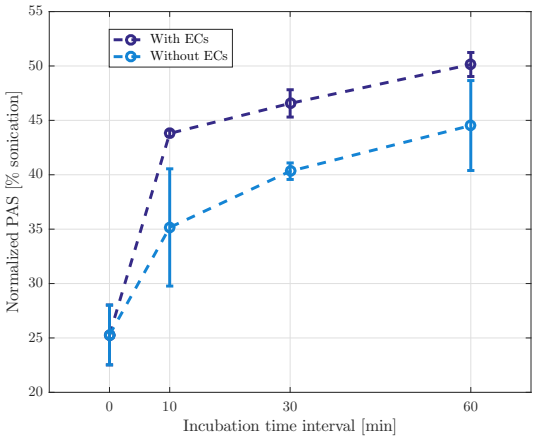

(c)

Figure 4.10: Trend of PAS % in time (mean ± SD, N=2 experiments, n=4) for shear activated platelets (i.e. (a) 30 dyne/cm^2, (b) 50 dyne/cm^2, (c) 70 dyne/cm^2 for 10 min) incubated with/without non activated HUVECs

Each plot is related to one of the three shear waveform. In particular, figure 4.10a is referred to 30 dyne/cm^2 stimulated platelets; figure 4.10b to 50 dyne/cm^2 stimulated platelets; figure 4.10c to 70 dyne/cm^2 stimulated platelets. It is evident that there is a time dependent increase in platelet activation, even in absence of ECs.
In order to compare the PAS % values related to shear activated platelets incubated with/without ECs, ANOVA test was performed. The aim was to determine if the presence of HUVECs has a significant effect on platelet activation.
In particular, for each of the three considered shear stimulation, ANOVA test was carried out to verify the equality of the two considered populations, i.e. i) platelets 1h incubated with HUVECs and ii) platelets 1h incubated alone. Despite a different activation trend was observed (i.e. activation of platelets incubated with HUVECs is higher than that of platelers alone), ANOVA did not suggest any significant difference at t=60 min (p-value > 0.05) for all the three shear stimulation.

- Concerning the flow cytometry results, the same procedure described in paragraph 3.4.2 was followed to obtain the histograms reported in figures 4.11 and 4.12. The analyzed samples are shear-activated platelets incubated for 30 and 60 minutes with non ac-

tivated ECs and alone (i.e. negative control at the same 2 time points). Only the results at 60 minutes are reported, since there were no difference between the two time points.

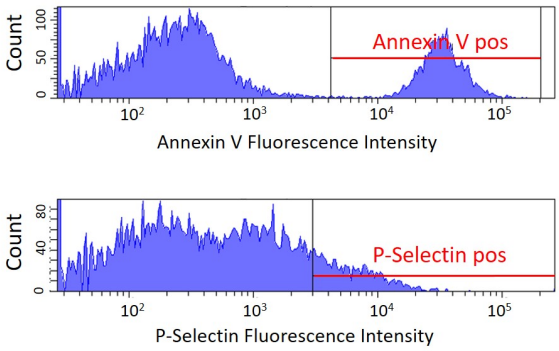

(a) 50 dyne/cm^2 activated platelets - post HSD

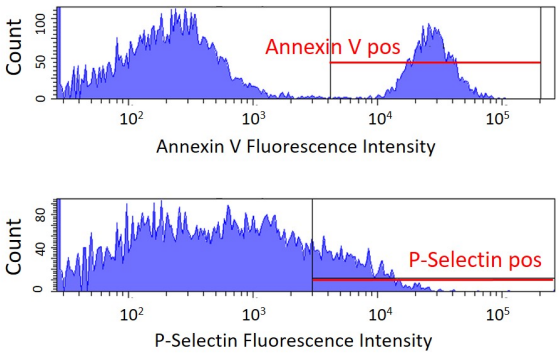

(b) 50 dyne/cm^2 activated platelets - after 1h incubation with HUVECs

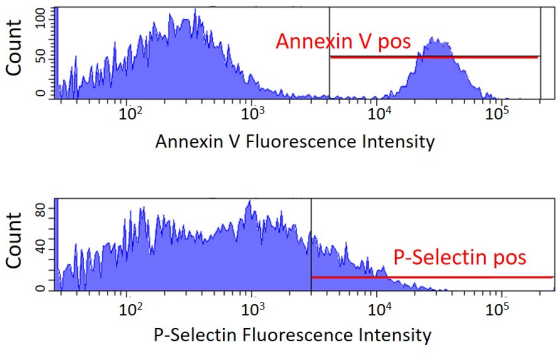

(c) 50 dyne/cm^2 activated platelets - after 1h incubation alone

Figure 4.11: Flow cytometry histograms for 50 dyne/cm^2 activated platelets expression of Annexin V (FITC- conjugated) and P-selectin (APC-conjugated) after incubation with non activated HUVECs

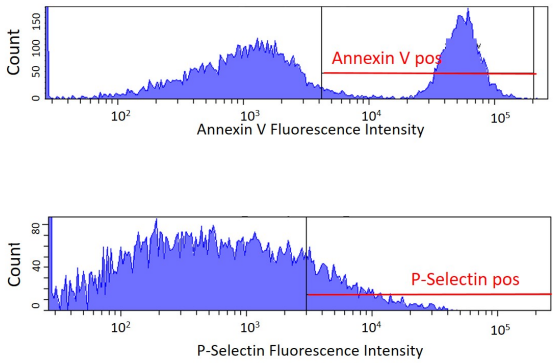

(a) 70 dyne/cm^2 activated platelets - post HSD

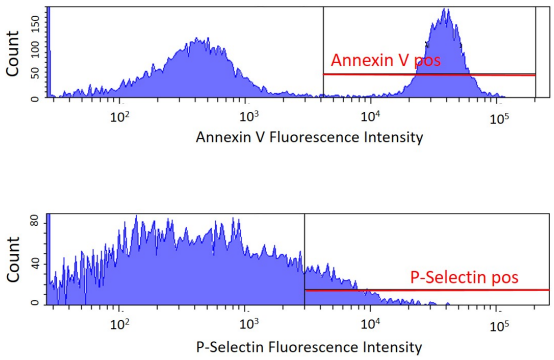

(b) 70 dyne/cm^2 activated platelets - after 1h incubation with HUVECs

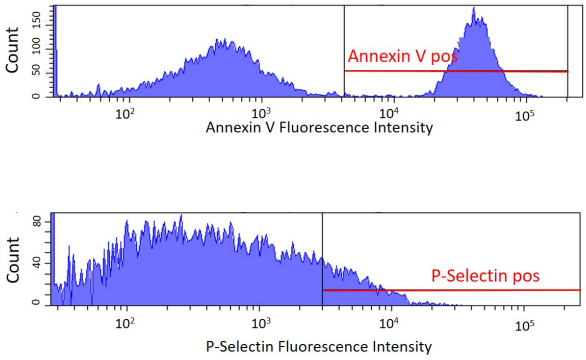

(c) 70 dyne/cm^2 activated platelets - after 1h incubation alone

Figure 4.12: Flow cytometry histograms for 50 dyne/cm^2 activated platelets expression of Annexin V (FITC- conjugated) and P-selectin (APC-conjugated) after incubation with non activated HUVECs

In addition, only the results after 50 and 70 dyne/cm^2 stimulation are presented, since no significant activation increase was pointed out in any case. In table 4.5, the sub-populations (i.e. percentage with respect to the entire population P1) positive for the two markers of interest are reported, based on the results of two experiments (N=2).

		Annexin V positive [%]	P-Selectin positive [%]
50 dyne/cm^2 sheared platelets	Post HSD	17.6 ± 3.81	9.50 ± 2.26
	1 h EC incubation	18.85 ± 5.58	10.80 ± 4.10
	1 h incubation alone	16.75 ± 5.30	11.20 ± 3.81
70 dyne/cm^2 sheared platelets	Post HSD	57.55 ± 27.6	14.5 ± 2.12
	1 h EC incubation	57.5 ± 26.2	12.35 ± 3.32
	1 h incubation alone	56 ± 26.8	13 ± 2.82

Table 4.5: Shear activated platelets sub-populations (mean ± SD, N=2, n=4), expressed as a % of the total platelets sample P1, positive to the markers of interest after incubation with HUVECs

In order to determine if the incubation with non-activated HUVECs produces any change in shear activated platelet expression of Annexin V or P-Selectin, ANOVA test was carried out to verify the equality of the considered populations, i.e. i) sheared activated platelets; ii) sheared activated platelets after 1h incubation with non-activated HUVECs and iii) sheared activated platelets after 1h incubation alone. According to our results, data are comparable (p-value > 0.05), i.e. there is not any statistically significant difference among data.
Together, PAS assay and flow cytometry indicate that the incubation with non-activated HUVECs or alone does not induce any platelet activation change, regardless of the initial platelet activation level.

- Moreover, it was of interest to evaluate if the contact with shear-activated platelets leads HUVECs to express their marker of activation. Flow cytometry for ICAM-1, VCAM-1 and E-Selectin was performed on ECs after 1 h incubation with HSD-stimulated

platelets. In particular, HUVECs underwent the procedure described in paragraph 3.4.2. In table 4.6 the values of the % subpopulations are collected, based on the results of two experiments (N=2).

HUVECs	ICAM-1 positive [%]	VCAM-1 positive [%]	E-Selectin positive [%]
No platelets incubation	53.7 ± 22.27	3.3 ± 3.25	1.5 ± 0.70
1h 50dyne/cm^2 sheared platelets	59 ± 31.11	4.3 ± 4.8	1.5 ± 0.70
1h 70dyne/cm^2 sheared platelets	59.5 ± 33.23	3.55 ± 3.46	1.3 ± 0.56

Table 4.6: HUVEC sub-populations (mean ± SD, N=2, n=4), expressed as a % of the total cellular sample P1, positive to the activation markers after incubation with shear activated platelets

HUVECs that were not incubated with platelets are used as control sample. The resulting positive sub-population after 1h incubation with 30 dyne/cm^2 activated platelets are not reported, since they were comparable with the other two cases.
From these data, it is possible to deduce that EC activation is not induced by the contact with activated platelets, regardless the platelet activation level, since no EC activation markers expression was highlighted. In order to prove it, ANOVA test was performed. In particular, the % positive subpopulations to the activation markers from i) HUVECs not incubated with platelets; ii) HUVECs incubated with 50 dyne/cm^2 sheared platelets and iii) HUVECs incubated with 70 dyne/cm^2 sheared platelets, were compared. According to our results, the expression level of the EC markers of activation does not change after incubation with sheared platelets (p-value > 0.05), regardless of the shear level.

2. Characterization of adhesion mechanism

   - Regarding the SEM images, they were acquired after 60 minutes incubation of shear activated platelets with non activated ECs. Figure 4.13 is referred to the case when platelets were activated by 30 dyne/cm^2 HSD stimulation before being incubated with HUVECs; figure 4.14 to the one when platelets were activated by 50 dyne/cm^2 HSD stimulation; figure 4.15 to the one when

platelets were activated by 70 dyne/cm^2 HSD stimulation. The images were all acquired at the same magnifications, i.e. 20'000X and 3'000X, in order to draw semi-quantitative conclusions.

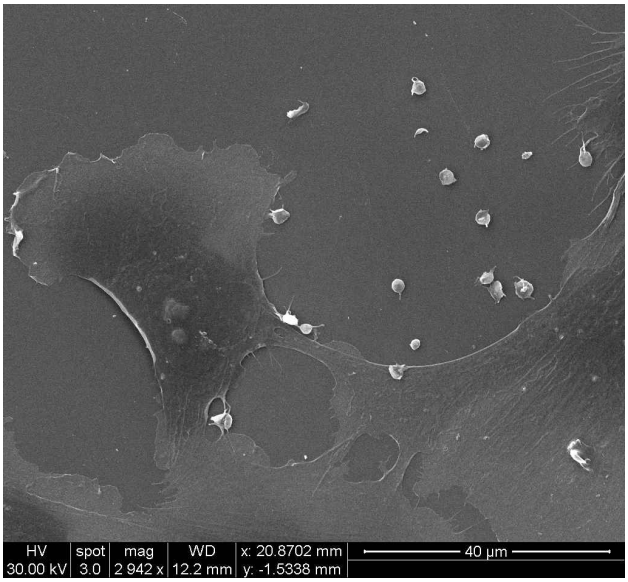

(a) Magnification 3000X

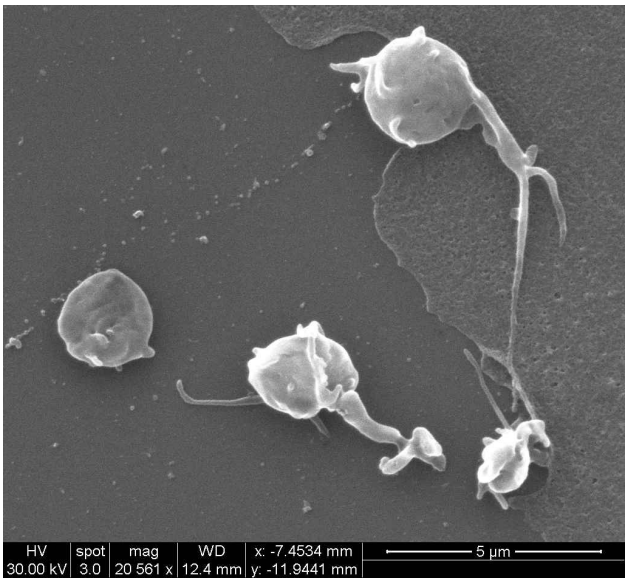

(b) Magnification 20'000X

Figure 4.13: SEM images acquired for 30 dyne/cm^2 activated platelets incubated with non activated ECs

Concerning the number of adhered platelets estimation, if platelets

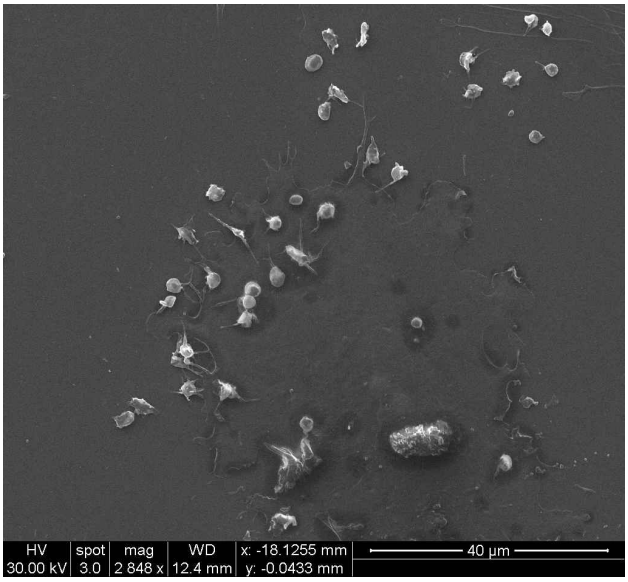

(a) Magnification 3000X

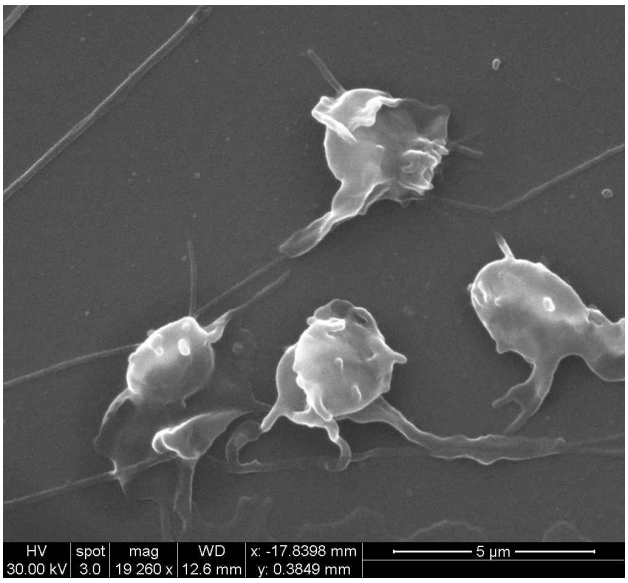

(b) Magnification 20'000X

Figure 4.14: SEM images acquired for 50 dyne/cm^2 activated platelets incubated with non activated ECs

are 30 dyne/cm^2 shear-activated, it is possible to estimate 15 adhered platelets in 10'000 μm^2; if platelets are 50 dyne/cm^2 shear-activated, it is possible to estimate 35 adhered platelets in 10'000 μm^2 and two platelet aggregates; if platelets are 70 dyne/cm^2

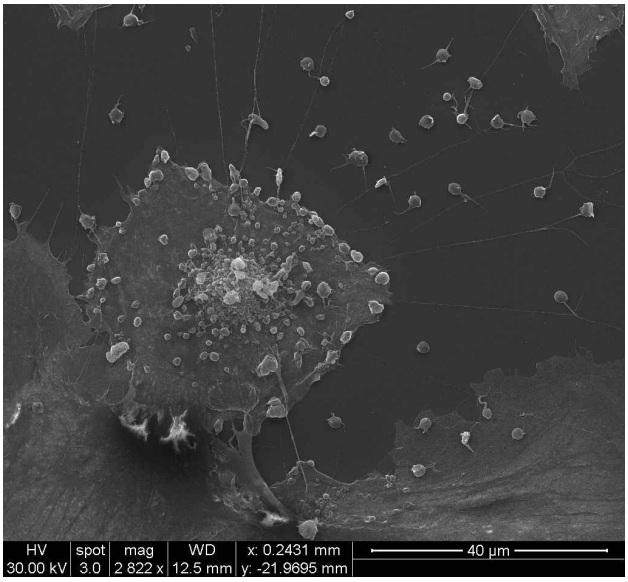

(a) Magnification 3000X

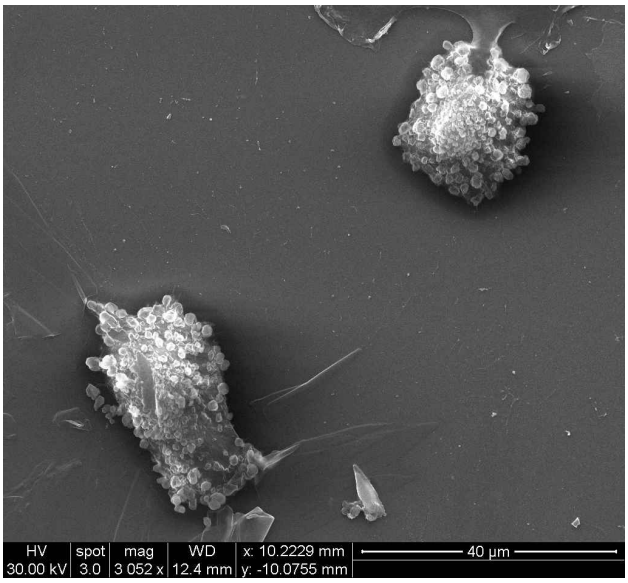

(b) Magnification 3000X

Figure 4.15: SEM images acquired for 70 dyne/cm^2 activated platelets incubated with non activated ECs

shear-activated, it is impossible to estimate the number of adhered platelets, since most of them are aggregated among each other. Therefore, there is a correlation between the activation level of platelets and their adhesion to ECs. Concerning the shape

assumed by platelets, 20'000X magnification images (i.e. figures 4.13b and 4.14b) shows that platelets are more spread and less rounded, which is the typical conformation of activated platelets.

- The evaluation of the binding between ECs and platelets was further evaluated through flow cytometry analysis for the endothelial marker $\alpha_v\beta_3$, binding integrin between platelets and ECs, whose results are shown in figure 4.16.

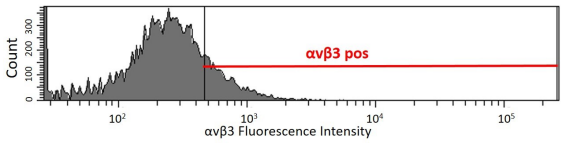

(a) HUVECs alone

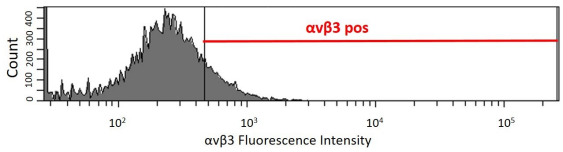

(b) HUVECs 1h incubated with 50 dyne/cm^2 conditioned platelets

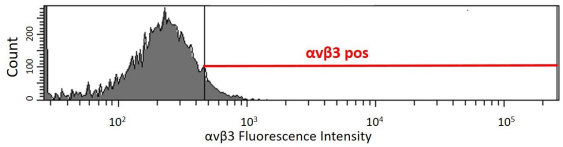

(c) HUVECs 1h incubated with 70 dyne/cm^2 conditioned platelets

Figure 4.16: Flow cytometry histograms for not activated HUVEC expression of $\alpha_v\beta_3$ (FITC - conjugated)

In particular, after 60 minutes of incubation with shear activated platelets, HUVECs were detached from their support and prepared as described in paragraph 3.4.2. Sub-populations which are $\alpha_v\beta_3$ positive (red straight lines in figure 4.16) are collected in table 4.7, based on the results of two experiments (N=2).

HUVECs that were not incubated with platelets were also evaluated as control.

In order to evaluate if there was a significant difference in the expression level of $\alpha_V\beta_3$, an ANOVA test was carried out. In particular, the % positive sub-population to $\alpha_V\beta_3$ from i) HUVECs not incubated with platelets; ii) HUVECs 1h incubated with 50 dyne/cm^2 sheared platelets and iii) HUVECs 1h incubated with

HUVECs	$\alpha_v\beta_3$ positive [%]
No platelets incubation	11.45 ± 1.20
1h incubation with 50 dyne/cm^2 sheared platelets	8.70 ± 0.84
1h incubation with 70 dyne/cm^2 sheared platelets	5.70 ± 0.28

Table 4.7: HUVEC sub-populations (mean ± SD, N=2, n=4), expressed as a % of the total cellular sample P1, positive to $\alpha_v\beta_3$

70 dyne/cm^2 sheared platelets, were compared. According to our results, there is a significant difference (p-value < 0.05) among data. Namely, the expression level of $\alpha_V\beta_3$ significantly decreases between these three populations, suggesting that this integrin is "hidden" because involved in the binding between HUVECs and activated platelets.

As such, with this experiment we were able to characterize two distinct effects mediated by activated platelets on EC markers expression: i) no effect on activation markers expression (i.e. ICAM-1, VCAM-1, E-Selectin) and ii) significant effect on adhesion marker expression (i.e. $\alpha_V\beta_3$).

4.2.3 Interaction between non activated platelets and activated ECs

With the aim of characterizing the interaction between non activated platelets and activated ECs, resting platelets were incubated with chemically activated HUVECs. Two chemical activation protocols were considered: 10 ng/ml TNF-α for 24h and 100 ng/ml TNF-α for 24h. As it will be shown, no platelet activation was observed through PAS assay, therefore flow cytometry for P-selectin and Annexin V was not performed. Additionally, SEM images were acquired.

1. Characterization of markers expression
   Concerning the PAS assay, platelets were collected after 10, 30 and 60 minuted of incubation with activated cells and then assayed. The same procedure described in section 4.2.1 was followed to compute the trends in time of the mean PAS % (N=3 experiments), one for each TNF-α concentration. Figure 4.17 shows the two curves associated with the

two considered activation levels of HUVECs.
It is evident that resting platelets do not increase their PAS % value after incubation with activated ECs, neither with the higher concentration of TNF-α. The PAS% value remains constant, as it was shown for the resting platelets incubated with non activated ECs. The two plots in figure 4.17 are comparable to the one reported in figure 4.6, indicating that pre-activation of HUVECs through TNFα does not cause any change in resting platelet activation.

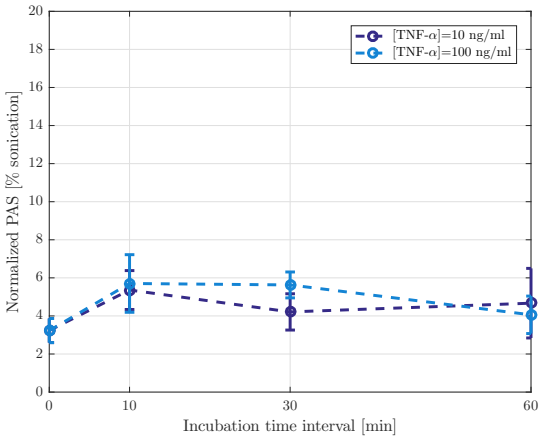

Figure 4.17: Trend of PAS % in time (mean ± SD, N=3 experiments, n=6) obtained incubating TNF-α activated HUVECs with resting platelets

2. Characterization of adhesion mechanism
SEM images were obtained after 60 minutes incubation of resting platelets with chemically activated HUVECs.
No differences were pointed out between the two considered EC activation levels (i.e. 10 ng/ml and 100 ng/ml for 24h), that is why only one image is reported in figure 4.18, representative of both the conditions. Chemically activated HUVECs are totally adhesive for resting platelets. It is impossible to estimate the number of adhered platelets, since they are too numerous.
Comparing figure 4.18 with figure 4.8, which shows the adhesion of non-activated platelets to non-activated HUVECs where few adhered platelets are present, the adhesive effect of TNFα is evident.

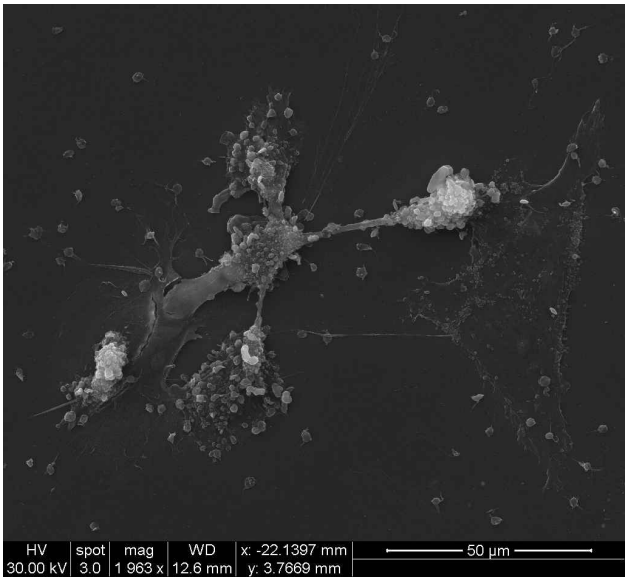

Figure 4.18: SEM image acquired for non-activated platelets incubated with chemically-activated HUVECs, magnification 2000X

4.2.4 Interaction between activated platelets and activated ECs

With the aim of characterizing the interaction between activated platelets and activated ECs, chemically activated HUVECs were incubated with shear-conditioned platelets. Again, two levels of chemical activation were considered, i.e. 10 and 100 ng/ml TNF-α for 24h, and three shear conditioning protocols were applied, i.e. 30, 50, 70 dyne/cm^2 for 10 min via HSD.

1. Characterization of markers expression

   - Regarding the PAS assay, platelets were collected after 30 and 60 minutes of incubation with activated and non-activated HUVECs and then assayed. The trends in time of the mean PAS % were calculated as described in paragraph 4.2.1. Since through SEM imaging it was noticed that many platelets were adhered to ECs, the PAS % values were normalized on platelet count values.
     The trends of the normalized PAS % are shown in figure 4.19, one for each of the three different shear stimulation considered.
     For each HSD stimulation, the count was performed immediately after the HSD run, i.e. before incubating the GFP with the ECs, so-called $count_{t=0}$, and at each time point, right after platelet collection, so called $count_{t=i}$, for i=10, 30, 60 [min]. Each sample

was analyzed four times with the particle counter and the mean value of the four count measurements was calculated. The PAS % value at each time point was normalized dividing it by the ratio R between the mean value of platelets concentration obtained at that time point and the value of platelet concentration obtained right after HSD, i.e. $R = count_{t=i}/count_{t=0}$. This procedure allows to take into account the platelets loss with the incubation with HUVECs, that was around 20% after 60 min of incubation with chemically activated HUVECs.

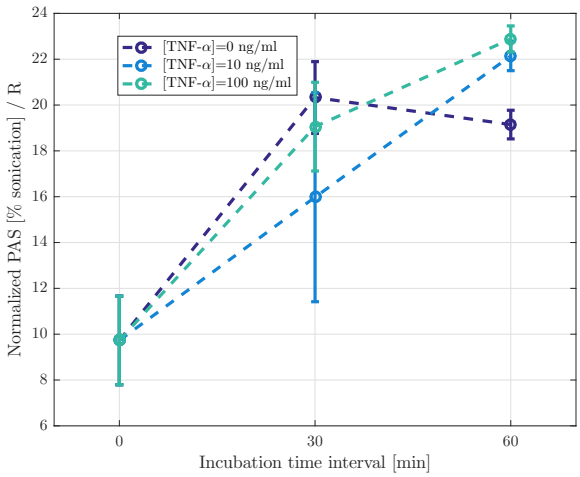

(a)

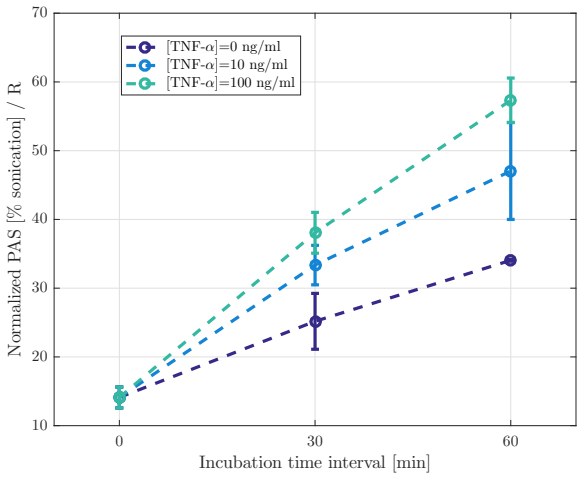

(b)

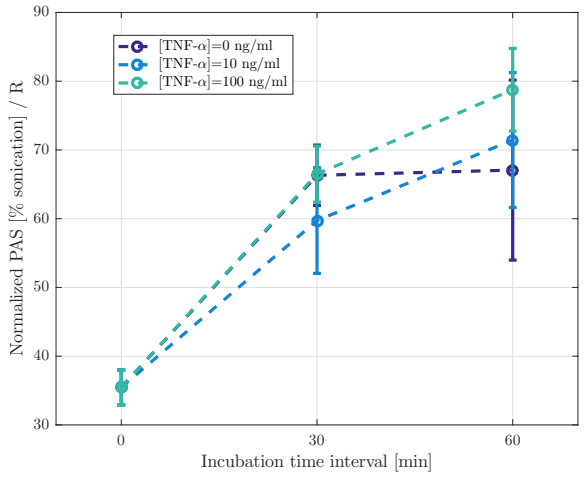

(c)

Figure 4.19: Normalized PAS % (i.e. divided by $R = count_{t=i}/count_{t=0}$, mean ± SD, N=2 experiments, n=4) for shear activated platelets, i.e. (a) 30 dyne/cm^2, (b) 50 dyne/cm^2, (c) 70 dyne/cm^2 for 10 min, incubated with chemically activated and non activated (negative control) HUVECs

The PAS% values increase over time for all the three considered conditions. In fact, according to the results illustrated in paragraph 4.2.2, sheared platelets incubated with non-activated HUVECs (i.e. condition [TNF-α=0[ng/ml] in figure 4.19) increase their PAS % value over time.
In order to compare the normalized PAS% values related to shear activated platelets incubated with activated and non-activated HUVECs, different ANOVA tests were performed. The aim was to determine if the presence of activated HUVECs has a significant effect on platelet activation at 60 minutes incubation.
In particular, for each of the three considered shear-stimulation, ANOVA test was carried out to verify the equality of the means of the three considered populations, i.e. i) sheared platelets incubated with non-activated HUVECs; ii) sheared platelets incubated with 10 ng/ml TNF-α activated HUVECs and iii) sheared platelets incubated with 100 ng/ml TNF-α activated HUVECs. ANOVA suggests a statistically significant difference at t=60 min (p-value < 0.05) for 30 and 50 dyne/cm^2 sheared platelets; for 70 dyne/cm^2 sheared platelets, no significant difference among data was pointed out (p-value > 0.05). These results suggest a signif-

icant role of TNF-α-activated HUVECs in platelet activation enhancement, exception made for the 70 dyne/cm^2 case, that could be ascribed to a platelet activation threshold mechanism (PAS% values between 70 and 80% in figure 4.19c).

- Concerning flow cytometry results, the procedure described in 3.4.2 was repeated to obtain the histograms in figure 4.20.

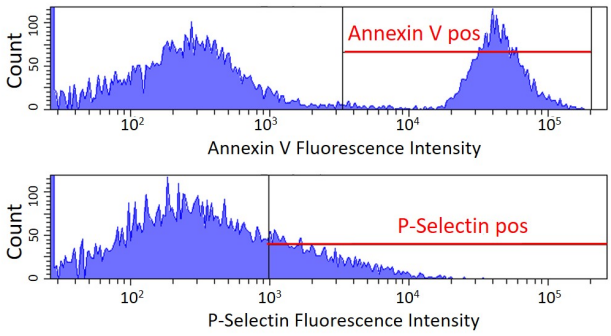

(a) 70 dyne/cm^2 activated platelets - post HSD

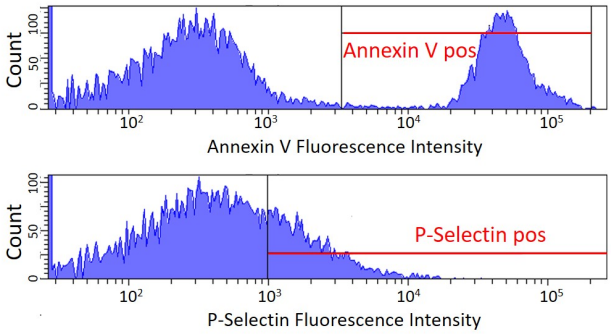

(b) 70 dyne/cm^2 activated platelets - after 1h incubation with non activated HUVECs

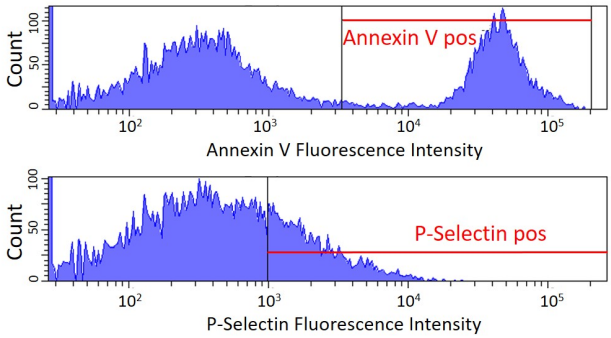

(c) 70 dyne/cm^2 activated platelets - after 1h incubation with 10 ng/ml TNFα activated HUVECs

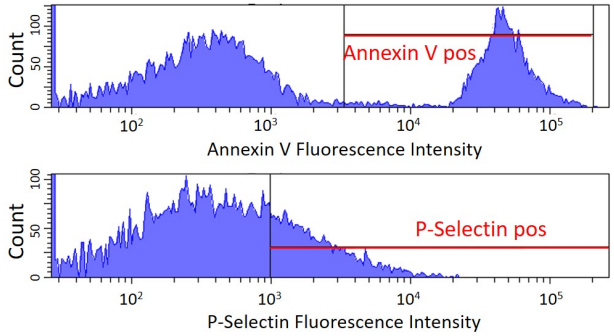

(d) 70 dyne/cm^2 activated platelets - after 1h incubation with 100 ng/ml TNFα activated HUVECs

Figure 4.20: Flow cytometry histograms for 70 dyne/cm^2 expression of Annexin V (FITC-conjugated) and P-Selectin (APC-conjugated) after incubation with activated and non activated HUVECs

The analyzed samples were shear activated platelets incubated with chemically activated HUVECs. In this case, the negative control is represented by shear-activated platelets incubated with non activated HUVECs (figure 4.20b, repetition of the experiment in paragraph 4.2.2), in order to estimate the TNFα effect on the platelets activation markers' expression.
Only the results after 70 dyne/cm^2 stimulation are shown, since no evident markers expression increase was obtained in any case. In table 4.8, the sub-populations positive to the markers of interest are reported (red straight lines in figure 4.20), based on the results of two experiments (N=2).

70 dyne/cm^2 sheared platelets	Annexin V positive [%]	P-Selectin positive [%]
Post HSD	32.6 ± 7.63	15.25 ± 3.18
1 h incubation ECs	33 ± 8.48	15.3 ± 7.49
1 h incubation 10 ng/ml TNF activated ECs	34.9 ± 6.5	15.75 ± 7.5
1 h incubation 100 ng/ml TNF activated ECs	35.35 ± 6.71	16 ± 7.63

Table 4.8: Shear activated platelets sub-populations (mean ± SD, N=2, n=4), expressed as a % of the total platelets sample P1, positive to the markers of interest, after incubation with chemically activated HUVECs

In order to verify if the incubation with activated HUVECs produce any change in the expression level of Annexin V and P-Selectin by sheared platelets, ANOVA test was performed to verify the equality of the considered populations, i.e. i) platelets after 70 dyne/cm^2 HSD stimulation; ii) 70 dyne/cm^2 sheared platelets after 1h incubation with HUVECs; iii) 70 dyne/cm^2 sheared platelets after 1h incubation with 10 ng/ml TNF-α activated HUVECs and iv) 70 dyne/cm^2 sheared platelets after 1h incubation with 100 ng/ml TNF-α activated HUVECs. According to our results, ANOVA did not suggest any significant difference (p-value > 0.05) among data, therefore the expression level of the platelets' activation markers does not change after incubation with activated HUVECs.

2. Characterization of adhesion mechanism

   - Regarding the SEM images acquisition, they were collected after 60 minutes incubation of shear activated platelets with chemically activated HUVECs.
     The samples are comparable, regardless the shear activation level of platelets (i.e. 30, 50, 70 dyne/cm^2) and the chemical activation of HUVECs (i.e. 10, 100 ng/ml TNFα for 24h). In particular, two meaningful images are reported in figure 4.21, representative for all the samples.

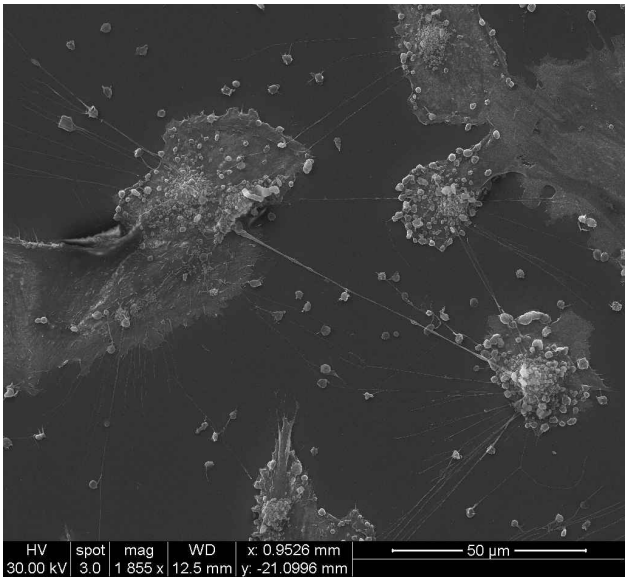

(a) Magnification 2000X

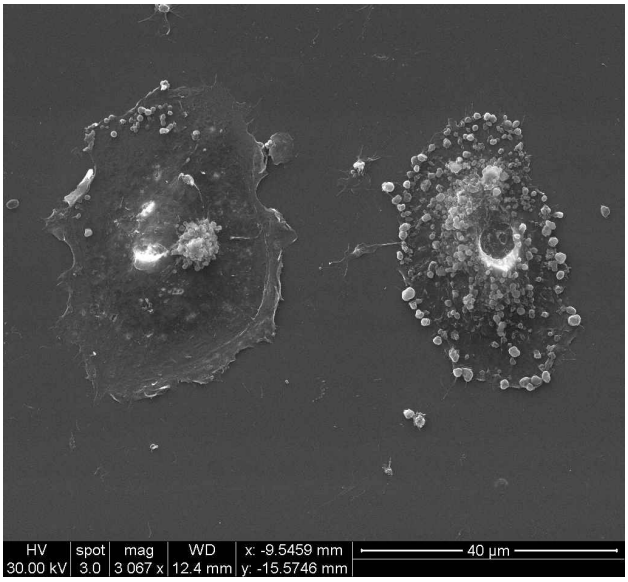

(b) Magnification 3000X

Figure 4.21: SEM images acquired for shear activated platelets incubated with chemically activated HUVECs

Chemically activated HUVECs represent a totally adhesive surface for shear activated platelets.

- To quantify the binding between chamically activated HUVECs and shear-activated platelets was further investigated via cytofluorimetric analysis of the HUVEC expression of the marker $\alpha_v\beta_3$ with the procedure described in section 3.4.2. The resulting histograms are shown in figure 4.22.
  The analyzed samples are TNFα-activated HUVECs incubated with shear conditioned platelets. TNFα-activated HUVECs that did not incubate with platelets are used as reference control sample (figure 4.22a). Only the results related to HUVECs activated through 10 ng/ml TNF-α are reported, since no difference was pointed out in terms of $\alpha_v\beta_3$ expression compared to 100 ng/ml TNF-α activated HUVECs.

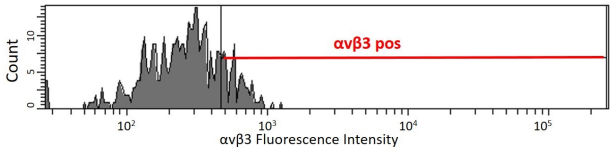

(a) 10 ng/ml TNFα activated HUVECs alone

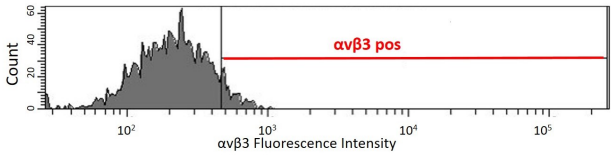

(b) 10 ng/ml TNFα activated HUVECs 1h incubated with 50 dyne/cm^2 conditioned platelets

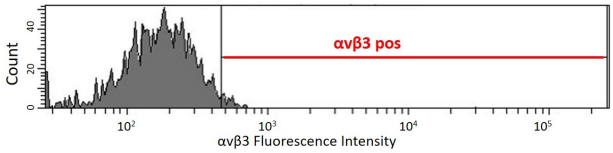

(c) 10 ng/ml TNFα activated HUVECs 1h incubated with 70 dyne/cm^2 conditioned platelets

Figure 4.22: Flow cytometry histograms for chemically activated HUVEC expression of $\alpha_v\beta_3$ (FITC-conjugated)

The values of the % sub-populations positive to $\alpha_v\beta_3$ (red straight lines in figure 4.22) are reported in table 4.9, based on the results of two experiments (N=2).

10 ng/ml activated HUVECs	$\alpha_v\beta_3$ positive [%]
No platelet incubation	16.45 ± 1.62
1h incubation with 50 dyne/cm^2 sheared platelets	9.05 ± 1.20
1h incubation with 70 dyne/cm^2 sheared platelets	4.1 ± 2.26

Table 4.9: Chemically activated HUVEC sub-populations (mean ± SD, N=2, n=4), expressed as a % of the total cellular sample P1, positive to the markers of interest

In order to evaluate if there was a significant difference in the expression level of $\alpha_V\beta_3$, an ANOVA test was carried out. In particular, the % positive subpopulations to $\alpha_V\beta_3$ from i) 10 ng/ml TNFα-activated HUVECs; ii) 10 ng/ml TNFα-activated HUVECs 1h incubated with 50 dyne/cm^2 sheared platelets and iii) 10 ng/ml TNFα-activated HUVECs 1h incubated with 70 dyne/cm^2 sheared platelets, were compared. According to our results, there is a significan difference (p-value < 0.05) among

data. Namely, the expression level of $\alpha_V\beta_3$ decreases between these three populations, suggesting that this integrin is "hidden" because involved in the binding between activated HUVECs and activated platelets. In addition, it is possible to underline that the expression level of the integrin is reduced in a more evident way in this condition (i.e. chemically activated HUVECs), compared to the case with non activated HUVECs (paragraph 4.2.2), confirming the SEM result, i.e. sheared platelets strongly adhere to activated ECs.

4.3 In silico model

As described in chapter 3, a numerical model was developed with the purpose to extract the WSS trends in the apical region of a HF-LV in presence of LVAD inflow cannula to exploit them to improve the experimental set up, introducing a perfusion unit, to mechanically stimulate ECs.
In the following sections the computational results are illustrated.

4.3.1 Mesh sensitivity analysis

With the procedure described in paragraph 3.6.1, a mesh sensitivity analysis was performed to determine the grid resolution for the two patient-specific geometries.
Regarding the healthy geometry, the selected grid is shown in figure 4.23.

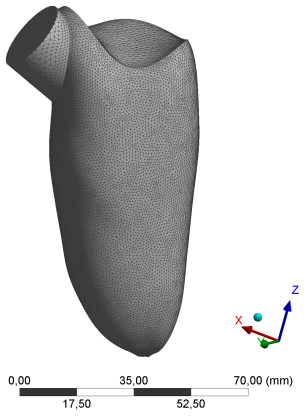

Figure 4.23: Healthy patient-specific LV geometry meshed with 445125 tetrahedral elements

The comparison between the averaged velocity magnitude obtained in the region 2 cm above the apex, considering the six different meshes listed in

section 3.6.1, is shown in figure 4.24a.
The percentage discrepancy of the time-averaged velocity was computed. A plateau was reached, as shown in figure 4.24b. The percentage difference between mesh 4 and mesh 5 was around 1.5 %, that is why mesh 4 (445125 elements) was chosen.

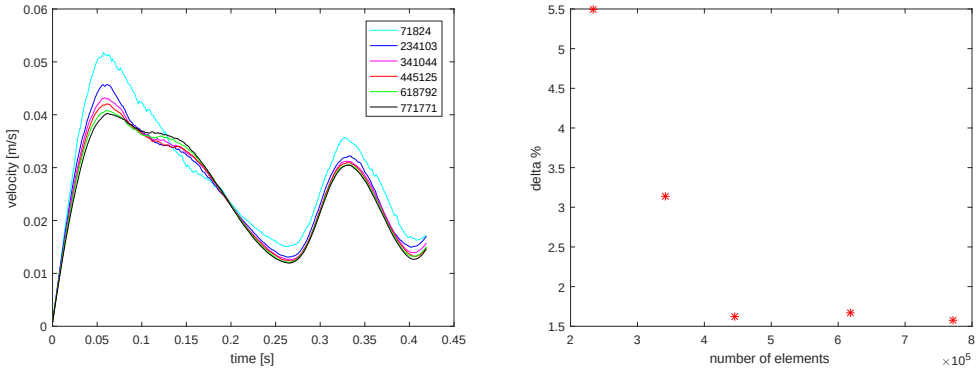

(a) (b)

Figure 4.24: Mean velocity magnitude in a region of the LV wall for the healthy patient-specific model 2 cm above the apex obtained with the six considered meshes (a). Percentage discrepancy between the current mesh and the previous one (b).

Regarding the HF geometry, the selected grid is shown in figure 4.25.

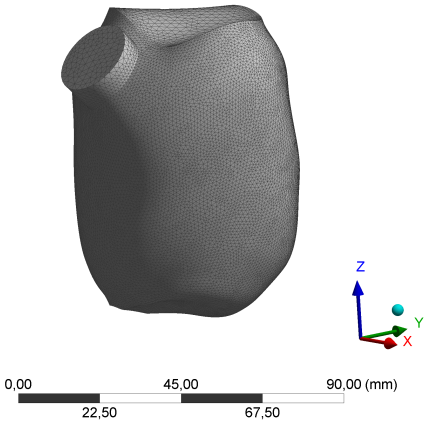

Figure 4.25: Pathological patient-specific LV geometry meshed with 473428 elements

The comparison between the averaged velocities in time obtained for the six different meshes listed in section 3.6.1, is shown in figure 4.26a. Since the percentage difference between the mesh 5 and the mesh 4 was around 2 %, as shown in figure 4.26b, the mesh 4 (473428 elements) was chosen.

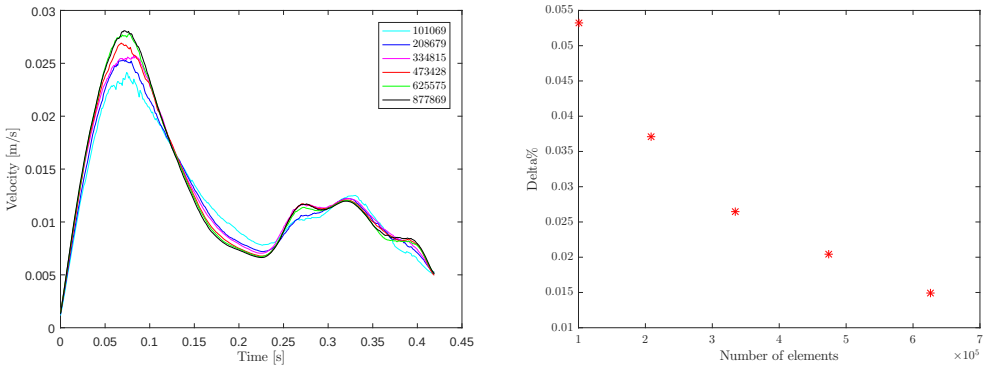

(a) (b)

Figure 4.26: Averaged velocity magnitude for the pathological patient-specific model in a region of the ventricular wall 2 cm above the apex obtained with the six considered meshes (a). Percentage discrepancy between the current mesh and the previous one (b).

4.3.2 Numerical inertia

With the purpose to determine a sufficient number of cycles to be run to guarantee a full development of the flow, the WSS trend in a region close to the ventricular apex was evaluated at each cardiac cycle. The obtained trends are shown in figure 4.27 for both systole and diastole. The percentage difference between the time-averaged WSS between the third and the fourth cycle is less than 2 %, that let us to consider as reliable the results obtained at the third cycle. Several studies in literature developed CFD models to simulate the fluid dynamics within the LV. All of these studies (e.g. Imanparast et al in [66]) reported that 3-4 cycles are enough to obtain representative results.

4.3.3 Grid motion

In paragraph 3.6.2, the grid motion UDFs implementation was deeply detailed. As mentioned, the so-obtained movement of the ventricular wall is characterized by twist and contraction during systole, untwist and dilation

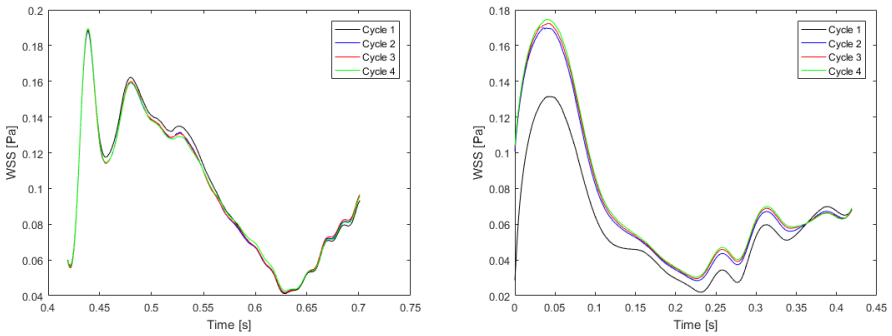

(a) (b)

Figure 4.27: WSS trend in time during systole (a) and diastole (b), computed running 4 consecutive cycles

during diastole. The better way to visualize the ventricular motion is to superimpose the resulting meshes at the end of the two phases of the cardiac cycle, i.e. end-systole and end-diastole, as it is shown in figure 4.28.

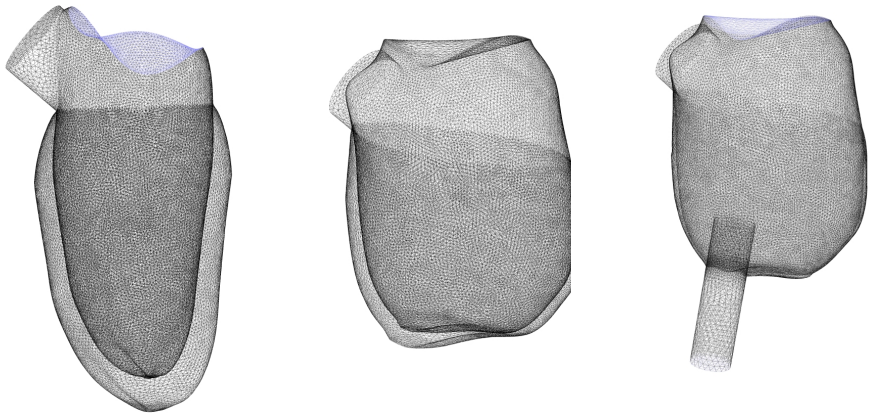

(a) (b) (c)

Figure 4.28: Superimposition of end-diastolic and end-systolic configurations for the patient-specific models: (a) healthy LV, (b) HF-LV and (c) HF-LV post LVAD implant

The volumetric difference between the two meshes determine the contractile capacity of the model, in particular, the healthy LV ejects 70 ml towards the aorta (figure 4.28a); the HF-LV 35 ml (figure 4.28b); the HF-LV post LVAD would eject 10 ml (figure 4.28c), but, as will be shown in the next section, the so-limited contractile capacity is not enough to direct the blood towards

the aorta.

4.3.4 Velocity streamlines

In order to characterize the different hemodynamics related to the patient-specific models, case and data files on Fluent were exported to CFD-Post, allowing to perform post-processing analysis. In particular, the streamlines of the velocity magnitude at both the diastolic and systolic peaks were extracted, for each patient-specific model. During the diastolic phase, the streamlines originate from the mitral valve, i.e. filling phase, while, during the systolic one, they originate from the ventricular wall, i.e. ejection phase. Figures 4.29a and 4.29b show the velocity streamlines extracted from the healthy LV. Figures 4.29c, 4.29d and 4.29e, 4.29f show the streamlines related respectively to the HF-LV with a reduced contractile capacity (i.e. ejected volume = 35 ml) and to the HF-LV with a negligible contractile capacity (i.e. ejected volume = 10 ml). Figures 4.29g and 4.29h represent the velocity streamlines extracted from the post LVAD implant HF-LV model.
The systolic peak velocity in the aortic root is equal to: 1.14 m/s for the healthy LV (figure 4.29b); 0.68 m/s for the HF-LV with reduced contractile capacity (figure 4.29d); 0.18 m/s for the HF-LV with negligible contractile capacity (figure 4.29f). In the HF-LV post LVAD implant model, no streamlines are directed toward the aorta, but all the blood is directed toward the inflow cannula, during both the phases of the cycle (figures 4.29g and 4.29h).

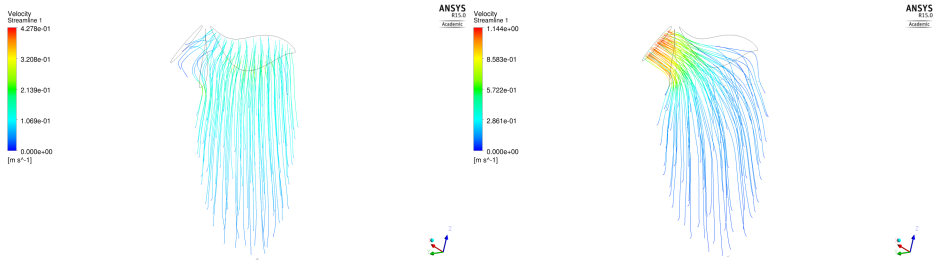

(a) (b)

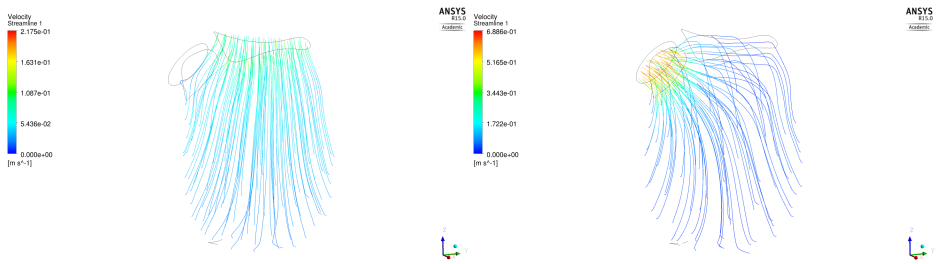

(c) (d)

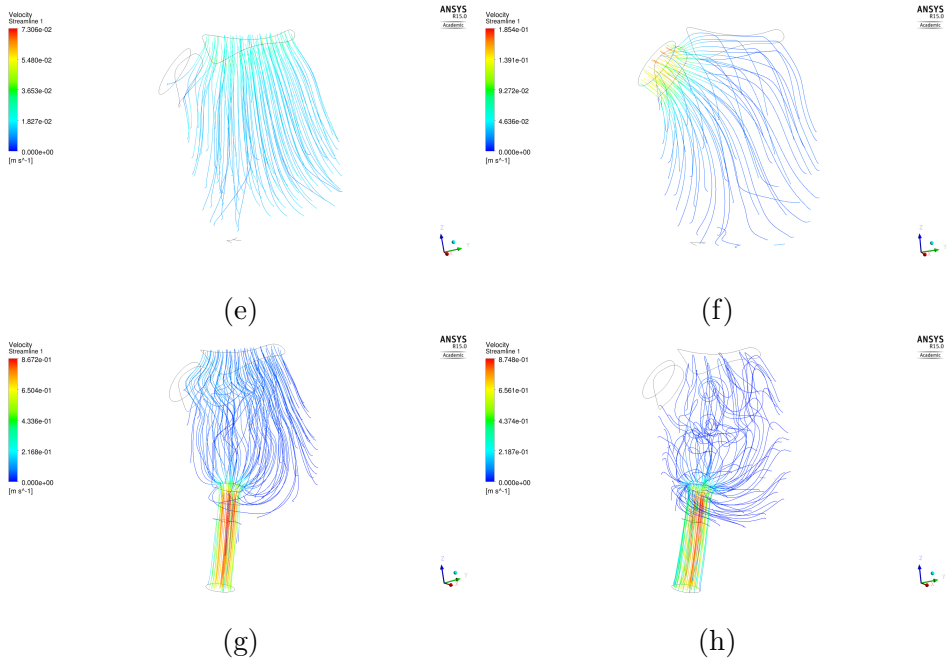

Figure 4.29: Velocity streamlines at the diastolic (a, c, e, g) and systolic (b, d, f, h) peaks extracted from the patient-specific models: (a-b) healthy LV, (c-d) HF-LV with reduced contractile capacity, (e-f) HF-LV with negligible contractile capacity, (g-h) HF-LV post LVAD implant

4.3.5 WSS extraction

As described in the paragraph 3.6.6, the WSS trend has a direct influence on the activation of the endothelium, since it is known that low and oscillating shear stresses can cause endothelial activation. For this reason, it was of interest to obtain the WSS trend during the cardiac cycle in the apical region of LVs.
Figure 4.30 shows the trends in time of the axial component (z component) of the WSS, referred to the patient-specific healthy LV (figure 4.30a), HF pre- and post-LVAD implant LVs (figures 4.30b and 4.30c).
WSS magnitude dramatically changes in the three models, as it is better pointed out in figure 4.31, that shows in the same plot the trends derived from the three models.
In particular, both the pre- and post-implant models showed very low values of WSSs (the peak values are one order of magnitude lower compared to the one derived from the healthy model), highlighting the presence of a stagnation region at the LV-LVAD cannula interface.

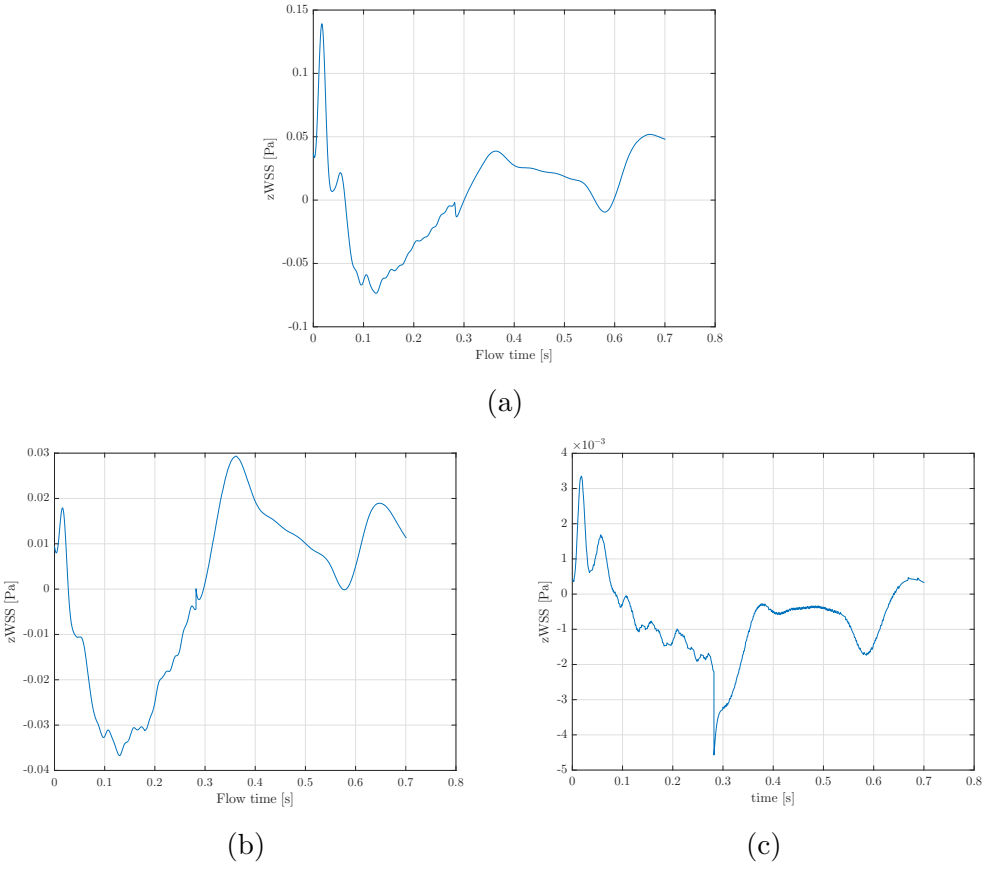

Figure 4.30: z-WSS trends (i.e. along the axial direction of the LV) during the cardiac cycle computed for the three models: (a) patient-specific healthy, (b) pathological pre-LVAD implant and (c) pathological post-LVAD implant

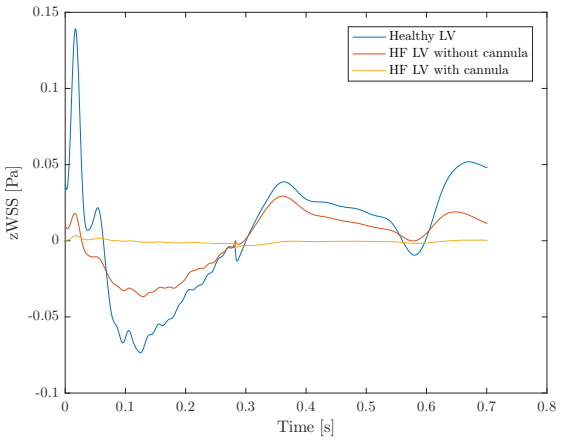

Figure 4.31: zWSS trends obtained for the three considered models

Chapter 5

Discussion and Conclusions

5.1 Discussion

LVAD is an established therapeutic strategy for patients with end-stage HF, both as bridge-to-transplant and destination therapy. Nevertheless, the clinical success of LVADs is still accompanied by significant post-implant complications, including thrombotic events. Like most other implanted devices, LVADs activate the coagulation system resulting in device-related thrombus formation, mostly at the interface between the LV and the LVAD inflow cannula.
So far, thrombus formation in LVAD recipients was mainly ascribed to shear-mediated platelet activation, due to the very high shear stress levels (hyper-shear) generated in the pump. Another important aspect of thrombus formation in LVAD recipients is related to EC inflammation leading to endothelial injury, which is known to enhance thrombosis. However, few studies are focused on the endothelial dysfunction in LVAD recipients.
Moreover, endothelial damage and the resulting dysfunction are known to induce complex interactions between circulating activated platelets and inflamed ECs. The two cell types communicate through receptor mediated cell-cell adhesion. The mechanism of platelets adhesion to endothelium leads to thrombus formation. Nevertheless, these interactions were poorly investigated.
In the present study, an experimental set-up able to characterize the mutual interaction between inflamed ECs and activated platelets was developed, in order to provide further insights into the mechanisms responsible for thrombosis in LVAD recipients. In particular, the mechanism of adhesion of platelets on ECs, known to lead to thrombus formation in vivo, was characterized. For this purpose, sheared platelets were incubated with cultured HUVECs and the interaction between the two cell types was evaluated in

terms of platelet adhesion.
The mutual interaction between platelets and ECs was clearly visualized through SEM images acquisition, demonstrating that the inflamed endothelium represents a totally adhesive surface for platelets, both activated and non-activated. The SEM imaging showed that activated HUVECs were entirely covered by single and aggregated platelets. Shear activated platelets were shown to adhere to non-activated ECs as well, result which is confirmed by Czervionke and co-workers [62]. Additionally, the number of adhered platelets resulted dependent on the initial platelet activation level. However, the adhesion amount to non-inflamed ECs is not comparable to the one visualized when ECs were inflamed.
Conversely, SEM imaging of HUVECs incubated with resting platelets showed a very small number of adhered platelet, in accordance to [63] and [62], who proved that resting platelets bind minimally to cultured HUVECs.
Binding of platelets to ECs was further confirmed by flow cytometry analysis for the endothelial integrin $\alpha_v\beta_3$: the expression level of this marker was found to be reduced after incubation with shear activated platelets. The higher was the activation level of platelets (i.e. HSD imposed), the lower was the expression of $\alpha_v\beta_3$ by HUVECs. This result is in accordance with a previous study [63], showing that platelets bind to endothelial $\alpha_v\beta_3$ integrin by forming bridges with fibrinogen, fibronectin and vWF.

Regarding EC inflammation, this was achieved incubating cultured HUVECs with a known chemical agonist, i.e. TNF-α, obtaining a modulation of the inflammation, dependent on both TNF-α concentration and exposure time. This modulation of HUVEC inflammation was proved through both ELISA and flow cytometry techniques for, respectively, soluble and surface ICAM-1, VCAM-1 and E-Selectin markers.
Concerning, flow cytometry analysis, our results are in accordance with the study of Mackay et al. [52], who demonstrated through flow cytometry that ICAM-1 is constitutively expressed by unstimulated HUVECs and its expression increases over time if incubated with 10 ng/ml TNF-α, while VCAM-1 is not expressed by unstimulated HUVECs but its expression increases over time if incubated with 10 ng/ml TNF-α.
The results of the ELISAs are confirmed by Boehme et al. [55], who demonstrated that the activation of ECs with 10 ng/ml of TNF-α results in a significant increase in the levels of the soluble ICAM-1 VCAM-1 and E-selectin at 24h. The fact that the EC response to TNF-α is concentration-dependent is in accordance with the study of Friedl et. al. [67], who exposed HUVECs to increasing TNF-α concentrations (from 0.1 to 1000 ng/ml), obtaining a dose-dependent expression of tissue factor.

The developed experimental platform was used to characterize the activation level of both platelet and ECs after being incubated together, to investigate the effect of the interaction between the two cell types.
It was demonstrated through flow cytometry that HUVECs do not increase the expression of activation markers after incubation with platelets, both resting and shear-activated, suggesting that the presence of platelet does not induce any significant response in terms of endothelial activation.
If platelets were shear-activated using the HSD, it was demonstrated through PAS assay that their activation level increases over time, up to 60 minutes of incubation with cultured HUVECs. However, shear activated platelets were shown to increase their PAS% value when incubated alone as well. The activation increase is more enhanced if sheared platelets are incubated with TNFα-activated HUVECs, demonstrating a significant role of inflamed endothelium on platelet activation. On the other hand, resting platelets do not increase their activation level after incubation with cultured HUVECs, both chemically inflamed and not, according to both PAS assay and flow cytometry results (i.e. PAS% values and expression level of P-selectin and Annexin V do not increase).

In order to settle the basis for a future improvement of the experimental set-up, namely the mechanical stimulation of cultured HUVECs through in-vivo like WSS waveforms, a CFD model was developed to simulate the hemodynamics of the LV in presence of LVAD inflow cannula. Several progresses were made in the present model compared to the state of the art. One of the most important limitation underlined in several studies, is the inaccuracy of the results given by the over-simplified geometry. For example, Ong et. al. [23] [68] developed axisymmetric 2D LV models, Liu et al [24] a semi-ellipsoid LV model. A quality of the present model is the use of patient-specific geometries, which provide more reliable results. Another advantage is the capability to simulate different contractile capacities, overtaken a limitation pointed out by Liao et. al. [25], who developed a static LV model, even though some contractility is still present in HF-LV after LVAD implant. The results related to the healthy LV simulations can be compared to the ones obtained by Nguyen et al. [69], whose patient-specific LV model was derived from MRI images. The velocity peaks for both systole and diastole (i.e. respectively $\backsimeq$ 1 m/s for the systolic peak on the aortic root and $\backsimeq$ 0.5 m/s for the diastolic peak on the mitral valve) are comparable to the ones obtained in the present study, both in terms of magnitude and distribution. Concerning the HF-LV post LVAD implant, Liu et al [24] evaluated the fluid dynamics within the LV in presence of inflow cannula with different

geometries. The case with the cannula with a blunt tip is very close to the cannula geometry considered in the present work. They obtained a velocity magnitude within the cannula around 0.85 m/s with a uniform distribution, confirming our results. Additionally, the Reynolds number computed within the cannula is comparable to the one obtained by [24], i.e. $\backsimeq$ 2600.
The close-to-zero velocity values in the apical region of the HF-LVs models (with and without LVAD) demonstrate the presence of blood stagnation. In addition, it is known that velocity values below 0.1 m/s represent a pro-thrombotic hemodynamic condition [24].
The model was exploited to extract the WSS trends in the apical region, that were one order of magnitude lower in presence of LVAD inflow cannula, flow condition that is known to be prone to shift ECs toward a thrombogenic phenotype.

5.2 Limitations and future developments

The present study is affected by various limitations that could be overcome.
A limitation of the developed experimental platform is the possibility of investigating only one of the mechanisms characterizing the process of thrombosis, i.e. the adhesion of activated platelets to inflamed endothelium. In order to provide a complete understanding of the mechanisms responsible for thrombus formation in LVAD recipients, it would be necessary to analyse many other aspects, such as the coagulation markers expression. On the other hand, the possibility to analyze a single mechanism of a complex phenomenon is an intrinsic characteristic of in-vitro models, which is also an advantage, allowing to characterize one mechanism at once.
Additionally, it is known that thrombus formation can be ascribed not only to the altered hemodynamics, but also to the blood contact with a foreign surface. In the present study, only the first thrombus-leading aspect was investigated, neglecting the platelet activation induced by the contact with artificial materials.
The proper cells that should be used to model the endothelium that lines the ventricle are endocardial primary cells, which are actually involved in the interaction with platelets in vivo. We used HUVECs instead, which are the most commonly used endothelial cellular line, since they were available at our laboratories (both at Politecnico di Milano and at the University of Arizona).
The interaction between platelets and ECs was studied up to 60 minutes. It

would be possible to characterize it for a longer period of time, to understand if the mutual effect vanishes or if it is enhanced over time.
Moreover, platelet activation was induced through HSD, stimulating platelets with a constant level of shear stress for ten minutes. An easy improvement could be to shear platelets through the HSD with LVAD-specific shear waveform, as performed by Chiu et al. [6], in order to induce a device-specific level of activation.
Concerning the computational model exploited to extract the WSS trends at the ventricular apical region, it displays some limitations that should be pointed out as well.
The interaction between blood, myocardial wall and the cannula was neglected. To take it into account, a Fluid Structure Interaction (FSI) model should be used.
A constant velocity boundary condition was applied at the inlet of the cannula. On the contrary, it is known that the suction flow rate depends on the impedance of the circulatory system.
Another limitation is due to the simplified boundary conditions that were used to simulate the HF-LV model, i.e. zero pressure on the aortic valve during systole and zero pressure on the mitral valve during diastole, that do not faithfully reproduce the physiological conditions. This choice was dictated by the impossibility to find in literature, at the best of our knowledge, the real pressure trends on the cardiac valves for HF-LV, as it was performed for the healthy model.
Finally, the inflow cannula was simply modeled as a cylinder inserted into the apex, whose penetration angle allowed the axis of the cannula to be directed toward the center of the mitral valve plane. It would be possible to extract from 3D-TT-ECHO data the precise cannula position (e.g. penetration depth, insertion angle) for each patient. In this way, the geometry would be totally patient-specific.

A very important future development of the present study is represented by the integration of the experimental platform with a perfusion set-up able to replicate WSS patterns extracted from the CFD model in order to mechanically stimulate cultured HUVECs. In this way, in-vivo like shear-induced inflammation of ECs would be obtained, instead of the chemically-induced inflammation.
In particular, it would be necessary to define a perfusion protocol able to replicate the in-silico-derived patient-specific WSS trends, in order to stimulate cultured HUVEC. In this way, the developed in-vitro platform would be able to investigate the interaction between inflammed ECs and shear-activated platelets on a patient-specific and device-specific basis.

Additionally, the implemented platform could be a useful tool to test the efficacy of anti-thrombotic (AT) drugs. It would be possible to exploit the experimental set-up and protocols developed to evaluate the EC-platelet interaction mechanisms in presence of AT drugs, also evaluating different therapies (single drug or combination of drugs, different drug dose, etc.), in order to evaluate patient-tailored AT protocols. Moreover, prospectively, a possible pharmacological target for EC inflammation might be identified.

5.3 Conclusions

In conclusion, the developed experimental platform is able to characterize the mechanism of platelet adhesion to endothelium, which leads to thrombosis in vivo. It was demonstrated that the inflammation of cultured HUVECs causes an evident adhesion of platelets to ECs and a decrease of the expression of the endothelial integrin $\alpha_v\beta_3$, which is involved in the binding between platelets and ECs. Thanks to the results obtained in the present study, it is possible to suppose a role of inflamed ECs in thrombus formation in LVAD recipients. Therefore, a pharmacological target for EC inflammation could be identified. These activities might potentially lead to decrease and/or limit thrombotic complications in LVAD recipients.

Appendices

A Analysis Techniques

A.1 AlamarBlue cell viability assay [70]

AlamarBlue assay is used to assess cell viability: the alamarBlue reagent functions as a cell health indicator, by using the reducing power of living cells to quantitatively measure the proliferation of a cell line. When cells are alive, they maintain a reducing environment within the cytosol. Resazurin, the active ingredient of alamarBlue reagent is a non-toxic, cell permeable compound that is blue in colour and non fluorescent. Upon entering cells, resazurin is reduced to resorufin, a compound that is red in colour and highly fluorescent. Viable cells continuously convert resazurin to resorufin, increasing the overall fluorescence and colour of the cell growth media.

A.2 ELISA

The Enzyme Linked ImmunoSorbent Assay (ELISA) is a laboratory technique used for the detection and quantification of a given Antigen (Ag) in a sample [71]. ELISAs are commonly performed in 96-well Polystyrene (PS) plates that allow for passive binding of proteins. Antibodies (Abs) are linked to enzymes (e.g. alkaline phosphatase - ALP) which convert a colorless substrate (e.g. p-nitrophenylphosphate - pNPP) to a colored (yellow p-nitrophenol) that can be then evaluated through a spectrophotometric analysys.
There are two main types of ELISA that can be performed:

- Indirect ELISA
  The indirect ELISA, whose scheme is illustrated in figure A.1a, is a 2-step method that exploits labeled Abs to detect an Ag of interest.
  In particular, micro-well plates are incubated with Ags, which adhere to PS because of charge interactions. Then, the not-adhered Ags are washed up. A solution of non-reactive proteins, such as Bovin serum

albumin (BSA) or casein, is added, in order to block the free binding sites.

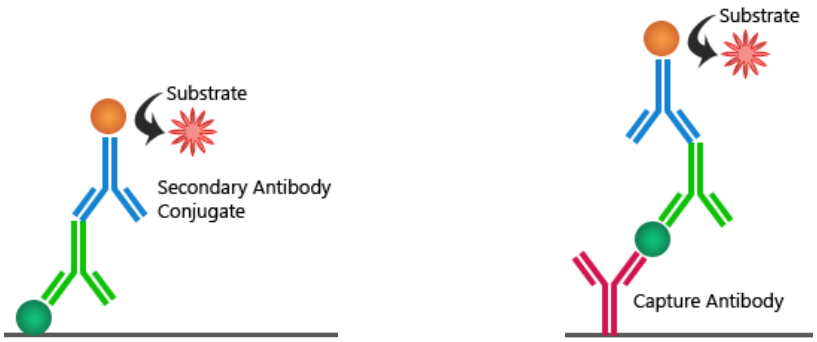

(a) (b)

Figure A.1: Schematic rapresentation of indirect ELISA (a) and sandwich ELISA (b)

Primary Abs, which are usually monoclonal (i.e. Abs specific for a particular epitope of the Ag, that are all identical because made by the same immune cell), are added and washed. This is followed by incubation with enzyme-labeled secondary Abs, which are usually polyclonal (i.e. obtained from different parent B cells, each identifying a specific epitope of the Ag) that recognize primary Abs. A substrate for the enzyme is added. The Ab-Ag interaction is detectable thanks to the emission of a chromogenic or fluorescent signal, quantified through a spectrophotometer. The measured signal (i.e. optical density or absorbance) is interpolated with a standard curve, obtained measuring the signal with known Ag concentrations.

- Sandwich ELISA
  The sandwich assay, whose scheme is illustrated in figure A.1b, allows the quantification of Ags between two layers of Abs. Two epitopes of the Ag to be measured are bound between two Abs, capture Ab and detection Ab. In particular, micro-well plates are coated with specific Ab (i.e. capture Ab). Washing procedure is followed by the blocking of free binding sites, as previously described. The solution containing the Ag that must be assayed is added. The non-captured Ags are washed. Enzyme-linked Abs are added (i.e. detection Abs) and then washed. After having added the substrate, the chromogenic or fluorescent signal can be measured. This assay is sensitive and robust. The main advantage with respect to the indirect ELISA is that it is able

to discriminate between different protein sharing common epitopes. On the other hand, little amount of proteins are difficult to be detected because the amplification of the signal given by the binding of more than one Ab to different epitopes of the same Ag is not possible.

A.3 Flow Cytometry [72]

Flow cytometry is a widely employed technology that allows simultaneous measurement and analysis of multiple physical characteristics of single particles, usually cells, as they flow in a fluid stream through a beam of light. A flow cytometer is made by four main components, whose schematic representation is shown in figure A.2:

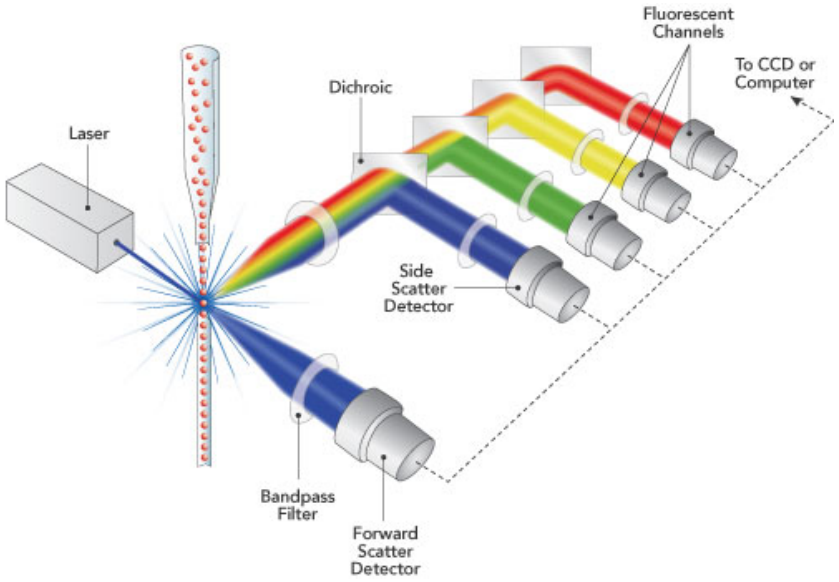

Figure A.2: Illustration of the flow cytometer main components

- a fluidics system, which allows the alignment of the cells into a stream of single particles that can be interrogated by the machine's detection system. It consists of a central channel where the sample is injected, enclosed by an outer sheath of faster flowing fluid able to crate a massive drag effect on the narrowing central chamber.

- a light source, which is usually a laser beam at one or more discrete frequencies, and detectors, which collect the scattered light and the fluorescence emission (if the particles are labeled with fluorochromes), providing information about the particles' properties. In particular,

when the laser beam strikes the stream, the light that is scattered in the forward direction is collected by a lens known as forward scattered channel (FSC) and its intensity roughly corresponds to the particle size. The light that is measured approximately at a 90^o angle to the excitation line is collected by the side scatter channel (SSC), providing information about the granular content within the cell (i.e. proportional to cell complexity). The fluorescence emission is collected by different fluorescence channels, whose specificity is controlled by optical filters, which select the proper wavelength. This measurement can provide quantitative and qualitative data about the fluorochrome-labeled cell surface receptor or intracellular molecules. For this detection, fluorescent probes, such as fluorochrome-conjugated antibodies, are added to the sample to target the antigen of interest.

- a computer with flow cytometry software, which analyzes the characteristics of each event (i.e. cell), based on the scattered light and on fluorescence properties. Collected data can be visualized with single parameter histograms (i.e. cell count on the y-axis and the measured parameter on the x-axis) or two parameters histograms (i.e. a dot plots in which each dot corresponds to a single cell, displaying two measured parameters on the two axes). It is possible to visualize only the cells of interest while eliminating unwanted particles (e.g. dead cells, aggregates or debris) subdividing the data by gating.

- Fluorescence-Activated Cell Sorter (FACS) is an optional equipment, which allows the physical separation of cells based on their characteristics. In practice, FACS isolate the cells of interest by vibrating the sample stream which is broken into drops. It applies a voltage to drops that meet the pre-defined sorting criteria (each drop contains a single cell). A negative and a positive charged plate are present on both side of the vibrating stream, deflecting the droplets to collection tubes based on their polarity (i.e. their property).

A.4 Scanning Electron Microscopy (SEM) [73]

Scanning electron microscope is a particular type of microscope that produces images of a solid specimen by scanning it with a focused beam of high-energy electrons. It's a method used for high resolution imaging of surfaces. The SEM has a much higher magnification and a greater depth of field with respect to a light microscopy. The signals that derive from the electron-sample interactions reveal information about the sample external morphology, chemical composition, crystalline structure and orientation of

materials. In most applications, data are collected over a selected area of the surface of the sample, and a 2-dimensional image is generated. The signals produced by SEM include secondary electrons (SE), backscattered electrons (BSE), diffracted backscattered electrons (used to determine crystal structures and orientations of minerals), photons (characteristic X-rays), visible light and heat. The signals result from interactions between the electrons and the atoms at various dephts within the sample. SE and BSE are commonly used for imaging samples. In the standard detection mode, i.e. the SEI (secondary electron imaging), the SE are emitted from very close to the surface. In this way a very high resolution image of a sample surface can be produced, revealing details less than 1 nm in size. On the other hand, BSE are reflected from the sample by elastic scattering. Since they emerge from deeper locations within the specimen, the resolution of BSE images is generally poorer than SE images. However, BSE are valuable for illustrating contrasts in composition in multiphase samples.
Samples are generally mounted on a specimen holder, called stub, using a conductive adhesive. For SEM imaging, specimens must be electrically conductive, at least at the surface and electrically grounded to prevent the accumulation of electrostatic charge. For this reason, non-conducting materials are usually coated with an ultrathin coating of electrically conductive material (gold, gold/palladium alloy, platinum, tungsten), deposited on the sample either by a low-vacuum sputter coating or by high-vacuum evaporation.
In addition, a specimen is normally required to be completely dry, since the samples chamber is at high vacuum. For biological samples, like living cells, tissues and whole organisms, a chemical fixation is required to preserve and stabilize the structure. The dry specimen is usually mounted on a specimen stub using epoxy resin or electrically conductive double-sided adhesive tape and sputter-coated with gold or gold/palladium alloy before examination in the microscope.
In a typical SEM, an electron beam is thermionically emitted from an electron source ("Gun") fitted with a tungsten filament cathode. The beam is generated in an electron column above the sample chamber. The column and the chamber are both at a moderate vacuum to allow the electrons to travel freely. The electron beam, which tipically has an energy ranging from 0.2 keV to 40 keV, is focused by one or two condenser lenses to a spot about 0.4 nm to 5 nm in diameter. The beam passes through pairs of scanning coils or deflector plates in the electron column, typically in the final lens, which deflect the beam in the x and y axes so that it scans in a raster pattern over a rectangular area of the sample surface. The primary beam interacts with the sample: the electrons lose energy by random scattering and absorption.

The energy exchange results in the reflection of high energy electrons, each of which can be detected by specialized detectors. Electronic amplifiers are used to amplify the signals, which are displayed as variations in brightness on a computer monitor. Each pixel of computer video memory is synchronized with the position of the beam on the sample in the microscope and the resulting image is a distribution map of the intensity of the signal emitted from the scanned area.
Magnification in a SEM can be controlled over a range of about 6 orders of magnitude, from about 10 to 50'000 times.
A schematic representation of the SEM is shown in figure A.3.

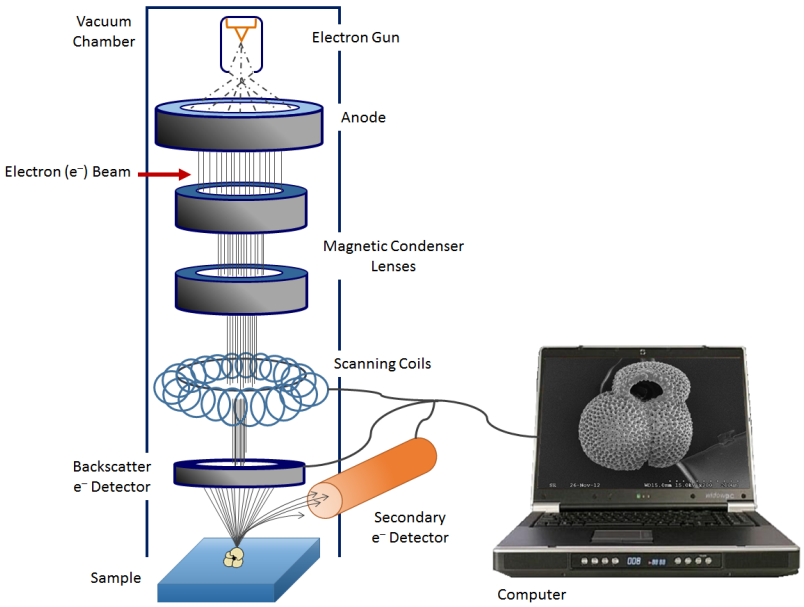

Figure A.3: Illustration of the SEM main components

Bibliography

[1] Clinton D Kemp and John V Conte. *The pathophysiology of heart failure.* Cardiovascular Pathology, 21(5):365–371, 2012.

[2] Longjian Liu and Howard J Eisen. *Epidemiology of heart failure and scope of the problem.* Cardiology clinics, 32(1):1–8, 2014.

[3] Joseph AR Englert III, Jennifer A Davis, and Selim R Krim. *Mechanical Circulatory Support for the Failing Heart: Continuous-Flow Left Ventricular Assist Devices.* The Ochsner Journal, 16(3):263–269, 2016.

[4] `http://rebelem.com/left-ventricular-assist-device/`.

[5] Arman Kilic, Michael A Acker, and Pavan Atluri. *Dealing with surgical left ventricular assist device complications.* Journal of thoracic disease, 7(12):2158, 2015.

[6] Wei-Che Chiu, Gaurav Girdhar, Michalis Xenos, Yared Alemu, Jõao S Soares, Shmuel Einav, Marvin Slepian, and Danny Bluestein. *Thromboresistance comparison of the HeartMate II ventricular assist device with the device thrombogenicity emulation-optimized HeartAssist 5 VAD.* Journal of biomechanical engineering, 136(2):021014, 2014.

[7] Randall C Starling, Nader Moazami, Scott C Silvestry, Gregory Ewald, Joseph G Rogers, Carmelo A Milano, J Eduardo Rame, Michael A Acker, Eugene H Blackstone, John Ehrlinger, et al. *Unexpected abrupt increase in left ventricular assist device thrombosis.* New England Journal of Medicine, 370(1):33–40, 2014.

[8] Mandeep R Mehra, Yoshifumi Naka, Nir Uriel, Daniel J Goldstein, Joseph C Cleveland Jr, Paolo C Colombo, Mary N Walsh, Carmelo A Milano, Chetan B Patel, Ulrich P Jorde, et al. *A fully magnetically levitated circulatory pump for advanced heart failure.* New England Journal of Medicine, 2016.

[9] Joseph G Rogers, Francis D Pagani, Antone J Tatooles, Geetha Bhat, Mark S Slaughter, Emma J Birks, Steven W Boyce, Samer S Najjar, Valluvan Jeevanandam, Allen S Anderson, et al. *Intrapericardial left ventricular assist device for advanced heart failure.* New England Journal of Medicine, 376(5):451–460, 2017.

[10] Samer S Najjar, Mark S Slaughter, Francis D Pagani, Randall C Starling, Edwin C McGee, Peter Eckman, Antone J Tatooles, Nader Moazami, Robert L Kormos, David R Hathaway, et al. *An analysis of pump thrombus events in patients in the HeartWare ADVANCE bridge to transplant and continued access protocol trial.* The Journal of Heart and Lung Transplantation, 33(1):23–34, 2014.

[11] Katharine H Fraser, Tao Zhang, M Ertan Taskin, Bartley P Griffith, and Zhongjun J Wu. *Computational fluid dynamics analysis of thrombosis potential in left ventricular assist device drainage cannulae.* ASAIO journal (American Society for Artificial Internal Organs: 1992), 56(3):157, 2010.

[12] Chitaru Kurihara, Minoru Ono, Takashi Nishimura, Aya Saito, Tsuyoshi Taketani, Motoyuki Hisagi, Kan Nawata, Osamu Kinoshita, Tetsurou Morota, Noboru Motomura, et al. *Use of DuraHeart® support for more than 1 year as the first successful bridge to heart transplantation in Japan.* Journal of Artificial Organs, 14(1):67–69, 2011.

[13] Ranjit John, Sandhya Panch, Jennifer Hrabe, Peng Wei, Anna Solovey, Lyle Joyce, and Robert Hebbel. *Activation of endothelial and coagulation systems in left ventricular assist device recipients.* The Annals of thoracic surgery, 88(4):1171–1179, 2009.

[14] David R Kumar, Erin Hanlin, Ingrid Glurich, Joseph J Mazza, and Steven H Yale. *Virchow's contribution to the understanding of thrombosis and cellular biology.* Clinical medicine & research, 8(3-4):168–172, 2010.

[15] KK Wu, MD and P Thiagarajan, MD. *Role of endothelium in thrombosis and hemostasis.* Annual review of medicine, 47(1):315–331, 1996.

[16] LESLIE V Parise, SUSAN S Smyth, and BARRY S Coller. *Platelet morphology, biochemistry and function.* Williams hematology, 7:1597–1645, 2001.

[17] Jawaad Sheriff, Danny Bluestein, Gaurav Girdhar, and Jolyon Jesty. *High-shear stress sensitizes platelets to subsequent low-shear conditions.* Annals of biomedical engineering, 38(4):1442–1450, 2010.

[18] Bente Thamsen, Bastian Blümel, Jens Schaller, Christian O Paschereit, Klaus Affeld, Leonid Goubergrits, and Ulrich Kertzscher. *Numerical analysis of blood damage potential of the HeartMate II and HeartWare HVAD rotary blood pumps.* Artificial organs, 39(8):651–659, 2015.

[19] Katharine H Fraser, Tao Zhang, M Ertan Taskin, Bartley P Griffith, and Zhongjun J Wu. *A quantitative comparison of mechanical blood damage parameters in rotary ventricular assist devices: shear stress, exposure time and hemolysis index.* Journal of biomechanical engineering, 134(8):081002, 2012.

[20] Jun Zhang, Albert F DeFelice, Joseph P Hanig, and Thomas Colatsky. *Biomarkers of endothelial cell activation serve as potential surrogate markers for drug-induced vascular injury.* Toxicologic pathology, 38(6):856–871, 2010.

[21] Dorothea I Siegel-Axel and Meinrad Gawaz. *Platelets and endothelial cells.* In Seminars in thrombosis and hemostasis, volume 33, pages 128–135. Copyright© 2007 by Thieme Medical Publishers, Inc., 333 Seventh Avenue, New York, NY 10001, USA., 2007.

[22] J Anthony Ware and Donald D Heistad. *Platelet-endothelium interactions.* New England Journal of Medicine, 328(9):628–635, 1993.

[23] ChiWei Ong, Socrates Dokos, BeeTing Chan, Einly Lim, Amr Al Abed, NoorAzuanBinAbu Osman, Suhaini Kadiman, and Nigel H Lovell. *Numerical investigation of the effect of cannula placement on thrombosis.* Theoretical Biology and Medical Modelling, 10(1):1, 2013.

[24] Guang-Mao Liu, Hai-Bo Chen, Fu-Liang Luo, Yan Zhang, Han-Song Sun, Jian-Ye Zhou, and Sheng-Shou Hu. *Numerical simulation of LVAD inflow cannulas with different tip.* International Journal of Chemical Engineering, 2012, 2012.

[25] Sam Liao, Benjamin Simpson, Michael Neidlin, Tim AS Kaufmann, Zhiyong Li, Maria A Woodruff, and Shaun D Gregory. *Numerical prediction of thrombus risk in an anatomically dilated left ventricle: the effect of inflow cannula designs.* BioMedical Engineering OnLine, 15(2):587, 2016.

[26] Anthony R Prisco, Alberto Aliseda, Jennifer A Beckman, Nahush A Mokadam, Claudius Mahr, and Guilherme JM Garcia. *Impact of LVAD Implantation Site on Ventricular Blood Stagnation.* ASAIO Journal, 2017.

[27] D Bluestein, KB Chandran, and KB Manning. *Towards non-thrombogenic performance of blood recirculating devices.* Annals of biomedical engineering, 38(3):1236–1256, 2010.

[28] Gaurav Girdhar, Michalis Xenos, Yared Alemu, Wei-Che , Bryan E Lynch, Jolyon Jesty, Shmuel Einav, Marvin J Slepian, and Danny Bluestein. *Device thrombogenicity emulation: a novel method for optimizing mechanical circulatory support device thromboresistance.* PloS one, 7(3):e32463, 2012.

[29] Matteo Nobili, Jawaad Sheriff, Umberto Morbiducci, Alberto Redaelli, and Danny Bluestein. *Platelet activation due to hemodynamic shear stresses: damage accumulation model and comparison to in vitro measurements.* ASAIO journal (American Society for Artificial Internal Organs: 1992), 54(1):64, 2008.

[30] Michalis Xenos, Gaurav Girdhar, Yared Alemu, Jolyon Jesty, Marvin Slepian, Shmuel Einav, and Danny Bluestein. *Device Thrombogenicity Emulator (DTE)- Design optimization methodology for cardiovascular devices: A study in two bileaflet MHV designs.* Journal of biomechanics, 43(12):2400–2409, 2010.

[31] Jolyon Jesty and Danny Bluestein. *Acetylated prothrombin as a substrate in the measurement of the procoagulant activity of platelets: elimination of the feedback activation of platelets by thrombin.* Analytical biochemistry, 272(1):64–70, 1999.

[32] Lorenzo Valerio, Filippo Consolo, Danny Bluestein, Phat Tran, Marvin Slepian, Alberto Redaelli, and Federico Pappalardo. *Shear-mediated platelet activation in patients implanted with continuous flow LVADs: A preliminary study utilizing the platelet activity state (PAS) assay.* In Engineering in Medicine and Biology Society (EMBC), 2015 37th Annual International Conference of the IEEE, pages 1255–1258. IEEE, 2015.

[33] Oddvar Tangen and Herbert J Berman. *Gel filtration of blood platelets: a methodological report.* In Platelet function and thrombosis, pages 235–243. Springer, 1972.

[34] Filippo Consolo, Lorenzo Valerio, Stefano Brizzola, Paolo Rota, Giulia Marazzato, Valentina Vincoli, Stefano Reggiani, Alberto Redaelli, and Gianfranco Fiore. *On the Use of the Platelet Activity State Assay for the In Vitro Quantification of Platelet Activation in Blood Recirculating Devices for Extracorporeal Circulation.* Artificial organs, 2016.

[35] Jawaad Sheriff, Phat L Tran, Marcus Hutchinson, Tracy DeCook, Marvin J Slepian, Danny Bluestein, and Jolyon Jesty. *Repetitive Hypershear Activates and Sensitizes Platelets in a Dose-Dependent Manner.* Artificial organs, 2015.

[36] Jawaad Sheriff, Gaurav Girdhar, Wei-Che Chiu, Jolyon Jesty, Marvin J Slepian, and Danny Bluestein. *Comparative efficacy of in vitro and in vivo metabolized aspirin in the DeBakey ventricular assist device.* Journal of thrombosis and thrombolysis, 37(4):499–506, 2014.

[37] CL Berman, EL Yeo, June D Wencel-Drake, BC Furie, MH Ginsberg, and B Furie. *A platelet alpha granule membrane protein that is associated with the plasma membrane after activation. Characterization and subcellular localization of platelet activation-dependent granule-external membrane protein.* Journal of Clinical Investigation, 78(1):130, 1986.

[38] Alan D Michelson and Mark I Furman. *Markers of Platelet Activation and Granule Secretion.* In Platelet Function, pages 301–314. Springer, 2005.

[39] M Griesshammer, H Beneke, B Nussbaumer, M Grünewald, M Bangerter, and L Bergmann. *Increased platelet surface expression of P-selectin and thrombospondin as markers of platelet activation in essential thrombocythaemia.* Thrombosis research, 96(3):191–196, 1999.

[40] Qijin Lu, Bryan V Hofferbert, Grace Koo, and Richard A Malinauskas. *In Vitro Shear Stress-Induced Platelet Activation: Sensitivity of Human and Bovine Blood.* Artificial organs, 37(10):894–903, 2013.

[41] Patrick J Trotter, Margaret A Orchard, and John H Walker. *Thrombin stimulates the intracellular relocation of annexin V in human platelets.* Biochimica et Biophysica Acta (BBA)-Molecular Cell Research, 1222(2):135–140, 1994.

[42] Eleni Tzima, Christel Poujol, Paquita Nurden, Alan T Nurden, Margaret A Orchard, and John H Walker. *Annexin V relocates to the periphery of activated platelets following thrombin activation: an ultra-*

structural immunohistochemical approach. Cell biology international, 23(9):629–635, 1999.

[43] Eleni Tzima, Patrick J Trotter, Margaret A Orchard, and John H Walker. *Annexin V relocates to the platelet cytoskeleton upon activation and binds to a specific isoform of actin.* European Journal of Biochemistry, 267(15):4720–4730, 2000.

[44] Jeanne Dachary-Prigent, Jean-Marie Freyssinet, Jean-Max Pasquet, Jean-Claude Carron, and Alan T Nurden. *Annexin V as a probe of aminophospholipid exposure and platelet membrane vesiculation: a flow cytometry study showing a role for free sulfhydryl groups.* Blood, 81(10):2554–2565, 1993.

[45] JD Hellums, DM Peterson, NA Stathopoulos, JL Moake, and TD Giorgio. *Studies on the mechanisms of shear-induced platelet activation.* In Cerebral ischemia and hemorheology, pages 80–89. Springer, 1987.

[46] Mitsuhiro Kuwahara, Mitsuhiko Sugimoto, Shizuko Tsuji, Hideto Matsui, Tomohiro Mizuno, Shigeki Miyata, and Akira Yoshioka. *Platelet shape changes and adhesion under high shear flow.* Arteriosclerosis, thrombosis, and vascular biology, 22(2):329–334, 2002.

[47] Ryan B Huang and Omolola Eniola-Adefeso. *Shear stress modulation of IL-1β-induced E-selectin expression in human endothelial cells.* PloS one, 7(2):e31874, 2012.

[48] JF Leeuwenberg, EF Smeets, JJ Neefjes, MA Shaffer, T Cinek, TM Jeunhomme, TJ Ahern, and WA Buurman. *E-selectin and intercellular adhesion molecule-1 are released by activated human endothelial cells in vitro.* Immunology, 77(4):543, 1992.

[49] V Videm and M Albrigtsen. *Soluble ICAM-1 and VCAM-1 as markers of endothelial activation.* Scandinavian journal of immunology, 67(5):523–531, 2008.

[50] Fan Zhang, Wei Yu, James L Hargrove, Phillip Greenspan, Roger G Dean, Ethan W Taylor, and Diane K Hartle. *Inhibition of TNF-α induced ICAM-1, VCAM-1 and E-selectin expression by selenium.* Atherosclerosis, 161(2):381–386, 2002.

[51] Vijayanand Modur, Guy A Zimmerman, Stephen M Prescott, and Thomas M McIntyre. *Endothelial Cell Inflammatory Responses to Tumor Necrosis Factor α Ceramide-dependent and -independent mitogen-*

activated ptotein kinase cascade. Journal of Biological Chemistry, 271(22):13094–13102, 1996.

[52] Fabienne Mackay, Hansruedi Loetscher, Dietrich Stueber, Gisela Gehr, and Werner Lesslauer. *Tumor necrosis factor alpha (TNF-alpha)-induced cell adhesion to human endothelial cells is under dominant control of one TNF receptor type, TNF-R55.* The Journal of experimental medicine, 177(5):1277–1286, 1993.

[53] Michelle Tsai, Ashley Kita, Joseph Leach, Ross Rounsevell, James N Huang, Joel Moake, Russell E Ware, Daniel A Fletcher, and Wilbur A Lam. *In vitro modeling of the microvascular occlusion and thrombosis that occur in hematologic diseases using microfluidic technology.* The Journal of clinical investigation, 122(1):408–418, 2012.

[54] PETER P Nawroth and DAVID M Stern. *Modulation of endothelial cell hemostatic properties by tumor necrosis factor.* The Journal of experimental medicine, 163(3):740–745, 1986.

[55] MWJ Boehme, U Raeth, WA Scherbaum, PR Galle, and W Stremmel. *Interaction of endothelial cells and neutrophils in vitro: kinetics of thrombomodulin, intercellular adhesion molecule-1 (ICAM-1), E-selectin, and vascular cell adhesion molecule-1 (VCAM-1): implications for the relevance as serological disease activity markers in vasculitides.* Clinical & Experimental Immunology, 119(1):250–254, 2000.

[56] Marco Franzoni, Irene Cattaneo, Bogdan Ene-Iordache, Alberto Oldani, Paolo Righettini, and Andrea Remuzzi. *Design of a cone-and-plate device for controlled realistic shear stress stimulation on endothelial cell monolayers.* Cytotechnology, 68(5):1885–1896, 2016.

[57] Adel M Malek, Seth L Alper, and Seigo Izumo. *Hemodynamic shear stress and its role in atherosclerosis.* Jama, 282(21):2035–2042, 1999.

[58] David C Chappell, Signe E Varner, Robert M Nerem, Russell M Medford, and R Wayne Alexander. *Oscillatory shear stress stimulates adhesion molecule expression in cultured human endothelium.* Circulation research, 82(5):532–539, 1998.

[59] Rosendo Estrada, Guruprasad A Giridharan, Mai-Dung Nguyen, Sumanth D Prabhu, and Palaniappan Sethu. *Microfluidic endothelial cell culture model to replicate disturbed flow conditions seen in atherosclerosis susceptible regions.* Biomicrofluidics, 5(3):032006, 2011.

[60] Wei Yin, Saravan Kumar Shanmugavelayudam, and David A Rubenstein. *The effect of physiologically relevant dynamic shear stress on platelet and endothelial cell activation.* Thrombosis research, 127(3):235–241, 2011.

[61] Wei Yin, Farzana Rouf, Saravan K Shanmugavelayudam, and David A Rubenstein. *Endothelial cells modulate platelet response to dynamic shear stress.* Cardiovascular Engineering and Technology, 5(2):145–153, 2014.

[62] Robert L Czervionke, John C Hoak, and Glenna L Fry. *Effect of aspirin on thrombin-induced adherence of platelets to cultured cells from the blood vessel wall.* Journal of Clinical Investigation, 62(4):847, 1978.

[63] Thomas Bombeli, Barbara R Schwartz, and John M Harlan. *Adhesion of activated platelets to endothelial cells: evidence for a GPIIbIIIa-dependent bridging mechanism and novel roles for endothelial intercellular adhesion molecule 1 (ICAM-1), $\alpha v\beta 3$ integrin, and GPIbα.* The Journal of experimental medicine, 187(3):329–339, 1998.

[64] Sherif F Nagueh, Christopher P Appleton, Thierry C Gillebert, Paolo N Marino, Jae K Oh, Otto A Smiseth, Alan D Waggoner, Frank A Flachskampf, Patricia A Pellikka, and Arturo Evangelista. *Recommendations for the evaluation of left ventricular diastolic function by echocardiography.* Journal of the American Society of Echocardiography, 22(2):107–133, 2009.

[65] Alaa Mabrouk Salem Omar, Sharath Vallabhajosyula, and Partho P Sengupta. *Left Ventricular Twist and Torsion Research Observations and Clinical Applications.* Circulation: Cardiovascular Imaging, 8(6):e003029, 2015.

[66] Ali Imanparast, Nasser Fatouraee, and Farhad Sharif. *The impact of valve simplifications on left ventricular hemodynamics in a three dimensional simulation based on in vivo MRI data.* Journal of biomechanics, 49(9):1482–1489, 2016.

[67] Josef Friedl, Markus Puhlmann, David L Bartlett, Steven K Libutti, Ewa N Turner, Michael FX Gnant, and H Richard Alexander. *Induction of permeability across endothelial cell monolayers by tumor necrosis factor (TNF) occurs via a tissue factor–dependent mechanism: relationship between the procoagulant and permeability effects of TNF.* Blood, 100(4):1334–1339, 2002.

[68] CW Ong, BT Chan, E Lim, NA Abu Osman, AA Abed, S Dokos, and NH Lovell. *Fluid structure interaction simulation of left ventricular flow dynamics under left ventricular assist device support.* In 2012 Annual International Conference of the IEEE Engineering in Medicine and Biology Society, pages 6293–6296. IEEE, 2012.

[69] Vinh-Tan Nguyen, Chong Jia Loon, Hoang Huy Nguyen, Zhong Liang, and Hwa Liang Leo. *A semi-automated method for patient-specific computational flow modelling of left ventricles.* Computer methods in biomechanics and biomedical engineering, 18(4):401–413, 2015.

[70] `https://www.thermofisher.com/it/en/home/references/protocols/cell-and-tissue-analysis/cell-profilteration-assay-protocols/cell-viability-with-alamarblue.html`.

[71] David Wild. *The immunoassay handbook: theory and applications of ligand binding, ELISA and related techniques.* Newnes, 2013.

[72] Notes from *"Biotechnological Applications"* course, academic year 2015-2016, prof. candiani.

[73] `https://serc.carleton.edu/research_education/geochemsheets/techniques/SEM.html`.